UNIVERSITÉ DE MONTRÉAL

KINETICS OF ALKALINE LEACHING OF ZINC OXIDE

Par

Hi Sun LEE
DÉPARTEMENT DE MÉTALLURGIE ET DE GÉNIE DES MATÉRIAUX
ÉCOLE POLYTECHNIQUE

THÈSE PRÉSENTÉE EN VUE DE L'OBTENTION
DU GRADE DE PHILOSOPHIAE DOCTOR (Ph.D.)
(GÉNIE MÉTALLURGIQUE)
mai 1994

ISBN 0-315-93388-7

Canada

UNIVERSITÉ DE MONTRÉAL

ÉCOLE POLYTECHNIQUE

Cette thèse intitulée:

KINETICS OF ALKALINE LEACHING OF ZINC OXIDE

présenté par: Hi Sun LEE

en vue de l'obtention du grade de: PHILOSOPHIAE DOCTOR (Ph.D.)

a été dûment acceptée par le jury d'examen constitué de:

M. Frank AJERSCH, Ph.D., president

M. Dominique L. PIRON, Ph.D., membre et directeur de recherche

M. Pierre CLAESSENS, Ph.D., membre extérieur

M. Marius D'AMBOISE, Ph.D., membre

SOMMAIRE

La dissolution de l'oxyde de zinc pur et des concentrés de zinc grillé dans une solution de NaOH est réalisée afin d'étudier la cinétique de la lixiviation alcaline de l'oxyde de zinc. Ce travail comporte trois parties: la première étudie la cinétique de la lixiviation alcaline de l'oxyde de zinc pur, la seconde étudie la cinétique de la lixiviation alcaline des concentrés de zinc grillé et la dernière étudie les variables du processus de la lixiviation qui offrent un plus haut taux de lixiviation et une plus faible consommation d'énergie. Des faibles concentrations de particules sont utilisées dans la première et la seconde partie, tandis que des hautes concentrations de particules sont utilisées dans la dernière partie de ce travail.

Dans un premier temps la surface spécifique des particules est mesurée par la technique BET. Ensuite, un réacteur agité mécaniquement est employé pour le processus de la lixiviation. Puis une centrifugeuse est utilisée pour séparer la solution de lixiviation du liquide contenant des particules. Et finalement, la concentration en zinc dans la solution de lixiviation est mesurée par spectrophotométrie d'absorption atomique.

Quatre types d'oxyde de zinc sont utilisés: l'oxyde de zinc pur de "haute pureté" (Fisher), l'oxyde de zinc pur fritté, les concentrés de zinc grillés de Zinc électrolytique du Canada (CEZ) et le mélange fritté d'oxyde de zinc et d'hématite. L'oxyde de zinc pur fritté a été préparé par frittage à 1523 K dans une atmosphère d'air durant 50 heures,

suivi d'un broyage. Le mélange fritté a été obtenu aussi par le frittage du mélange de l'oxyde de zinc et de l'hématite à 1373 K dans une atmosphère d'air durant 2 heures, et broyé par la suite.

La dissolution de l'oxyde de zinc pur dans une solution de NaOH est contrôlée par deux phénomènes; c'est à dire, par la réaction de surface et par la diffusion à travers la couche limite. La contribution du contrôle par transfert de masse a été calculée par l'équation semi-empirique de Rantz et Marshall. L'équation suivante permet de calculer le temps de lixiviation nécessaire pour atteindre une certaine conversion et ceci en concordance avec les résultats expérimentaux obtenus:

$$t_r = 2.1 \times 10^{-4} S_o^{-1} C^{-0.6} \exp(5170/T) [1-(1-\alpha)^{1/3}]$$

La dissolution des concentrés de zinc grillé dans une solution de NaOH est contrôlée par la diffusion à travers la couche de ferrite de zinc pendant la première étape du processus de la lixiviation et par la réaction de surface sur l'oxyde de zinc à l'étape ultérieure. Dans le modèle de la diminution du noyau, la diffusion à travers n'importe quelle couche solide peut être l'étape déterminante. Le coefficient de diffusion effectif et la constante de vitesse de réaction chimique du taux de lixiviation ont été calculés. Des énergies d'activation de 16 et de 11 kcal/mol ont été obtenues à partir des courbes d'Arrhenius pour la diffusion à travers la couche de ferrite de zinc et pour la réaction de surface sur l'oxyde de zinc, respectivement. Durant la lixiviation, la couche de ferrite

de zinc se transforme en une couche d'oxyde de fer plus poreuse, qui s'épaissit progressivement suite à la dissolution sélective de ferrite de zinc.

Pour un plus haut taux de lixiviation, il est nécessaire d'obtenir une suspension complète et non un écoulement turbulent. Le réacteur de lixiviation a été construit pour obtenir une suspension complète avec une consommation minimale de puissance. La vitesse d'agitation minimale pour la suspension complète est calculée par la corrélation de Zwietering: il diminue en augmentant le diamètre de l'agitateur, mais l'influence du diamètre de l'agitateur sur la vitesse d'agitation augmente lorsque le "clearance ratio" augmente. La formation du précipité à non-suspension a lieu en trois étapes: la dissolution, la supersaturation et l'élargissement.

ABSTRACT

The dissolution of pure zinc oxide and roasted zinc concentrates in NaOH solution were studied in order to understand the kinetics of alkaline leaching of zinc oxide. This work consists of three parts: first, a study of the kinetics of alkaline leaching of pure zinc oxide; second, a study of the kinetics of alkaline leaching of roasted zinc concentrates; and third, a study of the variables of leaching process, with respect to higher dissolution rates and less energy consumption. In the first and second parts, a low concentration of particles was used, and in the third part, a high concentration of particles was used.

A mechanically-agitated reactor was constructed. The specific surface area of the particles was measured by the BET adsorption technique. A centrifuge was used to obtain a pregnant solution from the mixture of particles and liquid, and the concentration of zinc ions in the pregnant solution was measured with an atomic absorption spectrophotometer.

Four kinds of zinc oxide were used in these studies: reagent grade pure zinc oxide (Fisher), sintered pure zinc oxide, roasted zinc concentrates of Canadian Electrolytic Zinc (CEZ), and a sintered mixture. Sintered pure zinc oxide was prepared by sintering in air at 1523 K for 50 hours and then grounding the sintered pellets. The sintered mixture was obtained by sintering the mixture of zinc oxide and hematite in air at 1373 K for 2 hours and then grounding the sintered pellets.

The dissolution of pure zinc oxide in NaOH solution is governed by mixed control of surface reaction and boundary layer diffusion. The contribution of mass transfer on the rate-determining step was calculated using a semi-empirical Rantz and Marshall equation. The following equation for leaching time required to attain a certain conversion was found to be in good agreement with experimentally obtained leaching times: $t_r = 2.1 \times 10^{-4} S_0^{-1} C^{-0.6} \exp(5170/T) [1-(1-\alpha)^{1/3}]$.

The dissolution of roasted zinc concentrates in NaOH solution is controlled by diffusion through the zinc ferrite layer during the early stage of the leaching process and by the surface reaction on the zinc oxide in the later stage. In the shrinking core model, diffusion through any solid layer can be the rate-determining step. The effective diffusion coefficient and the chemical rate constant in the leaching process were calculated from the experimental results. Activation energies of 16 and 11 kcal/mol were obtained from the Arrhenius plot for diffusion through the zinc ferrite layer and the surface reaction on the zinc oxide, respectively. The zinc ferrite layer changed to the more porous iron oxide as leaching proceeded, and this layer became progressively thicken due to the selective dissolution of zinc ferrite.

To obtain a fast leaching rate, complete suspension must be obtained, not a turbulent flow. The leaching reactor was designed to obtain complete suspension with minimal power consumption. The minimum agitation speed for complete suspension is

determined using the correlation of Zwietering: it decreased as the agitator diameter increased, but the influence of agitator diameter on the agitation speed increased as the clearance ratio increased. The formation of precipitate in no-suspension takes place in three stages: dissolution, supersaturation and thickening.

RÉSUMÉ

Le procédé électrolytique en milieu alcalin est une alternative technologique prometteuse au procédé électrolytique en milieu sulfate, puis qu'il permet l'opération à une densité de courant plus élevée avec plus basse consommation d'énergie. Ce dernier consomme typiquement d'environ 3.26 kWh/kg, alors que l'énergie spécifique typique du procédé alcalin n'est que d'environ 1.75 kWh/kg. De plus, du fait que le procédé alcalin opère à des densités de courant de 1000 A/m^2 ou plus, soit 500 A/m^2 de plus que le procédé au sulfate, les coûts d'investissements sont réduits et la productivité accrue.

Suite à ces résultats encourageants du procédé électrolytique en milieu alcalin, il est nécessaire d'étudier les étapes hydrométallurgiques. Et par conséquent, il est très important d'étudier le processus de lixiviation, puisqu'il est la première étape hydrométallurgique pour produire le zinc métallique.

L'objectif de ce travail est d'étudier la cinétique de la lixiviation alcaline de l'oxyde de zinc. Pour le réaliser, le travail a été réalisé en trois parties: la première consiste à étudier la cinétique de la lixiviation alcaline de l'oxyde de zinc pur, la seconde consiste à étudier la cinétique de la lixiviation alcaline des concentrés de zinc grillé et la troisième consiste à étudier les variables du processus de la lixiviation offrant un taux de lixiviation supérieure et une consommation d'énergie réduite. Des faibles concentrations de particules sont utilisées dans la première et la seconde partie tandis que des hautes

concentrations de particules sont utilisées dans la dernière partie de ce travail.

Lorsque la dissolution a lieu, les particules diminuent de taille, de même que leur surface active. Par conséquent, la vitesse totale de dissolution sera réduite. Cette situation est décrite par une formule mathématique appelée le modèle de la diminution du noyau. Des expressions mathématiques du taux de la réaction ont été développées pour décrire: le contrôle par transfert de masse à travers la couche limite ou par diffusion à travers la couche solide du produit de réaction, le contrôle par la réaction de surface et la combinaison de ces contrôles. Dans ce cas, les particules doivent être complètement en suspension. Ce critère dit que les particules ne restent pas dans le fond du réacteur au-delà d'une seconde. Ce critère se détermine par l'observation visuelle des particules, au fond du réacteur, à l'aide d'un miroir placé sous le réacteur.

L'appareillage utilisée dans les expériences de lixiviation consiste en un bécher en pyrex de deux litres (Corning No. 6947) partiellement enveloppe d'un manchon chauffant. Le bécher est couvert avec un plateau en pyrex ayant des ouvertures permettant la prise périodique d'échantillons, la mesure de la température, l'introduction d'un agitateur et l'adaptation d'un système de condensation des vapeurs. Un thermomètre de mercure a été employé pour mesurer la température. Le système de condensation permet de minimiser les pertes de l'électrolyte par évaporation. L'agitateur constitué d'une hélice avec quatre lames formant un angle de 45° a été actionné par un

moteur à vitesse variable. Des chicanes standards sont utilisées.

Un volume d'un litre de solution d'hydroxyde de sodium de concentration désirée a été placé dans le bécher. Lorsque la température de la solution est atteinte, une quantité prédéterminée d'oxyde de zinc a été ajoutée dans la solution. Un échantillon de 3 ml de volume a été prélevé à des intervalles réguliers. Ces échantillons ont été séparés par la centrifugeuse pour obtenir la solution lixiviée du mélange solide-liquide. Finalement, la concentration des ions a été mesurée.

La surface spécifique des particules a été mesurée par la technique d'adsorption BET (Flow Sorb II 2300 (Norcross, GA)). Une centrifugeuse est construite au laboratoire électrométallurgique de l'École Polytechnique de Montréal pour séparer la solution de la lixiviation. Ensuite, la concentration en zinc dans la solution de la lixiviation a été mesurée par un spectrophotomètre d'absorption atomique (Perkin-Elmer (Norwark, CT) AA 5000).

Quatre types d'oxyde de zinc sont utilisés: l'oxyde de zinc pur, l'oxyde de zinc pur fritté, les concentrés de zinc grillés et le mélange fritté d'oxyde de zinc pur et d'hématite pure. L'oxyde de zinc pur et l'hématite pure utilisés sont de "haute pureté" (Fisher). L'oxyde de zinc pur fritté a été préparé par frittage à 1523 K dans une atmosphère d'air durant 50 heures suivi d'un broyage. Les concentrés de zinc grillé ont

été préparés à partir des concentrés de sulfure de zinc grillé par Zinc électrolytique du Canada (CEZ). Le mélange fritté a été obtenu aussi par le frittage du mélange de l'oxyde de zinc et de l'hématite à 1373 K dans une atmosphère d'air durant 2 heures, et broyé par la suite.

La vitesse d'agitation influence le taux de lixiviation de l'oxyde de zinc pur. Le taux de lixiviation varie linéairement avec la surface spécifique. Le taux de lixiviation augmente avec l'accroissement de la concentration de NaOH mais alors l'exposant de la concentration sur le taux de lixiviation diminue. Une énergie d'activation de 10 kcal/mol a été obtenue à partir de la courbe d'Arrhenius. La dissolution de l'oxyde de zinc pur dans une solution de NaOH est contrôlée par la réaction de surface et par la diffusion à travers la couche limite.

Puisque le taux de lixiviation est, partiellement, contrôlé par la diffusion, la contribution du contrôle par transfert de masse a été calculée par l'équation semi-empirique de Rantz et Marshall. Ensuite, ces valeurs sont comparées avec les valeurs expérimentaux. Les valeurs obtenues à l'aide de l'équation semi-empirique de Rantz et Marshall concordent avec celles provenant des donnés expérimentales. L'importance relative de la réaction de surface et la diffusion à travers la couche limite sur le taux de la lixiviation dépend des conditions opératoires.

L'équation suivante permet de calculer le temps de lixiviation de l'oxyde de zinc pur nécessaire pour atteindre une certaine conversion en concordance avec les résultats expérimentaux obtenus: $t_r = 2.1 \times 10^{-4} S_o^{-1} C^{-0.6} \exp(5170/T) [1-(1-\alpha)^{1/3}]$.

Le taux de lixiviation des concentrés de zinc grillé est indépendant de la vitesse d'agitation et de la concentration de NaOH. Le taux de lixiviation augmente lorsque la taille des particules diminue. Aussi, le taux de lixiviation croît avec l'augmentation de la température. Particulièrement, le pourcentage absolu d'extraction de zinc augmente lorsque la température augmente. La cartographie de rayon X montre que l'oxyde de fer se situe à l'extérieur de la particule tandis que l'oxyde de zinc se trouve à l'intérieur. De plus, l'oxyde de fer entoure l'oxyde de zinc et la taille de la particule n'a pas diminuée après la lixiviation.

Selon le modèle de la diminution du noyau, la modification du contrôle de la diffusion à travers la couche solide de produit montre une valeur de la pente égale à deux, tandis que la modification du contrôle de la réaction de surface montre une valeur de la pente égale à un. La courbe entre log t (temps) et log R (rayon de la particule) des résultats expérimentaux montre une pente de deux pendant la première étape tandis que la pente devient unitaire dans l'étape ultérieure. L'analyse des résultats expérimentaux a représenté mathématiquement au modèle de la diminution du noyau.

Cependant, en pratique, l'utilisation du modèle de la diminution du noyau à partir des résultats expérimentaux présente deux problèmes. Premièrement, au début du processus de lixiviation, la couche solide de produit n'existe pas. Deuxièmement, malgré que la couche résiduelle est formée après quelque temps, la diffusion à travers cette couche ne peut pas contrôler le taux de lixiviation parce qu'à l'étape ultérieure, la réaction de surface devient l'étape déterminante. Au début du processus de la lixiviation, la couche de ferrite de zinc est existée, et cette couche oppose une résistance à la diffusion de la solution au cours de la première étape. Cependant, en considérant la couche de ferrite de zinc comme un barrière à la diffusion, le liquide doit diffuser à travers la couche de ferrite de zinc pour atteindre le noyau de l'oxyde de zinc et lors de la diffusion, il y a aussi lixiviation de l'oxyde de zinc contenu dans la couche de ferrite de zinc.

Pour résoudre les problèmes énoncé précédement, la porosité de la particule doit être considérée.

Pour un solide poreux, l'expression mathématique est la même que la formule entre la diffusion à travers la couche solide de réactif et la diffusion à travers la couche solide de produit puis qu'il s'agit du même type de gradient de concentration liquide dans les deux cas. Si la diffusion à travers la couche solide fournit la majeure partie de la résistance au processus de lixiviation, le processus a lieu dans une limite mince de

l'interface. Cette situation est identique à celle du modèle de la diminution du noyau. Donc, la diffusion à travers de n'importe quelle couche solide peut être l'étape déterminante dans le modèle de la diminution du noyau.

Lors de l'attaque par la solution de NaOH, la couche de ferrite de zinc se transforme en une couche d'oxyde de fer plus poreuse, qui s'épaissit progressivement suite à la dissolution sélective de ferrite de zinc. Après la tous formation en oxyde de fer plus poreux, la solution diffuse librement jusqu'à l'interface d'oxyde de zinc et c'est pourquoi l'étape déterminante change pour la réaction de surface dans l'étape ultérieure. La réaction globale de la dissolution des concentrés de zinc grillé est la suivante:

$$ZnFe_2O_4 + 2\ OH^- + H_2O \longrightarrow Zn(OH)_4^{2-} + Fe_2O_3$$

$$ZnO + 2\ OH^- + H_2O \longrightarrow Zn(OH)_4^{2-}$$

Le coefficient de diffusion effectif et la constante de vitesse réaction chimique ont été calculés à partir du modèle de la diminution du noyau. Les énergies d'activation de 16 et de 11 kcal/mol ont été obtenues à partir des courbes d'Arrhenius pour la diffusion à travers la couche solide et pour la réaction de surface respectivement.

L"impeller Reynolds number" a été calculé pour démontrer qu'il est nécessaire d'obtenir une suspension complète et non un écoulement turbulent pour obtenir un plus

haut taux de lixiviation. Le réacteur de lixiviation a été construit pour obtenir la suspension complète avec une consommation minimale de puissance. La vitesse d'agitation minimale pour la suspension complète est présentée en utilisant la corrélation de Zwietering. La corrélation entre log s (constant adimensionnelle) et log (D/D_T) a été obtenue en fonction de h/D_T. Cela montre que la vitesse d'agitation minimale pour la suspension complète diminue lorsque la diamètre de l'agitateur augmente. Cependant, l'influence du diamètre de l'agitateur sur la vitesse d'agitation augmente lorsque h/D_T augmente.

Les précipités formés lors de certaines réactions de la non-suspension ont été observée au microscope électronique à balayage (MEB). La précipitation a lieu en trois étapes: la première est la dissolution de l'oxyde de zinc en zincate qui accumule près de la particule, la seconde est la précipitation du film d'oxyde de zinc près de la particule et la troisième est l'accroissement graduel de la couverture du film d'oxyde de zinc sur la surface de la particule.

ACKNOWLEDGEMENT

The author extends his deepest thanks to the director of his thesis, Professor Dominique L. Piron, for his ideas, encouragements, kindness, and guidance in all aspects of this work.

Sincere appreciation also goes to Professors Frank Ajersch and Marius D'Amboise and to Dr. Pierre Claessens for accepting to be members of the committee for examination of the thesis.

The author is indebted to Dr. J. St-Pierre and Dr. C. Fan for useful discussions on this work.

The helpfulness and kindness of many friends in the laboratory are also gratefully acknowledged: K. Amuzgar, B. Behzadian, J. Ho, G. Kim, Y. Liu, N. Massé, H. Miao, I. Nakatsugawa, P. Paradis, M. Sider, P. Yin and Dr. M. Hu. I would especially like to thank C. Llerena, M. Rojas and A. Sleb for their help with French.

I also thank all the technicians and secretaries in the Département de Métallurgie et de Génie des Matériaux for their kindness and helpfulness.

I am grateful to Noranda's Canadian Electrolytic Zinc (CEZ) for the financial

support which permitted me to undertake my studies.

I realize that I could not have completed this work without the loving support and understanding from my parents. A very special thanks go to Jae-Yun, my wife, for her continued understanding and love and to Yunjoo and Anne-Marie Sooyoun, my daughters.

TABLE OF CONTENTS

PAGE

SOMMAIRE..... iv

ABSTRACT..... vii

RÉSUMÉ..... x

ACKNOWLEDGEMENT..... xiii

TABLE OF CONTENTS..... xx

LIST OF FIGURES..... xxvi

LIST OF TABLES..... xxxi

LIST OF SYMBOLS..... xxxiii

CHAPTER 1 - INTRODUCTION..... 1

CHAPTER 2 - LITERATURE REVIEW..... 7

2.1 Introduction..... 7

2.2 Shrinking Core Model..... 8

2.2.1 Dissolution of Pure Zinc Oxide..... 12

2.2.1.1 Diffusion through Boundary Layer..... 13

2.2.1.2 Surface Reaction..... 15

2.2.1.3 Mixed Control..... 16

2.2.2 Distinction between Diffusion Control and Surface Reaction Control..... 18

2.2.2.1 Temperature..... 18

2.2.2.2 Agitation Speed..... 18

2.2.3 Dissolution of Roasted Zinc Concentrates..... 19

2.2.3.1 Diffusion through Boundary Layer..... 19

2.2.3.2 Diffusion through Solid Product Layer..... 21

2.2.3.3 Surface Reaction..... 23

2.2.4 Combination of Resistance..... 23

2.3 Suspension of Particles..... 27

2.3.1 Criterion of Complete Suspension..... 27

2.3.2 Particle Suspension Correlations..... 28

2.3.3 Variables Which Affect Suspension of Particles..... 30

2.3.3.1 Clearance Ratio (h/D_T)..... 30

2.3.3.2 Impeller-to-Reactor Diameter Ratio (D/D_T).. 32

2.3.3.3 Liquid Height-to-Reactor Diameter Ratio (H/D_T)..... 32

2.3.4 Effect of Baffle..... 32

2.3.5 Particle Distribution in Complete Suspension..... 35

2.3.6 Mass Transfer in Mechanically-Agitated Reactor..... 35

CHAPTER 3 - EXPERIMENTAL..... 38

3.1 Apparatus..... 38

3.2 Electrolytic Solution..... 38

3.3 Materials..... 40

3.3.1 Pure Zinc Oxide..... 40

3.3.2 Sintered Pure Zinc Oxide..... 40

3.3.3 Sintered Mixture of Zinc Oxide and Hematite..... 43

3.3.4 Roasted Zinc Concentrates..... 45

3.4 Analysis..... 45

3.4.1 Surface Area Measurement..... 45

3.4.2 Separation of Liquid-Solid Mixture..... 46

3.4.3 Ion Concentration Measurement..... 49

3.5 Solubility of Zinc Oxide in NaOH Solution..... 51

3.6 Procedure..... 53

CHAPTER 4 - RESULTS..... 55

4.1 Leaching Kinetics of Pure Zinc Oxide..... 55

4.1.1 Effect of Agitation Speed..... 55

4.1.2 Effect of Particle Size..... 57

4.1.3 Effect of NaOH Concentration..... 60

4.1.4 Effect of Temperature..... 60

4.2 Leaching Kinetics of Roasted Zinc Concentrates..... 63

4.2.1 Effect of Agitation Speed..... 63

4.2.2 Effect of Particle Size..... 66

4.2.3 Effect of NaOH Concentration..... 69

4.2.4 Effect of Temperature..... 69

4.2.5 Dissolution of Iron..... 73

4.2.6 Morphology..... 77

4.3 Process Variables..... 79

4.3.1 Measurement of Kinematic Viscosity..... 79

4.3.2 Suspension of Particles..... 79

4.3.3 Precipitate..... 82

4.3.4 Effect of Baffles..... 85

4.3.5 Effect of Degree of Particle Concentration..... 88

4.3.6 Agitation Speed for Complete Suspension..... 91

4.3.7 Effect of Clearance Ratio..... 91

4.3.8 Effect of Impeller-to-Reactor Diameter Ratio..... 91

CHAPTER 5 - DISCUSSION..... 96

5.1 Leaching Kinetics of Pure Zinc Oxide..... 96

5.1.1 Data Treatment..... 96

5.1.2 Effect of Agitation Speed..... 98

5.1.3 Effect of Particle Size..... 100

5.1.4 Effect of NaOH Concentration..... 103

5.1.5 Effect of Temperature..... 103

5.1.6 Mixed Control..... 107

5.1.7 Prediction of Leaching Time..... 114

5.2 Leaching Kinetics Of Roasted Zinc Concentrates..... 118

5.2.1 Data Treatment..... 118

5.2.2 Rate-Determining Step..... 120

5.2.3 Extension of Shrinking Core Model..... 122

5.2.4 Analysis with Extended Shrinking Core Model..... 128

5.2.5 Dissolution of Zinc Ferrite..... 133

5.2.6 Determination of Effective Diffusion Coefficient, D_e and Chemical Rate Constant, k..... 134

5.2.7 Calculation of Activation Energy..... 139

5.2.8 Effect of Zinc Ferrite..... 143

5.2.9 Effect of Impurities..... 145

5.3 Process Variables..... 147

5.3.1 Degree of Particle Suspension..... 148

5.3.2 Formation of Precipitate..... 149

5.3.3 Complete Suspension..... 150

5.3.4 Correlation for Complete Suspension..... 152

5.3.5 Power Consumption..... 155

5.3.6 Avoidance of Vortex..... 156

5.4 Suggestion for Future Research..... 159

CHAPTER 6 - CONCLUSIONS..... 161

REFERENCES..... 165

LIST OF FIGURES

PAGE

Figure 1.1 E-pH diagram for the zinc-water system..... 3

Figure 2.1.a Shrinking particle model of the dissolution of particles in the solution..... 10

Figure 2.1.b Shrinking core model of the dissolution of particles in the solution..... 11

Figure 2.2 Schematic diagram of variables which affect the suspension of particles..... 31

Figure 2.3 Flow pattern of the leaching reactor..... 34

Figure 3.1 Schematic diagram of the experimental apparatus..... 39

Figure 3.2 Morphology of reagent grade pure zinc oxide..... 42

Figure 3.3 Schematic diagram of rotating plate with four 45^0 angle rotor of the experimental centrifuge..... 48

Figure 4.1 Effect of agitation speed on the dissolution of pure zinc oxide..... 56

Figure 4.2 Effect of temperature on the dissolution of pure zinc oxide (+20-38 μm)..... 58

Figure 4.3 Effect of particle size on the dissolution of pure zinc oxide..... 59

Figure 4.4 Effect of NaOH concentration on the dissolution of pure zinc oxide..... 61

Figure 4.5 Effect of temperature on the dissolution of pure zinc oxide (+180-355 μm)..... 62

Figure 4.6 Effect of agitation speed on the leaching rate of roasted zinc concentrates..... 64

Figure 4.7 Effect of agitation speed on the leaching rate of sintered mixture..... 65

Figure 4.8 Effect of temperature on the leaching rate of roasted zinc concentrates (+20-38 μm)..... 67

Figure 4.9 Effect of particle size on the leaching rate of roasted zinc concentrates..... 68

Figure 4.10 Effect of NaOH concentration on the leaching rate of roasted zinc concentrates..... 70

Figure 4.11 Effect of NaOH concentration on the leaching rate of sintered mixture..... 71

Figure 4.12 Effect of temperature on the leaching rate of roasted zinc concentrates (+75-150 μm)..... 72

Figure 4.13 Effect of temperature on the leaching rate of sintered mixture (+75-150 μm)..... 74

Figure 4.14 Dissolution of iron as a function of NaOH concentration in roasted zinc concentrates..... 76

Figure 4.15 Morphology and X-ray mapping of partially-leached particle of roasted zinc concentrates..... 78

Figure 4.16 Kinematic viscosity of NaOH solution as a function of temperature..... 80

Figure 4.17 Effect of agitation speed on the dissolution of pure zinc oxide..... 81

Figure 4.18 Suspension of particles (10 M, 298 K)
a) 300 rpm b) 600 rpm..... 83

Figure 4.19 Formation of precipitate of partially-leached particle (200 rpm, 328 K, 10 M)..... 84

Figure 4.20 Dissolution of pure zinc oxide at 200rpm..... 86

Figure 4.21 Effect of baffles on the dissolution of pure zinc oxide..... 87

Figure 4.22 Effect of number of baffles on the dissolution of roasted zinc concentrates..... 89

Figure 4.23 Effect of degree of particle concentration on the dissolution of roasted zinc concentrates..... 90

Figure 4.24 Effect of impeller-to-reactor diameter ratio and clearance ratio on the minimum agitation speed for complete suspension..... 92

Figure 4.25 Effect of clearance ratio on the dissolution of roasted zinc concentrates..... 93

Figure 4.26 Effect of impeller-to-reactor diameter ratio on the dissolution of roasted zinc concentrates..... 94

Figure 5.1 Effect of agitation speed on the leaching rate of pure zinc oxide analyzed by shrinking particle model..... 99

Figure 5.2 Effect of particle size on the leaching rate of pure zinc oxide analyzed by shrinking particle model..... 101

Figure 5.3 Relationship between rate constant and specific surface area..... 102

Figure 5.4 Effect of NaOH concentration on the leaching rate of pure zinc oxide analyzed by shrinking particle model..... 104

Figure 5.5 Change of power dependency on NaOH concentration..... 105

Figure 5.6 Effect of temperature on the leaching rate of pure zinc oxide analyzed by shrinking particle model..... 106

Figure 5.7 Activation energy from Arrhenius plot on the dissolution of pure zinc oxide..... 108

Figure 5.8 Relationship between rate constant and NaOH activity..... 112

Figure 5.9 Comparison of the calculated and the experimental leaching time as a function of particle size..... 116

Figure 5.10 Comparison of the calculated and the experimental leaching time as a function of temperature..... 117

Figure 5.11 Times to reach a given fractional conversion based on the original particle size of roasted zinc concentrates..... 124

Figure 5.12.a Analysis of experimental results using Equation (5.23) of the shrinking core model as a function of particle size (data from Figure 4.9)..... 129

Figure 5.12.b Analysis of experimental results using Equation (5.21) of the shrinking core model as a function of particle size (data from Figure 4.9)..... 130

Figure 5.12.c Analysis of experimental results by the shrinking core model as a function of particle size (data from Figure 4.9)..... 131

Figure 5.13 Analysis of experimental results by the shrinking core model as a function of temperature (data from Figure 4.12)..... 132

Figure 5.14 X-ray diffraction analysis of the particles..... 137

Figure 5.15 Analysis of experimental results using Equation (5.25)..... 140

Figure 5.16 Activation energy from Arrhenius plot determined from the leaching rate of roasted zinc concentrates..... 142

Figure 5.17 Effect of zinc ferrite on leaching rate..... 144

Figure 5.18 Schematic diagram of particle suspension as a function of agitation speed..... 148

Figure 5.19 Correlation for complete suspension..... 153

LIST OF TABLES

PAGE

Table 1.1 Comparison of the experimental conditions on the dissolution of pure zinc oxide..... 6

Table 3.1 Specific surface area measurements for three kinds of samples.. 41

Table 3.2 Effect of operating time of centrifuge on leaching rate (6M, 328K)..... 50

Table 3.3 Chemical analysis of the particles..... 52

Table 3.4 Experimental parameters..... 54

Table 4.1 The dissolution of iron in NaOH solution as a function of particle size (10M, 298 K, 600 rpm)..... 75

Table 5.1 Calculation of specific rate constant and specific mass transfer coefficient (600 rpm)..... 111

Table 5.2 Time needed to achieve the same fractional conversion for each particle size..... 123

Table 5.3 Dependence of chemical rate constant and effective diffusion coefficient on particle size (298 K, 600 rpm, 10 M)..... 135

Table 5.4 Calculation of values of A..... 138

Table 5.5 Dependence of chemical rate constant and effective diffusion coefficient on temperature (600 rpm, 10 M, +75-150 μm)..... 141

Table 5.6 Impeller Reynolds Number as a function of temperature, agitation speed and NaOH concentration..... 151

Table 5.7 Calculation of power consumption per unit mass as a function of agitation speed for complete suspension..... 156

LIST OF SYMBOLS

a = activity of NaOH solution, M

B = area of baffle, cm^2

C = concentration of NaOH solution in the bulk, M

C_1 = concentration of zincate ion, g l^{-1}

d = diameter of particles, cm

d_0 = initial diameter of particles, cm

D = agitator diameter, cm

D_b = baffle diameter, cm

D_d = diffusion coefficient, cm^2 sec^{-1}

D_e = effective diffusion coefficient, cm^2 sec^{-1}

D_T = reactor diameter, cm

g = acceleration of gravity, 980 cm sec^{-2}

H = fractional volumetric hold up of particles, cm^3 cm^{-3}

h = clearance between agitator and tank bottom, cm

k = rate constant, sec^{-1}

k_1 = mass transfer coefficient from Equation (2.1)

k_2 = mass transfer coefficient from Equation (2.18)

k_c = chemical rate constant, mol cm^{-2} min^{-1}

k_d = specific mass transfer coefficient, mol cm^{-2} min^{-1}

k_m = specific rate constant, mol cm^{-2} min^{-1}

k_n = mixed rate constant from Equation (2.16)

k_r = rate constant from Equation (5.2)

k_s = mass transfer coefficient obtained from slip velocity, cm sec^{-1}

k_t = mass transfer coefficient obtained from free settling velocity, cm sec^{-1}

K = equilibrium constant

K_1 = constant from Equation (2.8)

K_2 = constant from Equation (2.12)

K_3 = constant from Equation (2.21)

K_4 = constant from Equation (2.27)

L = liquid height in leaching reactor

M = molecular weight of particles, g M^{-1}

n = constant exponent

N = agitation speed, rpm

N_p = power number for the agitator, dimensionless

N_s = agitation speed for complete suspension, rpm

P = power input for the agitator, w

P_m = power input per unit mass of liquid, w kg^{-1}

R = initial mean radius of particles, cm

r_c = radius of particles at time t, cm

s = constant in Equation (2.34), dimensionless

S = surface area of particles at time t, cm^2

S_0 = initial specific surface area of particles, $cm^2\ g^{-1}$

t = time, min

T = temperature, K

v_s = slip velocity, $cm\ sec^{-1}$

v_t = free settling terminal velocity, $cm\ sec^{-1}$

V = volume of solution, l

W_o = initial weight of particles, g

W_t = weight of particles at time t, g

X = concentration of particles, $g\ l^{-1}$

Sh = Sherwood number, $k_s d/D_d$

Re = Reynolds number, $dv_s\rho_f/\mu$

Sc = Schmidt number, $\mu/\rho_f D_d$

Greek Letters

α = fraction reacted, $(W_o - W_t) / W_o$

δ = boundary layer thickness, cm

μ = viscosity, $g\ cm^{-1}\ sec^{-1}$

ρ = density of particles, $g\ cm^{-3}$

ρ_f = density of solution, $g\ cm^{-3}$

$\Delta\ \rho$ = density difference between particle and solution, $g\ cm^{-3}$

ν = kinematic viscosity, $cm^2\ s^{-1}$

σ = stoichiometric factor

CHAPTER 1

INTRODUCTION

The consumption of zinc metal in the western world has grown at the rate of 1.5 %/yr over the past two decades, and world demand for zinc metal was projected to grow an average of 1.7 %/yr during the 1990s (1). Around 80 % of world zinc production is obtained by the energy-intensive sulfate electrolytic process (2,3). Moreover, energy consumption constitutes approximately 35 % of the total cost of electrolytic zinc production, and this percentage will further increase (4). Since zinc production in the western world amounted to 5 million metric tons in 1990 (1), the reduction of energy consumption represents an important factor relative to the total production cost.

Among the possible alternatives for reducing energy consumption in zinc production, recent research results (5,6) show an alkaline electrolytic process to be very promising, and more economical than the sulfate electrolytic process. The specific energy consumption of the alkaline electrolytic process is approximately 1.75 kWh/kg (6), as compared with a value of 3.26 kWh/kg for the sulfate electrolytic process (7,8). Moreover, the alkaline electrolytic process requires less capital investment, since it operates at a current density of 1000 A/m^2 or higher, whereas the sulfate electrolytic process uses 500 A/m^2 (9,10).

The encouraging results of the alkaline electrolytic process show the necessity of

studying the leaching process, since it is the first hydrometallurgical step.

It is appropriate to discuss solution-solid equilibria in terms of the potential (E) - pH diagram to study the possibility of alkaline leaching of zinc oxide. The E-pH diagram describes the solution composition or solid phase stability as a function of electrode potential and pH. The possibility of alkaline leaching of zinc oxide is shown in the E-pH diagram for the zinc-water system, which simply shows in Figure 1.1. The dissolution of zinc oxide is favorable above pH 13.4 (11-13). In highly alkaline media, the metals exist as complex anions designated as zincate, $Zn(OH)_4^{2-}$; when a 1 M NaOH solution is used, 92 % of zinc ions in the leached solution are in the form of zincate; when a 4 M NaOH solution is used, 99 % of the ions are zincate (14).

Three sources of zinc oxide are available for alkaline leaching: roasted zinc concentrates, natural zinc oxide ores, and arc furnace steelmaking dusts. Roasted zinc concentrates are obtained by dead roasting of zinc sulfide concentrates in a fluidized bed reactor (15,16). Natural zinc oxide ores are zinc carbonates and hemimorphites which are directly obtained as natural ores (17,18). Arc furnace steelmaking dusts contain zinc oxide which forms from the vapors produced during the process (19-21). However, in this work, the roasted zinc concentrates are considered, due to the interest of Noranda's Canadian Electrolytic Zinc [CEZ].

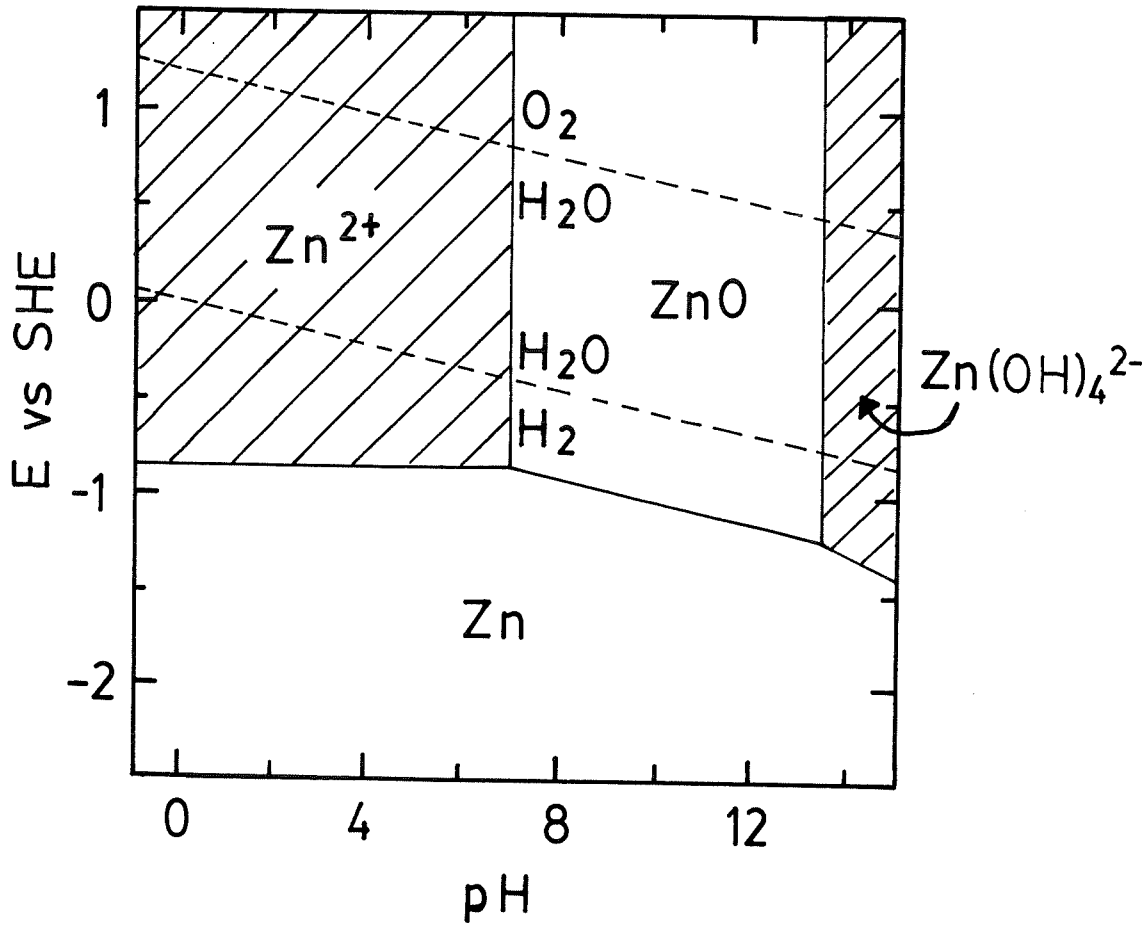

Figure 1.1 E-pH diagram for the zinc-water system.

CEZ uses the roasted zinc concentrates to produce zinc metal, which are produced by dead roasting zinc sulfide concentrates in a fluidized bed reactor. Zinc sulfide concentrates normally contain approximately 10 to 15 % iron, and when roasted, all of the iron is transformed into zinc ferrite $ZnFe_2O_4$, while the remaining zinc is converted to the zinc oxide ZnO (15,22,23). As the iron occurs in the original concentrates as marmatitic sphalerite (Zn,Fe)S, in which it is present as a solid solution in the zinc sulfide, the ferrite formation is almost complete during roasting (15,22-24).

However, no results have been published on the kinetics of alkaline leaching of roasted zinc concentrates, even though some practical tests were carried out in the pilot plant stage (25,26). In order to understand the leaching kinetics of roasted zinc concentrates, pure zinc oxide is first studied as a simple system. The effect of zinc ferrite is then studied, using roasted zinc concentrates and a sintered mixture of pure zinc oxide and hematite.

The objective of this project is to understand the kinetics of alkaline leaching of zinc oxide. In order to achieve this objective, this project consists of three parts.

In part one, the kinetics of alkaline leaching of pure zinc oxide are studied, using a low concentration of the particles. Two different rate-determining steps have been proposed in the dissolution of pure zinc oxide in alkaline solution. These have been

described as the surface reaction (27) or the diffusion process (28). Table 1.1 is a comparison of the experimental conditions of the present and previous works. As seen in this table, the disagreement on the dissolution mechanismstill exists. A through study was then required to elucidate the dissolution mechanism.

Part two is the study of the kinetics of alkaline leaching of roasted zinc concentrates, using low particle concentrations, which has not been published in a literature.

Part three is the study of the variables of the leaching process using high particle concentration to economize energy consumption. The production capacity of the unit depends directly on the particle concentration for commercial applications of the leaching reactor. Thus, such information is useful for designing and optimizing the leaching reactor.

A mechanically-agitated reactor was therefore constructed, and various experiments were carried out as a function of temperature, agitation speed, particle size and NaOH concentration. A centrifuge was used to obtain only a pregnant solution from the particle-liquid mixture, and the concentration of zinc ions in the pregnant solution was measured with an atomic absorption spectrophotometer.

Table 1.1 Comparison of the experimental conditions on dissolution of pure zinc oxide

	Rogers et al. (27)	Frenay (28)	This work
rds**	surface reaction	diffusion	surface reaction + diffusion
experimental method	mechanical agitation	rotating disk	mechanical agitation
reactor	no baffle	no baffle	baffle
C(M)	1 - 5	6	4 - 10
N(rpm)	1150	50 - 200	300 - 900
$d_0(\mu m)$	75-150		20-38, 38-63, 75-150, 180-355
$S_o^*(m^2/g)$	0.053		0.11
sample	double sintered pure ZnO particle	pressed pure ZnO disk	single sintered pure ZnO particle
T(K)	273 - 333	298	298 - 343

** rate-determining step

* Specific surface area of roasted zinc concentrates is 0.66 m^2/g for 75-150 μm.

CHAPTER 2

LITERATURE REVIEW

2.1 INTRODUCTION

Leaching is the process of dissolution of a valuable mineral from an ore or a concentrate using an aqueous solvent (12,29). The leaching process is therefore characterized by the reaction at the interface between particles and solution, generally carried out in a mechanically-agitated reactors (30-32). The main reasons (30,33) for using mechanical agitation are: 1) to promote the suspension of particles in the solution, 2) to promote the mass transfer process. Thus, in the leaching process using mechanical agitation, particles must be suspended in order to provide a large active surface area for the reaction.

As dissolution proceeds, the active part of each particle shrinks in size, the total surface area for the leaching reaction diminishes, and the overall rate of dissolution is reduced. This process can be analyzed using the shrinking core model (34-44).

The literature review therefore focuses on the following areas: the shrinking core model and the suspension of particles.

2.2 THE SHRINKING CORE MODEL

This model was first developed by Yagi and Kunii (36), who visualized five steps occurring in succession during a reaction in a gas-solid system. These five steps are as follows:

Step 1, diffusion of the gaseous reactant through the gas film surrounding the particle to the surface of the particle.

Step 2, diffusion of the reactant through the porous layer of reaction product to the surface of the unreacted core.

Step 3, reaction of the gaseous reactant with the particle at this reaction surface.

Step 4, diffusion of the gaseous product through the porous layer of reaction product back to the exterior surface of the particle.

Step 5. diffusion of the gaseous product through the gas film back into the main body of fluid.

In developing the kinetic equations for these steps, the surrounding fluid is, for convenience, considered to be a gas, but this analysis applies equally well to liquids (36-39). Thus, this model is applied to a particle-solution system.

Mathematical rate expressions for the model were developed based on diffusion control through the liquid boundary layer or through the solid product layer, on surface

reaction control at the particle surface, and on a combination of these.

At times some of these steps do not exist. For example, if no solid product layer is formed, Steps 2 and 4 do not contribute to the resistance to the reaction. Also, the resistance of the different steps usually vary greatly. In such cases the step with the highest resistance is considered to be a rate-determining step.

In the dissolution of pure zinc oxide in NaOH solution, the particles shrinks during the reaction, and finally disappear. Figure 2.1.a represents the shrinking particle. The reaction steps are as follows:

Step 1, diffusion of reactant OH^- through the liquid boundary layer, i.e., the liquid film surrounding the particle, to the surface of the particle.

Step 2, reaction of OH^- with the particle at this reaction surface.

Step 3, diffusion of product, zincate $Zn(OH)_4^{2-}$, through the liquid boundary layer back into the bulk of the electrolyte.

In roasted zinc concentrates, the particles remain unchanged in size even if the active part of the particle shrinks. Figure 2.1.b represents the shrinking core model. The steps are:

Step 1, diffusion of the reactant OH^- through the liquid boundary layer surrounding the particle to the surface of the particle.

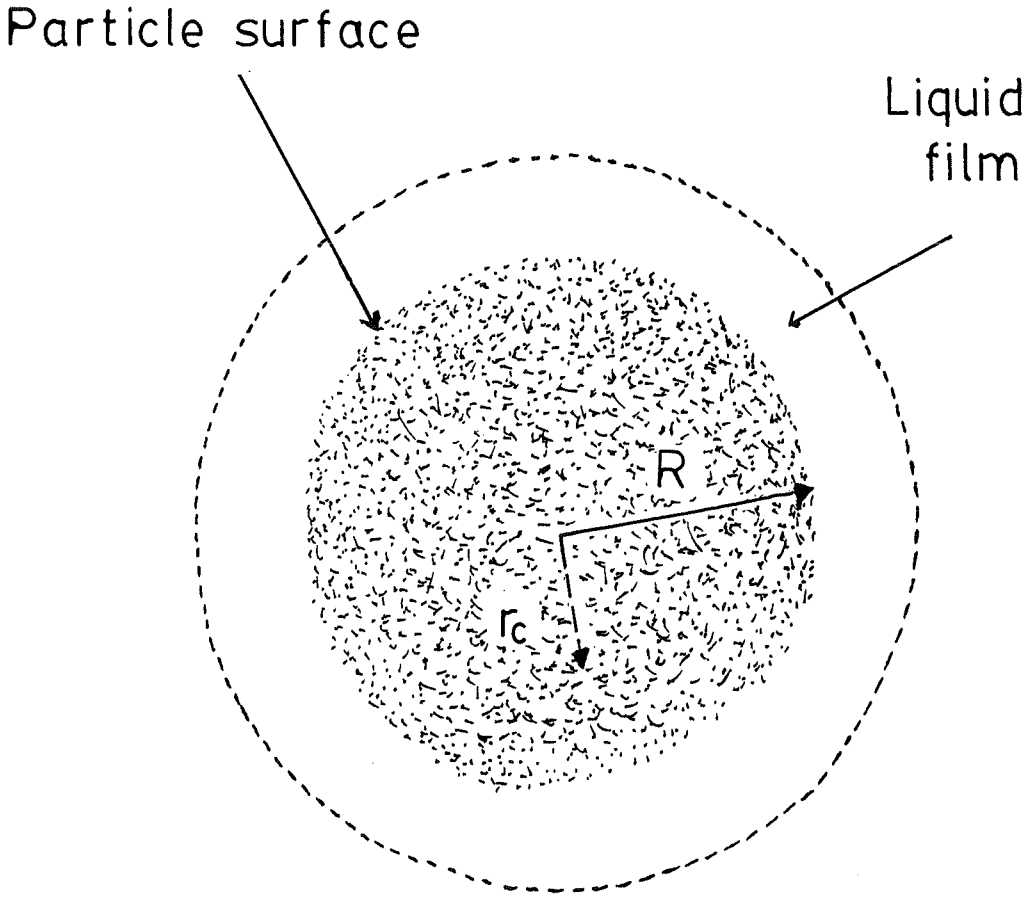

Figure 2.1.a Shrinking particle model of the dissolution of particles in the solution

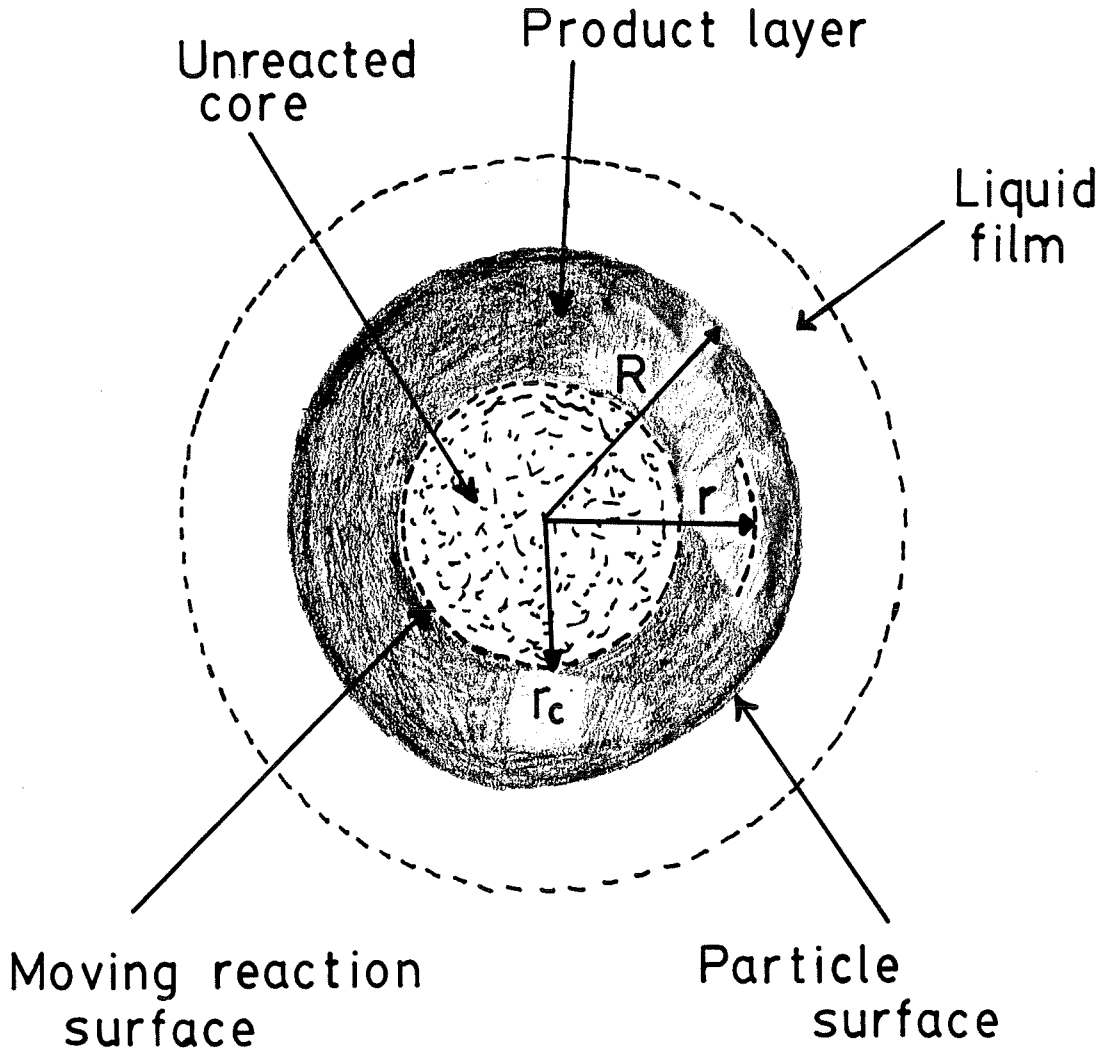

Figure 2.1.b Shrinking core model of the dissolution of particles in the solution

Step 2, diffusion of the reactant OH^- through the porous solid layer to the surface of the unreacted core of the particle.

Step 3, reaction of the reactant OH^- with the particle at this reaction surface.

Step 4, diffusion of the product, zincate $Zn(OH)_4^{2-}$, through the porous solid layer to the exterior surface of the particle.

Step 5, diffusion of the product through the liquid boundary layer back into the bulk of the electrolyte.

2.2.1 Dissolution of Pure Zinc Oxide

Two types of general rate equations for leaching are available: dW/dt and dn/dt. W and n are the weight and the number of mole of particles, respectively, and t is time. In the rate expression dW/dt, the rate constant includes molecular weight, which is not expressed in the formula. In dn/dt, the rate constant includes molecular weight in the formula, but in the experimental results, the leaching rate is expressed by weight ratio, i.e., the fraction reacted (α) = W/W_o. W and W_o represent the dissolved and initial weight of particles, respectively. Therefore, the rate expressions were obtained by combining two equations, and the rate equations were deduced for convenience.

As a result of the existence of a boundary layer, the leaching reaction can be diffusion-controlled, surface-reaction-controlled, or mixed-controlled, depending on the slowest step.

2.2.1.1 Diffusion through Boundary Layer

A particle, originally of size R, has shrunk to size r_c.

$$\frac{dW}{dt} = - k_1 M \sigma 4\pi r_c^2 (C - C_i) \qquad (2.1)$$

where: C is the reactant concentration in the bulk

C_i is the reactant concentration at the surface of the particle

k_l is the mass transfer coefficient

M is the molecular weight

r_c is the radius of the particle at time t

t is time

W is particle weight

σ is a stoichiometric factor

Whenever the resistance to diffusion through the boundary layer controls the rate, no reactant is present at the surface of the particle; hence the concentration driving force, given by C - C_i, is therefore constant at all times during the reaction of the particle.

$$W = \frac{4}{3}\pi r_c^3 \rho \qquad (2.2)$$

where: ρ is particle density

The differentiation of Equation (2.2) gives:

$$\frac{dW}{dt} = 4\pi\, r_c^2\, \rho\, \frac{dr_c}{dt}$$

From Equations (2.1) and (2.3),

$$-\, k_1\, M\, \sigma\, C = \rho \frac{dr_c}{dt} \qquad (2.4)$$

The integration of Equation (2.4) gives:

$$\rho R[(\frac{r_c}{R})-1] = -\, k_1\, M\, \sigma\, C\, t \qquad (2.5)$$

The fraction reacted, α, can be obtained as follows:

$$\alpha = \frac{W - W_{r_c}}{W_R} = \frac{R^3 - r_c^3}{R^3} = 1 - (\frac{r_c}{R})^3 \qquad (2.6)$$

$$\therefore \quad \frac{r_c}{R} = (1-\alpha)^{\frac{1}{3}} \qquad (2.7)$$

From Equations (2.5) and (2.7), a rate expression in terms of the fraction reacted, α, is obtained as follows:

$$1 - (1 - \alpha)^{\frac{1}{3}} = \frac{k_1 M \sigma C}{\rho R} t = K_1 t \qquad (2.8)$$

The plot of $1 - (1 - \alpha)^{1/3}$ against t should give a straight line. In this case, the reaction rate is controlled by diffusion through the liquid boundary layer.

2.2.1.2 Surface Reaction

The quantity of material reacted is proportional to the available surface of the unreacted core of the particle.

$$\frac{dW}{dt} = - k_c M \sigma 4\pi r_c^2 C \qquad (2.9)$$

where: k_c is a chemical rate constant

From Equations (2.3) and (2.9),

$$k_c M \sigma C = - \rho \frac{dr_c}{dt} \qquad (2.10)$$

Integrating Equation (2.10) gives:

$$\rho R[(\frac{r_c}{R})-1] = - k_c M \sigma C t \qquad (2.11)$$

From Equations (2.7) and (2.11), a rate expression in terms of the fraction reacted, α, is obtained as follows:

$$1 - (1 - \alpha)^{\frac{1}{3}} = \frac{k_c M \sigma C}{\rho R} t = K_2 t \qquad (2.12)$$

The plot of $1 - (1 - \alpha)^{1/3}$ against t should give a straight line. In this case, the reaction rate is controlled by the surface reaction at the surface of the particle.

2.2.1.3 Mixed Control

The general case in hydrometallurgical systems treating industrial mineral particles, such as in the agitating leaching process, would have a mixed control by diffusion and the surface reaction.

If the rate of the surface reaction at the interface is much faster than the rate of the diffusion through the liquid layer to the interface, the general equation for the leaching reaction is as follows:

$$\frac{dW}{dt} = - k_1 M \sigma S (C - C_i) \qquad (2.13)$$

If the rate of the surface reaction is much slower than that of diffusion, the general equation is as follows:

$$\frac{dW}{dt} = - k_c M \sigma S C_i \qquad (2.14)$$

In the intermediate-control, both rates are the same. From Equations (2.13) and (2.14),

$$C_i = \frac{k_1}{k_1 + k_c} C \qquad (2.15)$$

Substituting Equation (2.15) into Equation (2.14),

$$\frac{dW}{dt} = - M \sigma S C \frac{k_1 k_c}{k_1 + k_c} = - k_n M \sigma S C \qquad (2.16)$$

Thus, when $k_i << k_c$, the process is diffusion-controlled, and when $k_i >> k_c$, the process is surface-reaction-controlled. Therefore, the individual resistance can be combined directly to give a total resistance. Equation (2.16) is the same formula as Equations (2.1) and (2.9). The integration of Equation (2.16) therefore leads to the same formula as Equations (2.8) and (2.12).

2.2.2 Distinction between Diffusion Control and Surface Reaction Control

As studied in sections 2.2.1.1 to 2.2.1.3, it is not possible from the kinetics alone to determine the rate-determining step, since the shrinking particle model has the same mathematical form for surface reaction control and boundary layer diffusion control when a solid product layer is not formed. If the leaching rate is dependent both on the agitation speed and on temperature, the rate-determining step is a combination of the two. Therefore, the effect of temperature and agitation speed on the observed kinetics must be separately evaluated to distinguish between the two.

2.2.2.1 Temperature

A diffusion-controlled process is characterized by being slightly dependent on temperature, while a chemical-reaction-controlled process is strongly dependent on temperature. The activation energy of the diffusion-controlled process is therefore characterized as being 1 to 3 kcal/mol, while for the surface-reaction-controlled process it is usually greater than 10 kcal/mol (35). Therefore, in this situation, the activation energy must be obtained to determine whether diffusion or the surface reaction is the rate-determining step.

2.2.2.2 Agitation Speed

When the stirring rate is increased in a solid-liquid reaction, an increase in the dissolution rate takes place when particles were suspended. This is the case when the

leaching process is diffusion-controlled through the boundary layer, because such a process follows the rate law:

$$\frac{dW}{dt} = \frac{D_d}{\delta} M \sigma S C \qquad (2.17)$$

Since the thickness of the boundary layer, δ, decreases with increasing agitation speed, the rate of dissolution increases as a consequence. However, the surface-reaction-controlled process is independent of the agitation speed.

2.2.3 Dissolution of Roasted Zinc Concentrates

In this case, all of the steps of the dissolution mechanisms may contribute to the resistance to the reaction. The particle therefore remains unchanged in size even though the active part of the particle reduces.

2.2.3.1 Diffusion through the Boundary Layer

$$\frac{dW}{dt} = - k_2 M \sigma 4\pi R^2 (C - C_i) \qquad (2.18)$$

where: k_2 is the mass transfer coefficient

Whenever the resistance to diffusion through the boundary layer controls the leaching rate, no reactant is present at the particle surface; hence the concentration driving force, given by $C - C_i$, is therefore constant at all times during the reaction of the particle.

From Equations (2.3) and (2.18),

$$M \sigma R^2 k_2 C = - r_c^2 \rho \frac{dr_c}{dt} \qquad (2.19)$$

The integration of Equation (2.19) gives:

$$\frac{\rho R}{3} [(\frac{r_c}{R})^3 - 1] = - k_2 M \sigma C t \qquad (2.20)$$

From Equations (2.7) and (2.20), a rate expression in terms of the fraction reacted, α, is obtained as follows:

$$\alpha = \frac{3 k_2 M \sigma C}{\rho R} t = K_3 t \qquad (2.21)$$

The plot of α against t should give a straight line. In this case, the reaction rate is controlled by the boundary layer.

2.2.3.2 Diffusion through the Solid Layer

To develop a rate expression between a reaction time and the radius of the particle, a two-step analysis is required: first, we examine a typical partially-reacted particle, writing the flux relationships for this condition. We then apply this relationship for all values of r_c; that is, we integrate r_c between R and 0.

Both reactants, i.e., lixiviant and the boundary of the unreacted core, move inward toward the center of the particle, and the reaction rate of the reactant at any instant is given by its rate of diffusion to the surface of the particle.

$$-\frac{dW}{dt} = M\,\sigma\,4\pi r^2\,Q = M\,\sigma\,4\pi r^2\,D_e\,\frac{dC}{dr} \qquad (2.22)$$

where: D_e is the effective diffusion coefficient

Q is the flux of materials

r is the radius of the particles

Integration across the solid layer from R to r_c gives:

$$- \frac{dW}{dt}\left(\frac{1}{r_c} - \frac{1}{R}\right) = 4\pi M \sigma D_e (C - C_i) \qquad (2.23)$$

Whenever the resistance to diffusion through the solid layer controls the leaching rate, no reactant is present at the particle surface; hence the concentration driving force, given by C - C_i, is therefore constant at all the times during the reaction of particle.

From Equations (2.3) and (2.23),

$$- r_c^2 \rho \frac{dr_c}{dt}\left(\frac{1}{r_c} - \frac{1}{R}\right) = M \sigma D_e C \qquad (2.24)$$

Integrating Equation (2.24) gives:

$$- \rho \int_R^{r_c} \left(r_c - \frac{r_c^2}{R}\right) dr_c = M \sigma D_e C \int_0^t dt \qquad (2.25)$$

$$\therefore \quad - \frac{\rho R^2}{6}\left[3\left(\frac{r_c}{R}\right)^2 - 2\left(\frac{r_c}{R}\right)^3 - 1\right] = M \sigma D_e C t \qquad (2.26)$$

From Equations (2.7) and (2.26), a rate expression in terms of the fraction reacted, α, is obtained as follows:

$$1 - \frac{2}{3}\alpha - (1-\alpha)^{\frac{2}{3}} = \frac{2 M \sigma D_e C}{\rho R^2} t = K_4 t \qquad (2.27)$$

The plot of 1 - 2/3 α - (1 - α)$^{2/3}$ against t should give a straight line. In this case, the rate-determining step is diffusion through the solid layer.

2.2.3.3 Surface Reaction

When the surface reaction controls the leaching rate, the result is the same as when no solid product layer is formed, because the progress of the reaction is unaffected by the presence of a reaction product layer. Thus, the quantity of material reacted is proportional to the available surface of the unreacted core of the particle.

$$1 - (1 - \alpha)^{\frac{1}{3}} = \frac{k_c M \sigma C}{\rho R} t = K_2 t \qquad (2.12)$$

2.2.4 Combination of Resistance

In hydrometallurgical systems treating industrial mineral particles such as in the agitating leaching process, the relative importance of the controlling mechanisms will vary as conversion progresses.

If diffusion through the solid layer controls the leaching rate, normally the resistance of the boundary layer is negligible as compared with the resistance through the solid layer; the leaching process is then controlled by the rate of the diffusion through the solid layer. The kinetics of the reaction may be governed by the porous or nonporous character of the solid product layer (35). If it is porous, the rate will not be affected by

the solid product layer, but if it is nonporous, the reagent has to diffuse through the solid product layer, and the kinetics will therefore be markedly different. As can be seen in section 2.2.2.2, we can determine if diffusion through the boundary layer constitutes the rate-determining step by examining the effect of agitation speed on the leaching rate.

To account for the simultaneous action of these resistances is straightforward since they act in series and are all linear in the concentration of the solution.

If the rate of the surface reaction is faster than the rate of diffusion through the solid layer, the general equation for the leaching reaction is obtained as follows:

$$- \frac{dW}{dt} \left(\frac{1}{r_c} - \frac{1}{R}\right) = 4\pi M \sigma D_e (C - C_i) \qquad (2.28)$$

If the rate of the surface reaction is much slower than the rate of diffusion through the solid layer, the general equation is:

$$- \frac{dW}{dt} = k_c M \sigma 4\pi r_c^2 C_i \qquad (2.29)$$

Substituting Equation (2.29) into Equation (2.28) to eliminate C_i gives:

$$-\frac{dW}{dt}\left(\frac{1}{r_c}-\frac{1}{R}+\frac{D_e}{k_c r_c}\right)=4\pi M\sigma D_e C \qquad (2.30)$$

From Equations (2.3) and (2.7), the following equation can be obtained:

$$\frac{dW}{dt}=-\frac{4\pi R^2 \rho}{3}\frac{d\alpha}{dt} \qquad (2.31)$$

Substituting Equations (2.7) and (2.31) into Equation (2.30) gives:

$$\frac{d\alpha}{dt}\left[R\left(\frac{1}{(1-\alpha)^{1/3}}-1\right)+\frac{D_e}{K_c}\frac{1}{(1-\alpha)^{2/3}}\right]=\frac{3 M\sigma D_e C}{R\rho} \qquad (2.32)$$

Integrating Equation (2.32) yields:

$$R\int_0^{\alpha}\left[\frac{1}{(1-\alpha)^{1/3}}-1\right]d\alpha+\frac{D_e}{k_c}\int_0^{\alpha}\frac{1}{(1-\alpha)^{2/3}}d\alpha=\int_0^{t}\frac{3 M\sigma D_e C}{R\rho}c$$

Therefore,

$$\left[1-\frac{2}{3}\alpha-(1-\alpha)^{2/3}\right]+\frac{2D_e}{R k_c}\left[1-(1-\alpha)^{1/3}\right]=\frac{2M\sigma D_e C}{R^2\rho}t \qquad (2.33)$$

It is evident from Equation (2.33) that the integral form simply includes the sum of the expression for two types of controls. The plot of the left side of Equation (2.33) against t should give a straight line if the leaching rate is controlled by the combination of two rate-determining steps at the same time throughout the reaction.

2.3 SUSPENSION OF PARTICLES

The dissolution of particles in a liquid is facilitated by suspending the particles in a fluid stream as a dispersion with a high interfacial area between the reactants.

Some principles of efficient contact in the continuous flow of the dispersed-phase may be seen from the relationship as follows (45):

$$A = \frac{6\,H}{d} \qquad (2.34)$$

where: A is the interfacial area per unit volume between particles and solution

d is particle diameter

H is fractional volumetric hold-up of particles

The interfacial area may be increased by increasing the hold-up of particles and/or reducing the diameter of the particles. This argument then favors the use of fine-grained dispersions.

2.3.1 Criterion of Complete Suspension

Many particle suspension investigators (46-50) have used visual observation to

determine how well the particles in a reactor are suspended in the liquid. The criterion for complete suspension is that no particles should remain on the bottom of the reactor more than 1 second. This criterion can be determined by observing the particles on the reactor bottom with a mirror placed beneath the reactor (46,50).

2.3.2 Particle Suspension Correlations

Zwietering (50) used dimensional analysis to determine suitable dimensionless groups for analyzing his experimental data, which used baffles and high concentration of particles ranging from 0.5 to 20 wt%. The minimum agitation speed (N_s) for complete suspension (50) was related to other system parameters by the following equation:

$$N_s = \frac{s\,\nu^{0.1}\,d^{0.2}\,\left(\frac{g\,\Delta\rho}{\rho}\right)^{0.45}\,X^{0.13}}{D^{0.85}} \qquad (2.35)$$

where: d is particle diameter

D is agitator diameter

s is a dimensionless constant which is a function of D/D_T and h/D_T

X is concentration of particles

ν is kinematic viscosity

$\Delta\rho$ is density difference between particle and solution

ρ is density of particles

The exponents of ν, d, $(g\ \Delta\rho)/\rho$, X and D were found to be independent of impeller type, vessel size, clearance ratio (h/D_T) and impeller-to-reactor diameter ratio (D/D_T) (51). Equation (2.35), generally adopted for the systems of particle suspension is used for an estimation of N_s, and has been verified by other studies (30,49,51). The use of this equation to calculate N_s has been especially recommended for propellers and 45° pitched-blade turbines (51).

The following phenomena can be expected from Equation (2.35), because N_s is a function of the following parameters. First, an increase in N_s is expected as particle diameter increases since a higher settling velocity should require a higher liquid velocity to suspend the particles. Second, since an increase in particle-fluid density difference increases the particle settling velocity, its increase increases N_s. Third, increasing particle concentration increases N_s when interference between particles is not significant.

The kinematic viscosity of the liquid was increased from 10^{-6} to 5×10^{-6} m^2s^{-1} using a sugar solution, but no significant effect on N_s was observed. This is because N_s is insensitive on the kinematic viscosity of the liquid as seen in Equation (2.35). The configuration used was that for which Baldi (46) predicted N_s to be independent of viscosity, though Zwietering (50) found a very weak dependence.

2.3.3 Variables Which Affect the Suspension of Particles

The effects of various variables are valid for the range of equipment and system parameters on which they were based, so that a divergence in the effect of variables on N_s can occur. However, although the results of different investigators for N_s do not agree well, some general information is available. Figure 2.2 illustrates the variable dimensions of the agitated reactor.

2.3.3.1 Clearance Ratio (h/D_T)

The agitation speed, N_s, strongly depends on the clearance ratio. A decrease in the agitation speed can be obtained by decreasing the clearance ratio. The agitation speed decreases as the clearance ratio decreases between a turbine with disk-supported blades and the flat bottom of a baffled cylindrical vessel (46,47,49).

It is clear that the flow pattern is more sensitive to the clearance ratio (49). For an impeller with six disk-supported blades, the flow pattern had a strong horizontal stream at mid-elevation of the impeller blades. When $h/D_T > 1/5$, the stream split into two parts at the reactor wall, one flowing up and the other down. The latter stream then turned inward along the bottom of the reactor and returned to the suction side of the impeller. At $h/D_T < 1/6$, all of the impeller discharge stream sloped down to the bottom of the reactor before it reached the cylindrical wall, where it turned up. For this type of flow pattern, N_s was lower than that for the $h/D_T > 1/5$ flow pattern.

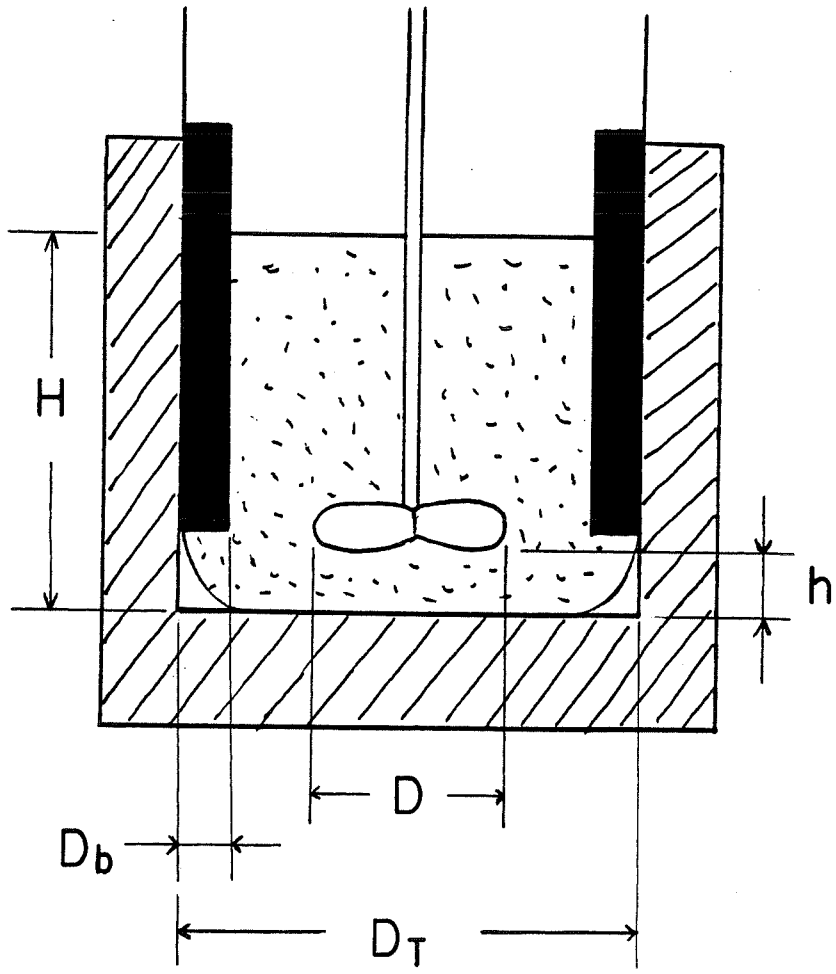

Figure 2.2 Schematic diagram of variables which affect the suspension of particles

2.3.3.2 Impeller-to-Reactor Diameter Ratio (D/D_T)

A maximum diameter of an impeller is reached when the annular free space between impeller tip and wall becomes too restricted to permit free flow of the rising impeller stream to a vertical direction with minimum velocity loss due to impingement on the wall surface (52). In the particle suspension, there is usually an optimum D/D_T ratio which is a function of the percent particle, settling velocity and process criterion.

2.3.3.3 Liquid Height-to-Reactor Diameter Ratio (H/D_T)

The ratio of liquid height to reactor diameter should be selected on the basis of the height of the circulation pattern. Axial flow impellers provide an unidirectional vertical pattern which is not suitable for slurry mixing in tall vertical tanks, because more power is required by axial flow turbine than radial flow turbine to obtain satisfactory suspension (52).

The optimum H/D_T ratio for particle suspension is normally about 0.6 to 0.7 with a single impeller. When H/D_T ratios get much higher than this, the power requirement increases dramatically with a single impeller.

2.3.4 Effect of Baffle

If a low-viscosity liquid is stirred in an unbaffled tank by an axially mounted agitator, there is tendency for a swirling flow pattern to develop, regardless of the type

of impeller. In other words, the formation of a vortex in a mechanically-agitated unbaffled reactor is inevitable. This phenomenon is explained in Figure 2-3-a (53).

A vortex is produced by a centrifugal force acting on the rotating liquid. Vertical velocities in a vortexing low-viscosity liquid are low relative to circumferential velocities in the reactor. The swirl inhibits the production of a uniform concentration of the particles. Moreover, the onset of air entrainment is observed when a critical vortex depth is reached (35,54).

It is obvious that an increase of the impeller speed results in deeper vortices. Moreover, the relative vortex depth may be considerably increased if an impeller of a relatively larger diameter is employed (54). However, the relative vortex depth decreases with increasing reactor size and/or with decreasing impeller clearance (54,55).

Baffling makes the flow direct vertically and prevents the particle size classification that results from an uncontrolled swirl. The use of baffles results in a large top-to-bottom circulation without vortexing (53). This phenomenon is shown in Figure 2-3-b. As stirrer speed is further increased and suspension becomes complete, baffled vessels establish an increasing superiority.

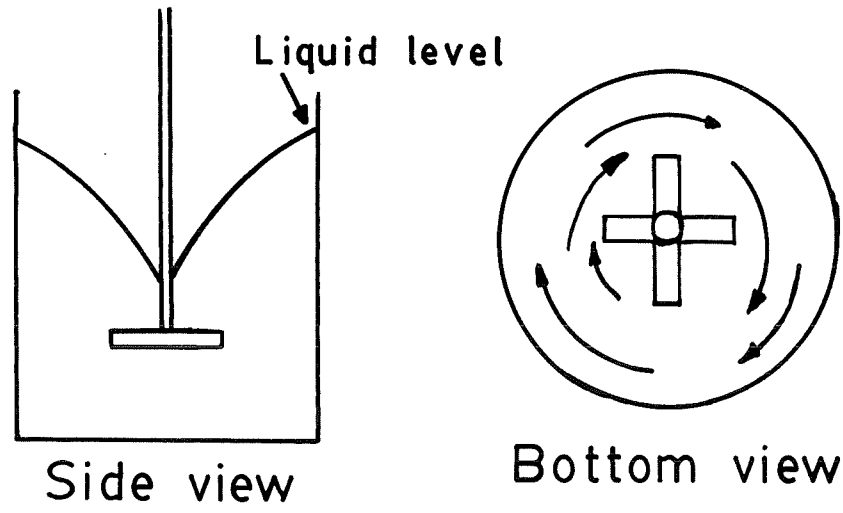

a) unbaffled reactor

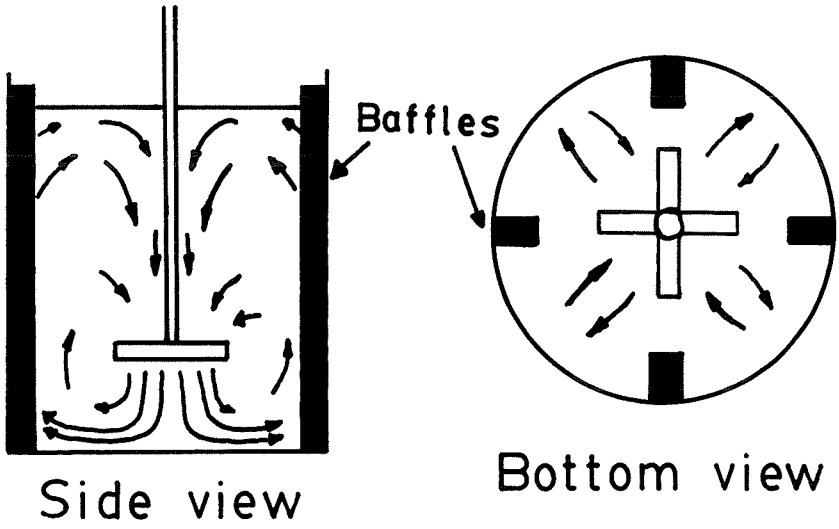

b) baffled reactor

Figure 2.3 Flow pattern of the leaching reactor

2.3.5 Particle Distribution in Complete Suspension

In the majority of cases of particle suspensions, the biggest variation in particle concentration in the agitated liquid is in the axial direction, and a peak in the particle concentration occurs at the agitation speed, N_s for complete suspension (56). Moreover, the concentration of the particles increases nearly exponentially with the liquid depth from a region just below the liquid surface.

2.3.6 Mass Transfer in Mechanically-Agitated Reactor

Rotating impellers are also used to promote the transfer of dissolved molecules to or from the surface of the particles in a leaching process. The rate of transfer of molecules between the surface of the suspended particles and the bulk of the liquid phase is limited by turbulent diffusion (46).

Mass transfer from the suspended particles in mechanically-agitated reactors has been explained by slip-velocity theory (57-61). It implies that the coefficient is related to that which could be obtained if the particle moved at its terminal velocity.

Mass transfer to fixed spheres submerged in flowing fluid is usually described by the equation of Rantz and Marshall.

$$Sh = 2 + 0.6\, Re^{1/2}\, Sc^{1/3} \qquad (2.36)$$

where: Sh is Sherwood number, $k_s d/D_d$

Re is Reynolds number, $dv_s\rho_f/\mu$

Sc is Schmidt number, $\mu/\rho_f D_d$

k_s is mass transfer coefficient obtained from slip velocity

d is diameter of particle

D_d is diffusion coefficient

v_s is slip velocity

ρ_f is density of solution

μ is viscosity

The above equation correlates mass transfer data well over a range of Reynolds numbers and it has gained widespread acceptance in the literature (60-62).

The Reynolds number requires a knowledge of the slip velocity of the particles, which is the velocity of the fluid relative to the particle. Even though the slip velocity can not be obtained, it can be replaced by the free-falling terminal velocity of a particle. However, if the terminal velocity is used to calculate the Reynolds number, Equation (2.36) gives the minimum value to be expected for the transfer coefficient for suspended particles.

Harriot (51,59) therefore recommended the following method of predicting the mass transfer coefficient for particles suspended in a baffled tank:

First, calculate the free-falling terminal velocity and the corresponding Reynolds number based on the particle diameter.

Second, calculate the mass transfer coefficient for free-falling particles, k_t, from Equation (2.36) by replacing k_s into k_t.

Third, get an approximate k_s by multiplying k_t by 2.

CHAPTER 3

EXPERIMENTAL

3.1 APPARATUS

The reaction system used in the leaching experiments (Figure 3.1) consists of a two-liter pyrex reaction flask (Corning No. 6947) partially immersed in a heating mantle. The flask was fitted with a pyrex glass lid with ports to permit access for periodic sampling, temperature measurement, stirring and condenser placement. A mercury thermometer was used to measure the temperature of the NaOH solution. A reflux condenser inserted in one port kept vapor losses of the solution to a minimum. The stirrer is a four-blade axial flow turbine, with a 45 ° angle, driven by a variable speed motor. The standard baffle was principally used.

3.2 ELECTROLYTE SOLUTION

Experiments were performed with solutions of NaOH and KOH (6). KOH solution is more conductive than NaOH solution. The specific energy to produce zinc from the electrowinning in the NaOH solution is 1.75 kWh/kg, while that in the KOH solution is 1.69 kWh/kg (at 1000 A/m^2, 348 K and with 2.5 cm between electrodes). The diminution of 0.06 kwh/kg is then obtained using the KOH solution, but since the price of KOH is approximately twice that of NaOH, NaOH was chosen as the electrolyte.

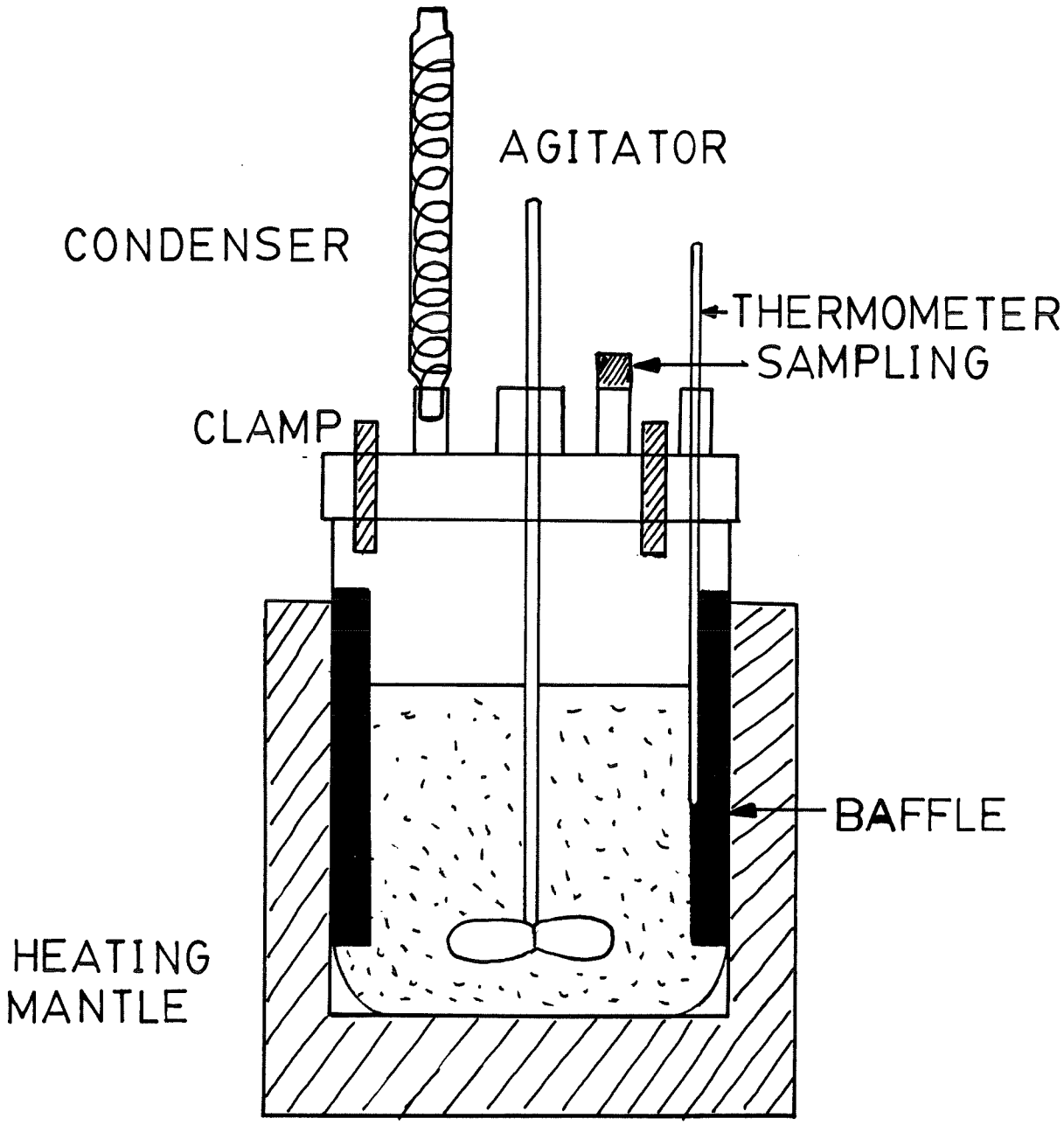

Figure 3.1 Schematic diagram of the experimental apparatus

3.3 MATERIALS

Four kinds of zinc oxide were used for these experiments: pure zinc oxide, sintered pure zinc oxide, a sintered mixture of zinc oxide and hematite, and roasted zinc concentrates. Table 3.1 shows different particle sizes of three kinds of zinc oxides prior to the leaching reaction.

3.3.1 Pure Zinc Oxide

The reagent grade zinc oxide (Fisher) is manufactured by vaporizing and oxidizing a high grade zinc metal. These oxides have a high chemical purity (99.9 %) and a fine particle size. Their specific surface area ranges from 3 to 5 m^2/g, which is equivalent to an average spherical diameter of 0.5 μm (62). The SEM in Figure 3.2 illustrates the porous morphology of reagent grade pure zinc oxide. The portion of desired size of the pure zinc oxide was obtained with a laboratory test sieve ASTM E 11. These particles are fragile.

3.3.2 Sintered Pure Zinc Oxide

Because the reagent grade zinc oxide particles dissolved very quickly due to their large specific surface area, larger particles were needed in order to study the kinetics of the leaching process and to correspond to the typical particle size used in the industrial process. The particles of reagent grade zinc oxide were therefore sintered. The amount

Table 3.1 Specific surface area measurements for three kinds of samples

d_o (μm)	S_o (m^2/g)
sintered pure ZnO	
+20-38	0.35
+38-63	0.18
+75-150	0.11
+180-355	0.05
sintered mixture of zinc oxide and hematite	
+38-45	0.93
+63-75	0.79
+75-150	0.38
+150-180	0.30
roasted zinc concentrates	
+20-38	2.90
+38-45	2.63
+45-63	2.21
+63-75	1.37
+75-150	0.66
as received*	2.18

* not classified with wet-screening

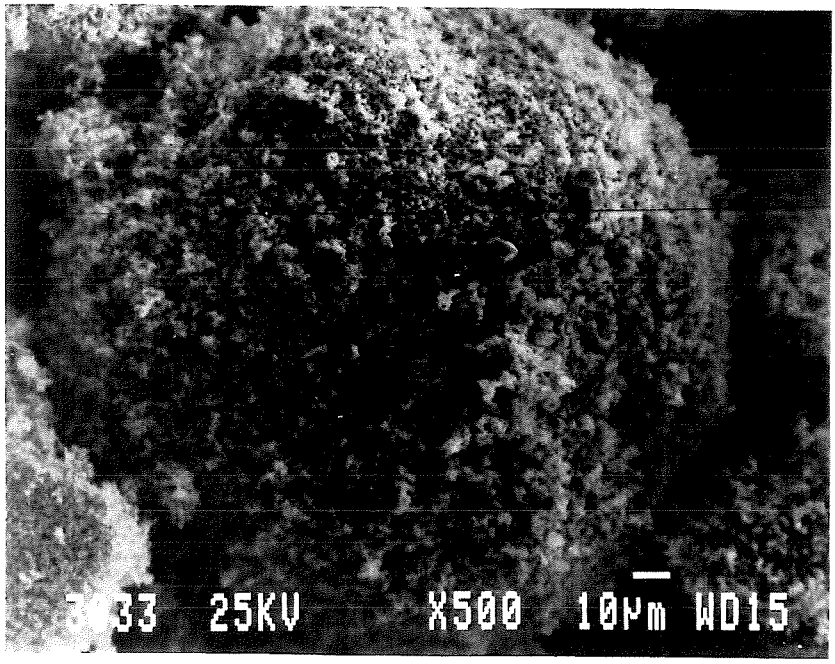

Figure 3.2 Morphology of reagent grade pure zinc oxide

of increase in grain size during sintering depends on sintering time and sintering temperature (28,63-67). When the sintering time and/or the sintering temperature increase, the grain size increases.

Large particles were obtained by sintering using the following process. In order to avoid the utilization of agglomerates, the - 38 μm portion of the reagent grade zinc oxide was collected as a base material for sintering. These powders were pressed at 3 tons (Fred S. Carver laboratory press) in a double-action steel die to form disk-shaped pellets 10 to 15 mm thick and 20 mm in diameter. A few drops of double-distilled water were mixed with the powders to improve cohesiveness. The resulting pellets were sintered in air at 1523 K for 50 hours in a pure magnesia crucible using an electric furnace. Samples were cooled to room temperature (by turning the furnace off and allowing it to cool for approximately 12 hours) and crushed in a pulverizer. These powders were wet-screened into closely-sized fractions for the dissolution experiments. The different size fractions were then dried in an oven at 383 K for 20 hours. The sizes of the sintered particles were matched with those of the roasted zinc concentrates used in CEZ, as seen in Table 3.1.

3.3.3 Sintered Mixture of Zinc Oxide and Hematite

In order to avoid the utilization of agglomerates, the - 38 μm portion of reagent grade zinc oxide and hematite (Fisher) was collected as a base material, because the solid-

state reaction for the formation of zinc ferrite is $ZnO + Fe_2O_3 \longrightarrow ZnFe_2O_4$. The two oxides were mixed with a weight ratio of 4 to 1 of zinc oxide and hematite, respectively, in order to correspond to the composition of the roasted zinc concentrates of CEZ.

Even though a greater amount of zinc ferrite formed as the contact between hematite and zinc oxide increased and the temperature increased, temperatures over 1573 K are not recommended, because of the volatility of ZnO (28,67). The ferrite formation proceeds at a relatively slow rate in the temperature range from 908 to 1053 K, because of the slow solid-solid reaction rate (68,69). However, both high temperatures and long periods (for example, more than 1 hour at 1573 K or 2 hours at 1473 K) may cause thermal decomposition of zinc ferrite and a decrease in the ratio of ferritization (28). The mixture was therefore sintered in air at 1373 K for 2 hours, using an electric furnace in order to form zinc ferrite and to correspond to the particle size of CEZ.

Samples were cooled to room temperature (by turning the furnace off and allowing it to cool for approximately 12 hours). After crushing the mixture, these powders were wet-screened into closely-sized fractions, which were then dried in an oven at 383 K for 20 hours. The sizes of the sintered particles were matched to those of the roasted zinc concentrates used in CEZ.

3.3.4 Roasted Zinc Concentrates

A new fluidized bed roaster has been installed at CEZ to roast zinc sulfide concentrates prior to conventional leaching (70). The roasted zinc concentrates of CEZ were wet-screened into closely-sized fractions. The different size fractions were then dried in an oven at 383 K for 20 hours.

3.4 ANALYSIS

Various experimental methods were carried out to study the kinetics of alkaline leaching. The general procedure of these experiments consists of various steps: surface area measurement of the particles, separation of a solid-liquid mixture, and ion concentration measurement of the leached solution.

3.4.1 Surface Area Measurement

The specific surface area of the particles was determined by a Flow Sorb II 2300 (Norcross, GA) BET adsorption technique, which has proven to be very reliable for powdered materials (71-74). This technique involves a determination of the quantity of gas necessary to form a monomolecular layer on the surface of the particles to be measured. The number of molecules required to form this layer may be evaluated, and since the area occupied by each molecule is known, the surface area of the material may be calculated.

The adsorption of nitrogen gas at the temperature of liquid nitrogen is generally used for the surface area measurement (71). The surface area of the zinc oxide particles was measured using the Flow Sorb II 2300. For a nitrogen and helium mixture of 30 vol.% nitrogen, the most favorable conditions for the formation of a monolayer of absorbed nitrogen are established at atmospheric pressure and the temperature of liquid nitrogen.

Calibration was accomplished with 1.0 cm^3 of nitrogen gas, corresponding to 2.84 m^2 of standard sample surface in the Flow Sorb. In this case, liquid nitrogen was used to set the absorbing temperature, and ambient conditions are 22°C and 760 mmHg (75).

The specific surface area of each particle size of the three kinds of zinc oxides which are mentioned in section 3.3 are listed in Table 3.1. As seen in this table, the specific surface area increases as the particle size decreases, regardless of the kinds of the particles.

3.4.2 Separation of Liquid-Solid Mixture

Normally NaOH solutions are so viscous that a solid-liquid mixture can not be separated through a filtration process. However, the mixture can be separated by a centrifugal process if the density difference between the solid and the liquid is sufficient (76,77). The particles are subjected to centrifugal forces which make them move

radially through the liquid.

If the centrifugal force is large enough to overcome the Brownian diffusion forces, it can settle very fine particles. High speed centrifuges are therefore used for separating colloidal suspensions and emulsions which would not separate under the action of gravitational field.

An experimental centrifuge was constructed in the electrometallurgical laboratory of the École Polytechnique de Montréal. The maximum speed of 1350 rpm was obtained by a motor. The rotating plate with four 45° angle rotor is illustrated in Figure 3.3. Various operating times from 1 to 5 minutes were used to obtain the optimum time for separating the mixture at each NaOH concentration. An optimum time of 3.5 minutes was obtained at each NaOH concentration.

To consider the effect of the operating time of the centrifuge on the leaching rate, two types of preliminary experiments were carried out. The first one is no-suspension experiments. Two samples were obtained under the same conditions: solution and mixture of solution-particles. The mixture was separated using the centrifuge for 3.5 minutes. The concentration of zinc ion (Zn(II)) of the two solutions was measured with a spectrophotometer. The second one is partial suspension. Two samples of the mixtures of solution-particles were obtained under the same conditions. The solution

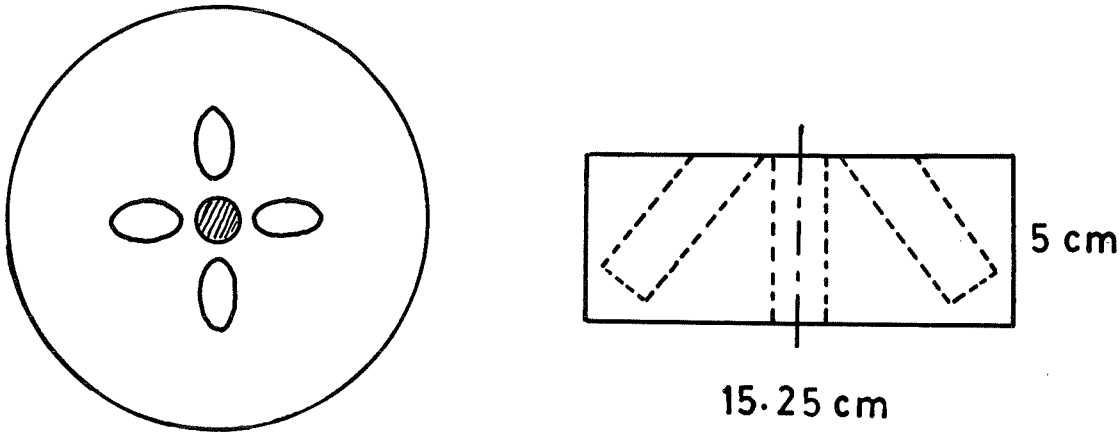

Figure 3.3 Schematic diagram of rotating plate with four 45° angle rotor of the experimental centrifuge

was separated with different operating times, 3.5 and 6 minutes. The concentration of zinc ion of the two solutions was measured with a spectrophotometer. Table 3.2 shows the results of the two experiments. As seen in this table, the effect of the operating time of the centrifuge on the leaching rate is negligible.

3.4.3 Ion Concentration Measurement

The concentration of the zinc ion (Zn(II)) and the ferric ion (Fe(III)) in the leached solution is measured with a Perkin-Elmer (Norwark, CT) AA 5000 atomic absorption spectrophotometer. Atomic absorption spectrophotometry may be defined as a method for determining the concentration of an element in a sample by measuring the absorption of radiation in atomic vapor produced from the sample at a wavelength that is specific and characteristic of the element under consideration (78,79). This method is rapid, simple and relatively precise compared to the time-consuming chemical method.

The development of this method depends on the improvement of producing gaseous atomic species of the test sample. The most convenient method of obtaining vapors of a particular element is to use a flame with some means of injecting it into a solution containing the element. When the concentration of the sample vapor increases, the increased partial pressure of the atom vapor will produce a broader resonance, with a corresponding reduction in absorption.

Table 3.2 Effect of the operating time of the centrifuge on the leaching rate (6 M, 328 K, 5 minutes)

experimental condition	(1) no-suspension (0 rpm)	(2) partial suspension (400 rpm)
sampling	(a) solution (b) solution + particles	solution + particles
operating time (minutes)	3.5	(c) 3.5 (d) 6
Zn(II) (g/l)	(a) 3.6 (b) 3.5	(c) 33.7 (d) 33.7

Calibration was accomplished with standard solution, which dissolves 0.500 g of zinc metal in 1 liter solution with 1 % HCl. The compositions of each metal element of the roasted zinc concentrates of CEZ and the sintered mixture at each particle size were determined by the atomic absorption spectrophotometer after dissolving the materials in a concentrated HCl solution at 383 K for 2 hours. Table 3.3 shows the result of chemical analysis of these materials.

The measurement of Zn(II) in the pregnant solution was carried out by the potential oscillation method (80,81) using a three electrode system (82-84). Potential oscillation of a zinc cathode immersed in an alkaline solution constitutes a new and interesting cyclic phenomenon which can be investigated by measuring oscillation period. However, the oscillation periods were erratic at higher zinc oxide concentrations ranging from 0.7 to 1.0 M zinc oxide and at high current densities ranging from 40 to 50 mA/cm^2. Thus, only the atomic absorption spectrophotometer was used to measure the zinc ion concentration of the pregnant solution, since the potential oscillation method must be further developed to be used in the measurement of zinc ion concentration.

3.5 SOLUBILITY OF ZINC OXIDE IN NaOH SOLUTION

The solubility of zinc oxide in sodium hydroxide solutions of various concentrations is in reasonable agreement with previous studies (18,19), from which

Table 3.3 Chemical analysis of particles

	Zn (%)	Fe (%)	Cd (%)	Cu (%)	Pb (%)	S (%)
sintered mixture of zinc oxide and hematite						
+38-45 μm	32.00	37.35				
+63-75 μm	40.50	30.40				
+75-150 μm	64.35	15.30				
+150-180 μm	66.00	12.00				
roasted zinc concentrates						
+20-38 μm	57.60	13.60	0.16	0.71	0.69	2.25
+38-45 μm	58.10	13.30	0.15	0.66	0.65	2.05
+45-63 μm	58.80	12.35	0.15	0.68	0.66	2.05
+63-75 μm	58.30	10.80	0.16	0.69	0.67	2.15
+75-150 μm	62.30	10.80	0.15	0.67	0.66	2.35

maximum solubilities were obtained as a function of NaOH concentration. 40, 56 and 100 g/l of the zinc ion concentration, $Zn(II)_{tot}$, were obtained for 6, 8 and 10 M NaOH concentrations, respectively. Zinc ion concentrations increase with NaOH concentrations.

3.6 PROCEDURE

Sodium hydroxide solution was prepared from doubly distilled water and reagent grade chemicals. A 1-liter volume of the desired concentration of the sodium hydroxide solution was placed in the reactor. When the selected reaction temperature was reached, the desired weight of pure zinc oxide or iron-containing zinc oxide, respectively, was added to the solution. 3 mL samples were then taken, at appropriate intervals, from 2 to 120 minutes. A centrifuge was used to obtain only a leached solution from the samples of the liquid-solid mixture. The concentrations of Zn(II) and Fe(III) from the pregnant solution were then measured. Table 3.4 is a summary of the experimental parameters of the present work.

Table 3.4 Experimental parameters

C (M/l)	4, 5, 6, 8, 10
T (K)	298, 313, 328, 343, 358, 371
N (rpm)	0, 200, 300, 400, 600, 900, 1200
C_s (g/l)	1.0, 1.2, 50.2, 70.4, 125.3
d_o (μm)	+20-38, +38-45, +45-63, +63-75, +75-150, +150-180, +180-355
h/D_T	0.05, 0.1, 0.2, 0.3
D/D_T	0.23, 0.38, 0.54, 0.69
D_b (cm)	1/10 D_T

CHAPTER 4

RESULTS

This chapter consists of three parts. Part one studies the kinetics of alkaline leaching of pure zinc oxide. Part two studies the kinetics of alkaline leaching of roasted zinc concentrates. These two parts have been studied as a function of agitation speed, particle size, NaOH concentration and temperature, using low concentrations of the particles. The objective of part three, however, is to study the variables of the leaching process using high concentration of the particles in order to reduce energy consumption. These are studied as a function of particle suspension, baffles, degree of particle concentration, clearance ratio and impeller-to-reactor diameter ratio.

4.1 LEACHING KINETICS OF PURE ZINC OXIDE

4.1.1 Effect of Agitation Speed

As illustrated in section 2.3.1, complete suspension of the particles may be judged visually. According to this test, an agitation speed of 400 rpm is enough to give complete suspension under the present experimental conditions, in which standard baffles are used.

Figure 4.1 shows the effect of agitation speed on the leaching rate. The leaching rate increased as the agitation speed increased from 300 to 400 rpm. The particles are

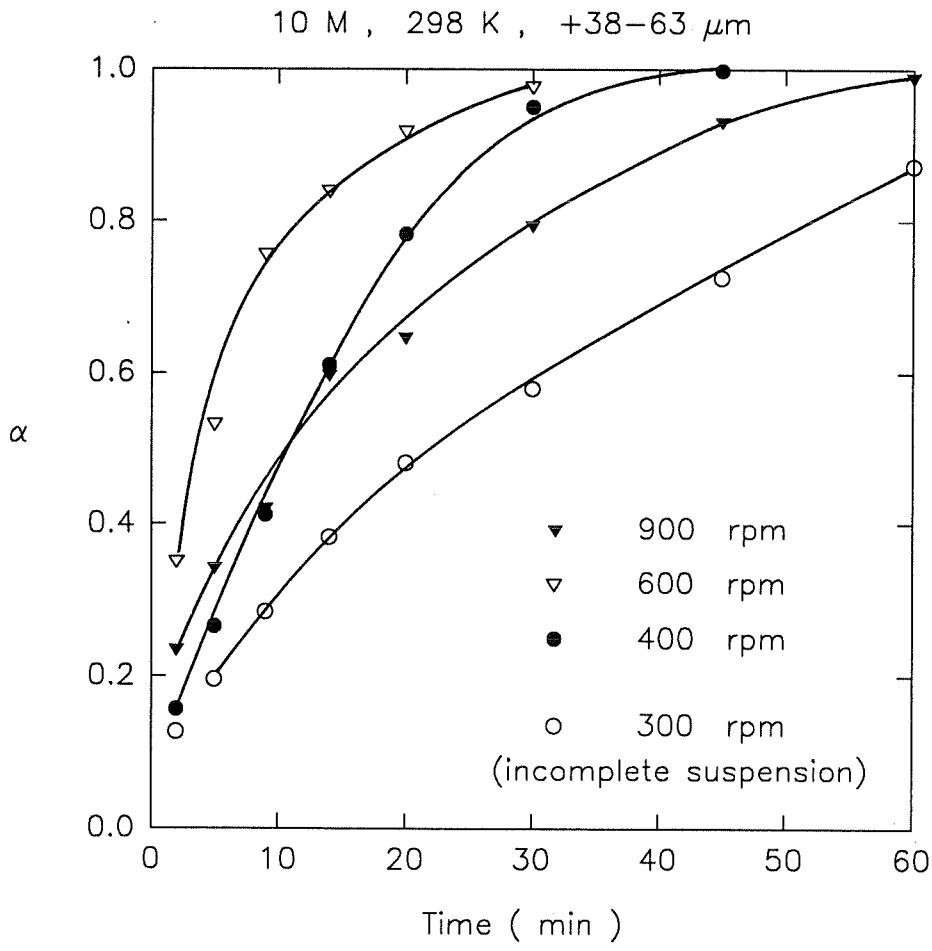

Figure 4.1 Effect of agitation speed on the dissolution of pure zinc oxide

suspended at 400 rpm, but some of them are settled on the bottom of the reactor at 300 rpm. Moreover, the leaching rate increased as the agitation speed increased from 400 to 600 rpm, i.e., for complete suspension. However, the leaching rate decreased as the agitation speed increased from 600 to 900 rpm. Thus, there exists an optimum agitation speed which yields the highest leaching rate.

In this experiment, the particle size of +38-63 μm was tested, since this constitutes the largest weight percentages among the particle sizes of the roasted zinc concentrates of CEZ. However, since small particles dissolve quickly at high temperature, as seen in Figure 4.2, large particles, for example +180-355 μm, are needed to analyze the effect of temperature on the leaching rate. An agitation speed of 600 rpm is necessary to give complete suspension for this particle size, as determined by visual observation. This is because the agitation speed for complete suspension increases as the particle size increases. The determination of the minimum agitation speed for complete suspension can be easily made, due to the low concentration of the particles. Therefore, in all subsequent experiments, the agitation speed was set at 600 rpm.

4.1.2 Effect of Particle Size

The effect of particle size on the leaching rate is shown in Figure 4.3. The rate of dissolution increased with decreasing particle size or with increasing specific surface area. As seen in Table 3.1, the specific surface area increased with decreasing particle

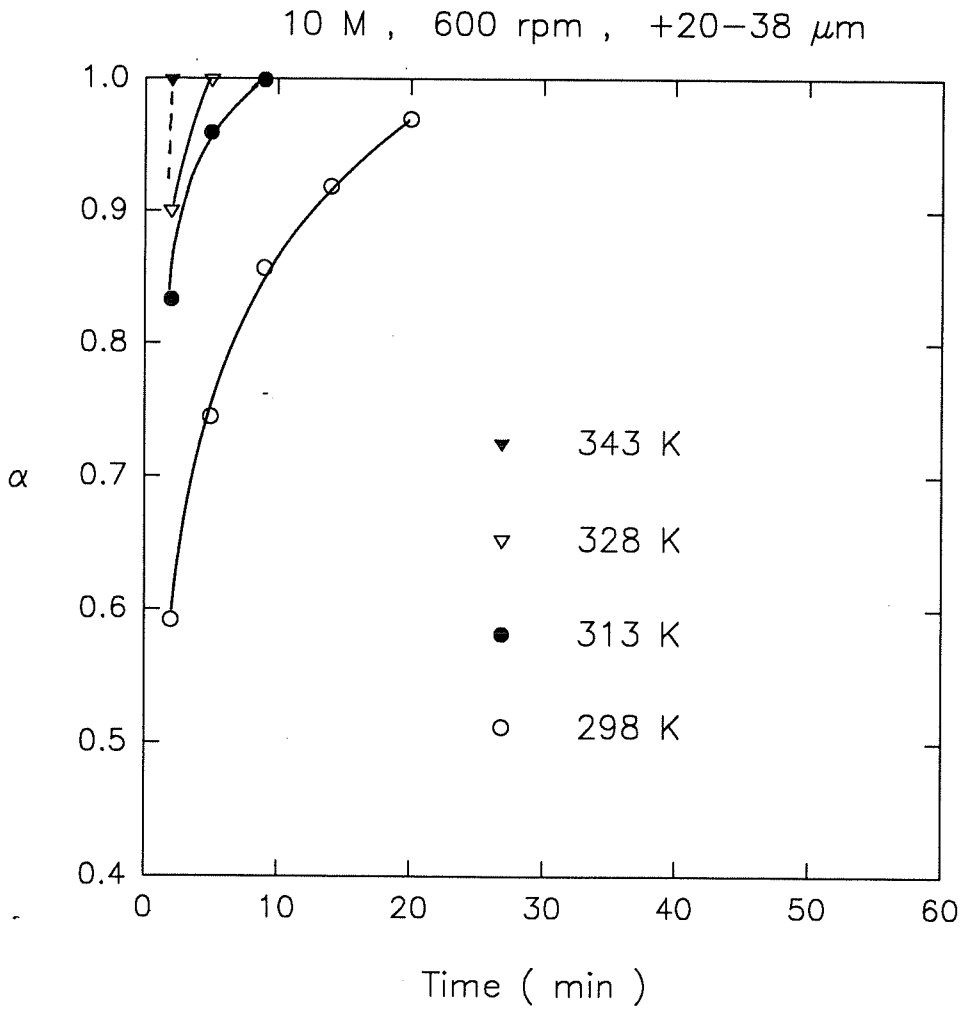

Figure 4.2 Effect of temperature on the dissolution of pure zinc oxide

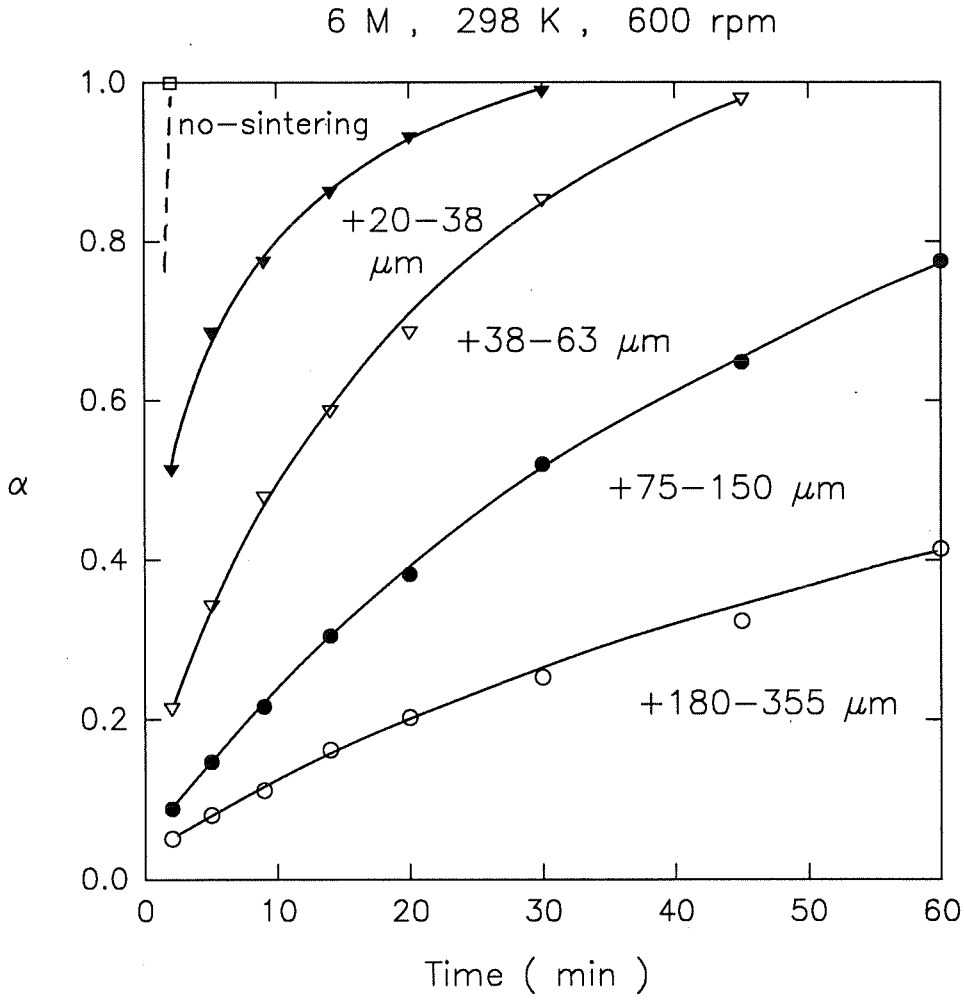

Figure 4.3 Effect of particle size on the dissolution of pure zinc oxide

size. As explained in section 3.3.2, non-sintered particles, i.e., reagent grade particles, had a much faster leaching rate than sintered particles.

4.1.3 Effect of NaOH Concentration

A group of experiments were performed to establish the dependence of NaOH solution on the leaching rate. Figure 4.4 shows the effect of NaOH concentration on the dissolution of zinc oxide. As illustrated, the leaching rate increased as NaOH concentration increased.

4.1.4 Effect of Temperature

Figure 4.5 shows the effect of temperature on dissolution of zinc oxide. The temperature influences the dissolution of zinc oxide, and the leaching rate increased as temperature increased.

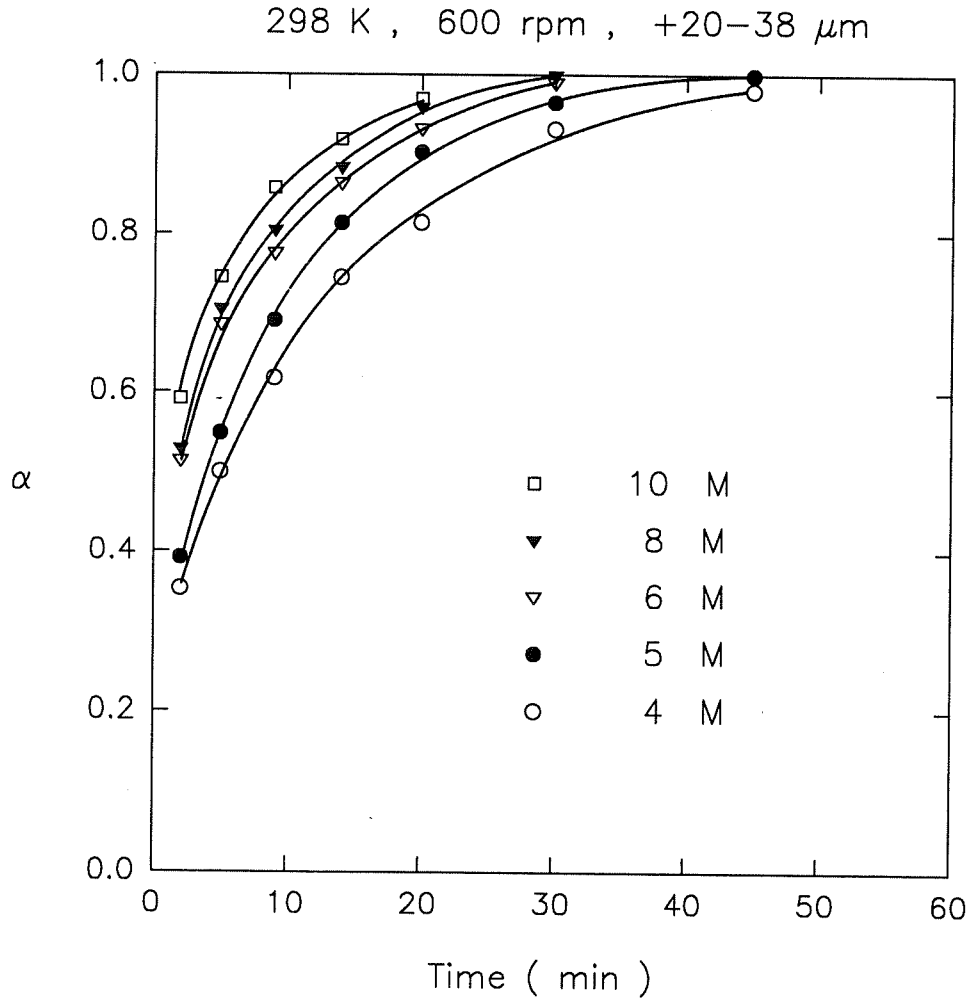

Figure 4.4 Effect of NaOH concentration on the dissolution of pure zinc oxide

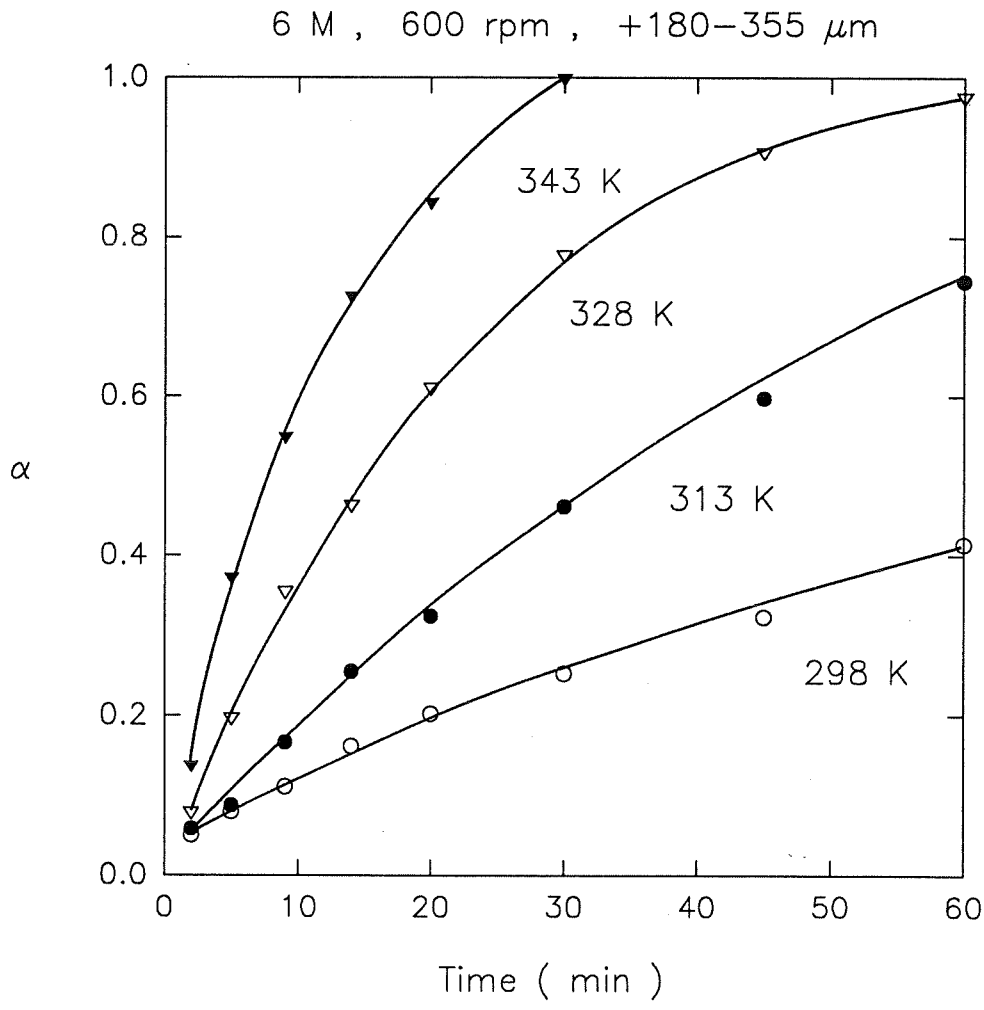

Figure 4.5 Effect of temperature on the dissolution of pure zinc oxide

4.2 LEACHING KINETICS OF ROASTED ZINC CONCENTRATES

4.2.1 Effect of Agitation Speed

An agitation speed of 300 rpm is enough to give complete suspension for the present experimental conditions in which standard baffles are used. This was determined visually. This value is less than the agitation speed of 400 rpm for the pure zinc oxide. The agitation speed for complete suspension is a function of the density difference between the particle and the solution. The specific densities for zinc oxide, hematite and zinc ferrite are about 5.66, 5.26 and 5.33, respectively (85). Roasted zinc concentrates and a sintered mixture are more porous so that their apparent bulk densities are less than that of pure zinc oxide. Thus, their agitation speeds for complete suspension are less than that for pure zinc oxide.

Figure 4.6 shows the effect of the agitation speed on the leaching rate of the roasted zinc concentrates. The leaching rate increased as agitation speed increased from 150 to 300 rpm. The particles are suspended at 300 rpm, but some of them are settled on the bottom of the reactor at 150 rpm. However, the leaching rate is independent of agitation speed from 300 to 900 rpm, i.e., for complete suspension. Therefore, it is no longer controlled by diffusion through the boundary layer. Figure 4.7 illustrates the effect of agitation speed on the leaching rate of the sintered mixture. Three agitation speeds for complete suspensions were used in order to compare a leaching trend with the

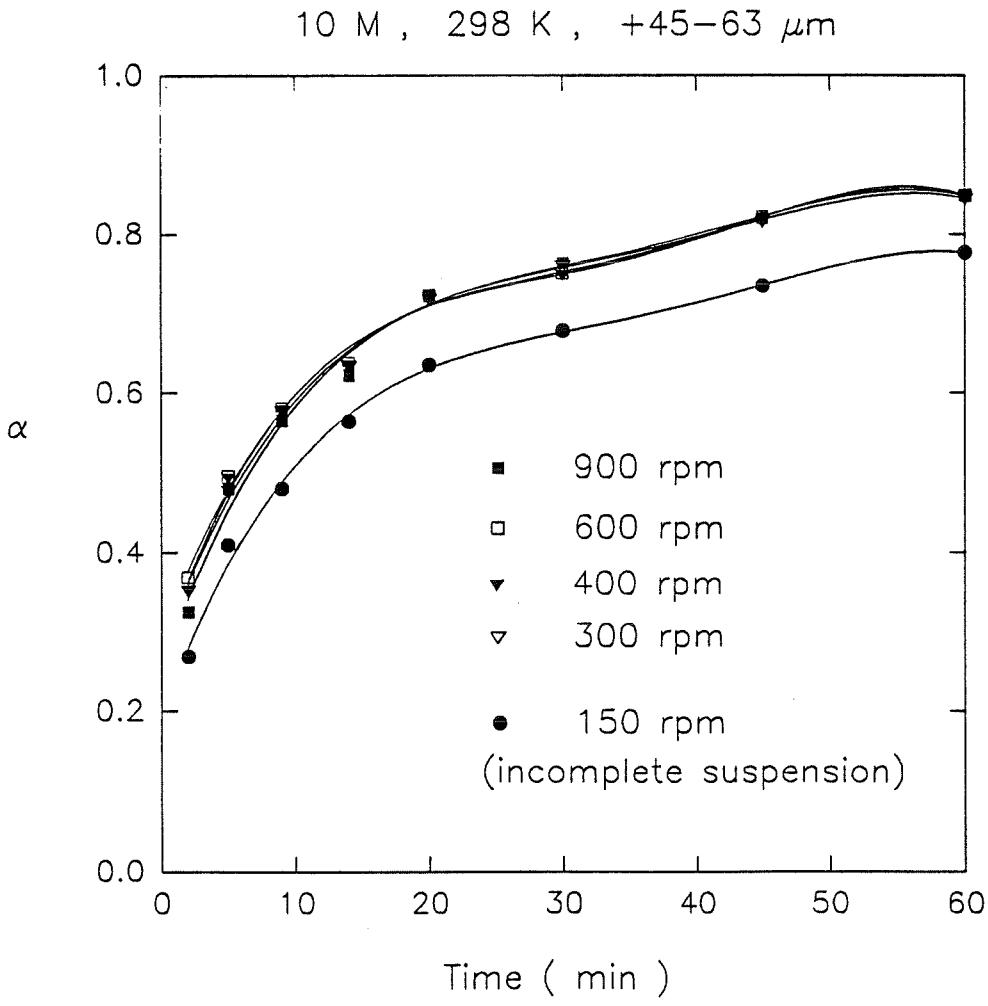

Figure 4.6 Effect of agitation speed on the leaching rate of roasted zinc concentrates

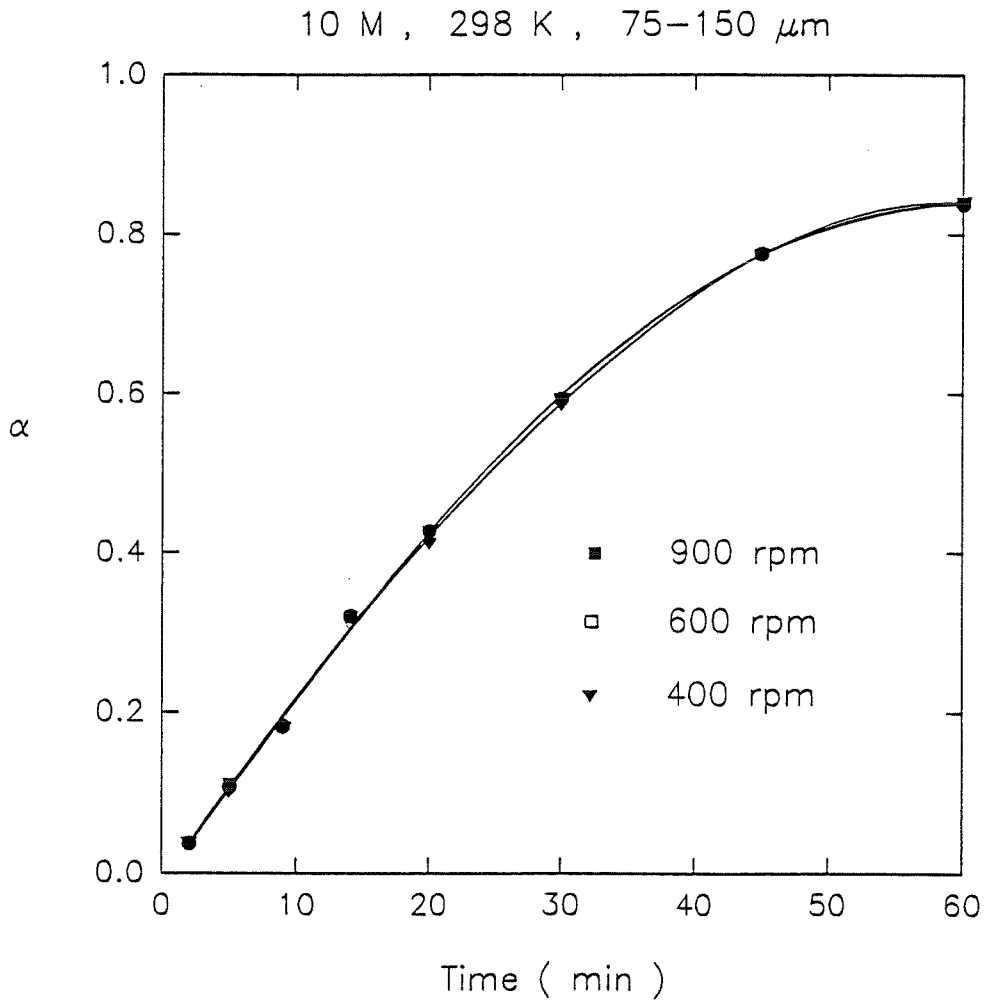

Figure 4.7 Effect of agitation speed on the leaching rate of sintered mixture

roasted zinc concentrates. As in the case of the roasted zinc concentrates, the leaching rate of the sintered mixture was independent of the agitation speed. Their dissolution behavior is therefore totally different from that of pure zinc oxide.

As seen in Figure 4.8, since small particles of the roasted zinc concentrates also dissolve quickly at high temperature, large particles (+75-150 μm) are required to determine the effect of temperature on the leaching rate. Therefore, the agitation speed was set at 600 rpm. At this agitation speed, the diffusion resistance through the boundary layer immediately surrounding the particles can be minimized.

4.2.2 Effect of Particle Size

The effect of particle size on the leaching rate is shown using five size fractions of the roasted zinc concentrates in Figure 4.9. The rate of dissolution was found to increase with decreasing particle size or with increasing specific surface area. As seen in Table 3.1, specific surface area increased with decreasing particle size.

The amounts of the elements of the sintered mixture change depending on the particle size as compared with the roasted zinc concentrates (Table 3.3). Therefore, in the sintered mixture, +75-150 μm particles were used in order to compare the leaching trend with the roasted zinc concentrates.

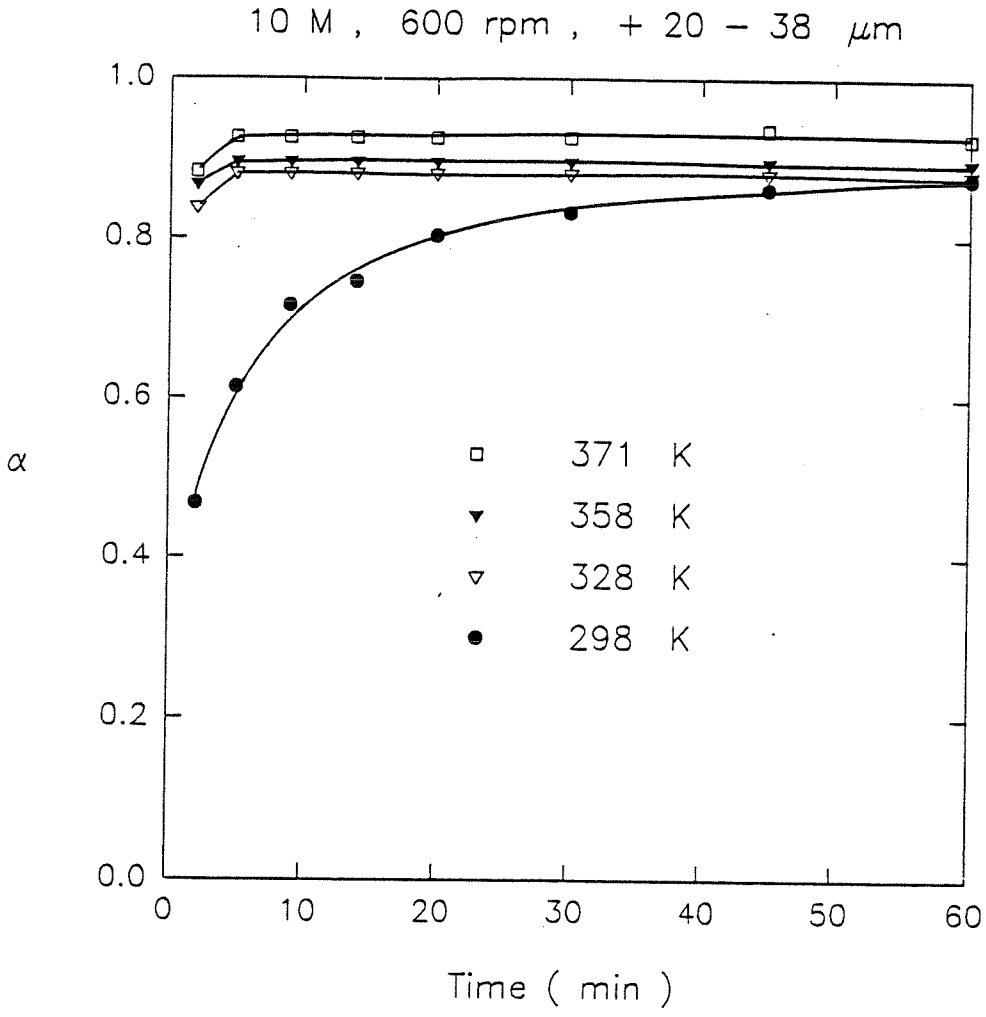

Figure 4.8 Effect of temperature on the leaching rate of roasted zinc concentrates

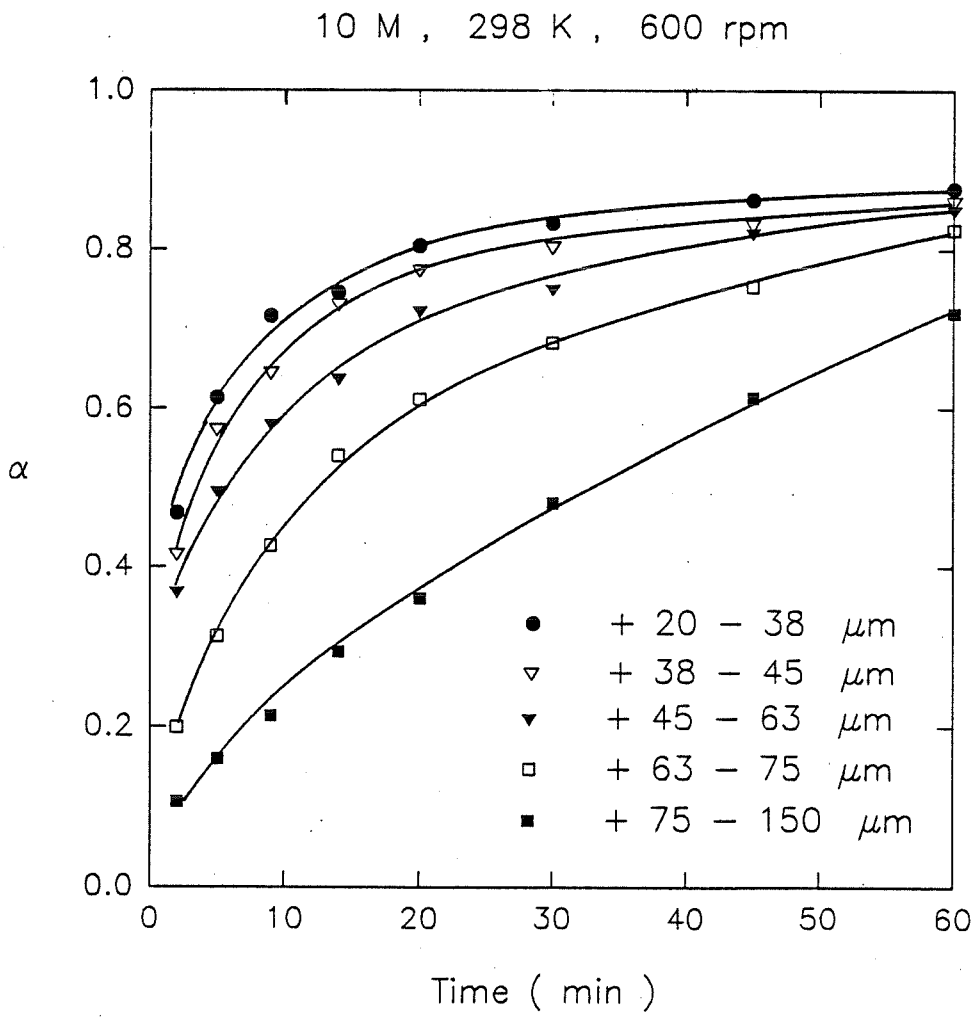

Figure 4.9 Effect of particle size on the leaching rate of roasted zinc concentrates

4.2.3 Effect of NaOH Concentration

A group of experiments were conducted to establish the dependence of the leaching rate on NaOH concentration. Figure 4.10 shows the effect of NaOH concentration on the dissolution of the roasted zinc concentrates. As seen in this figure, the leaching rate is independent of NaOH concentrations ranging from 4 to 10 M. Figure 4.11 illustrates the effect of NaOH concentration on the dissolution of the sintered mixture. Two experiments using 6 and 10 M NaOH were carried out in order to compare the leaching trend with that of the roasted zinc concentrates. As in the case of the roasted zinc concentrates, the leaching rate of the sintered mixture is independent of NaOH concentration. Thus, the sintered mixture has the same trend as the roasted zinc concentrates. However, their dissolution behaviors are totally different from that of sintered pure zinc oxide.

4.2.4 Effect of Temperature

Figure 4.12 illustrates the effect of temperature on dissolution of the roasted zinc concentrates. As the temperature increased, the leaching rate increased. Particularly, as seen in Figures 4.8 and 4.12, absolute extraction percentages became higher and higher as temperature increased. For example, in +75-150 μm, the absolute extraction percentages were about 98, 93 and 90 % at 371, 358 and 328 K, respectively. In +20-38 μm, they were about 93, 90 and 88 %, respectively.

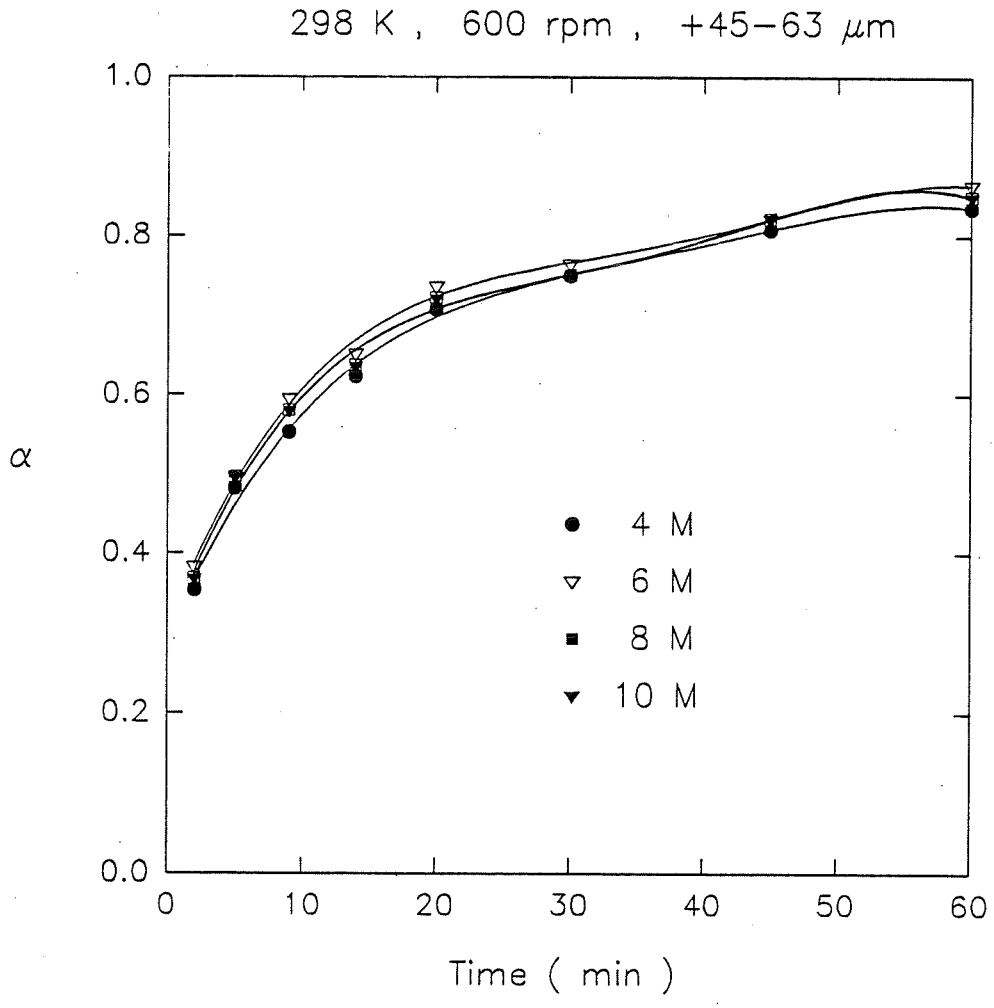

Figure 4.10 Effect of NaOH concentration on the leaching rate of roasted zinc concentrates

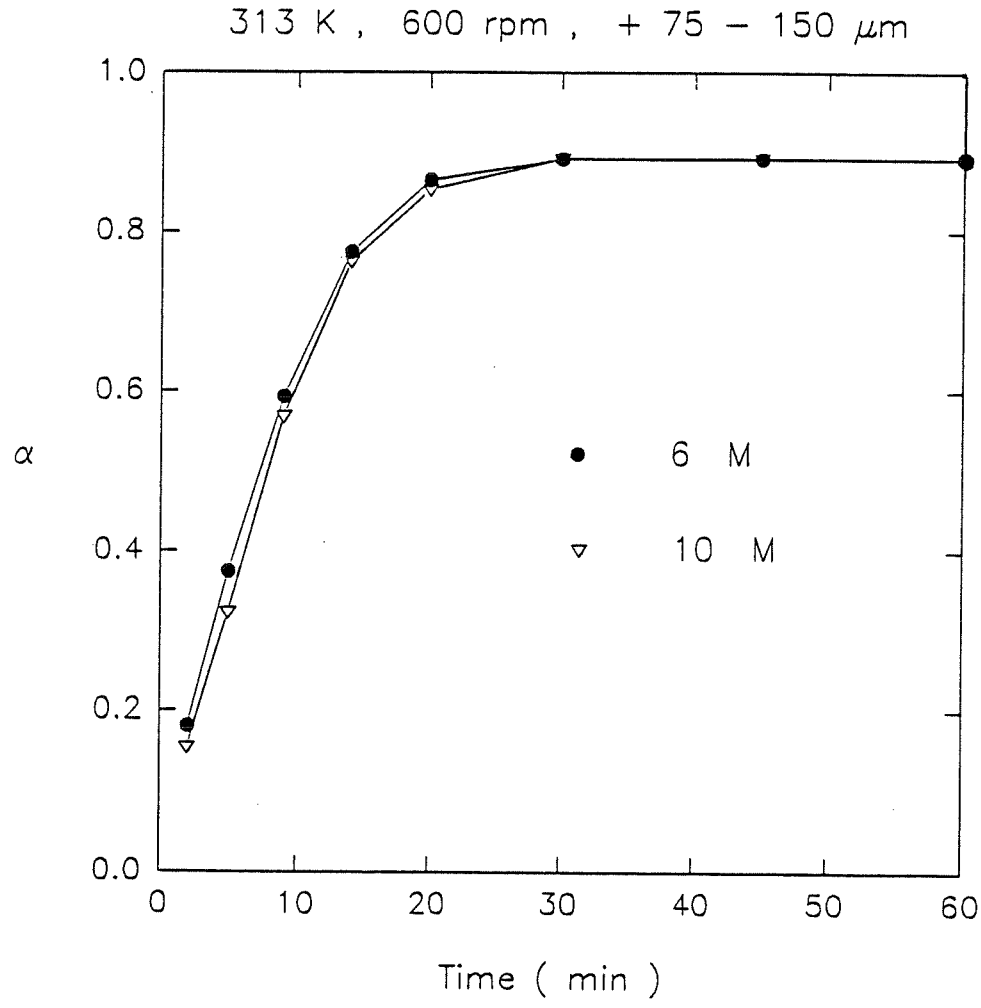

Figure 4.11 Effect of NaOH concentration on the leaching rate of sintered mixture

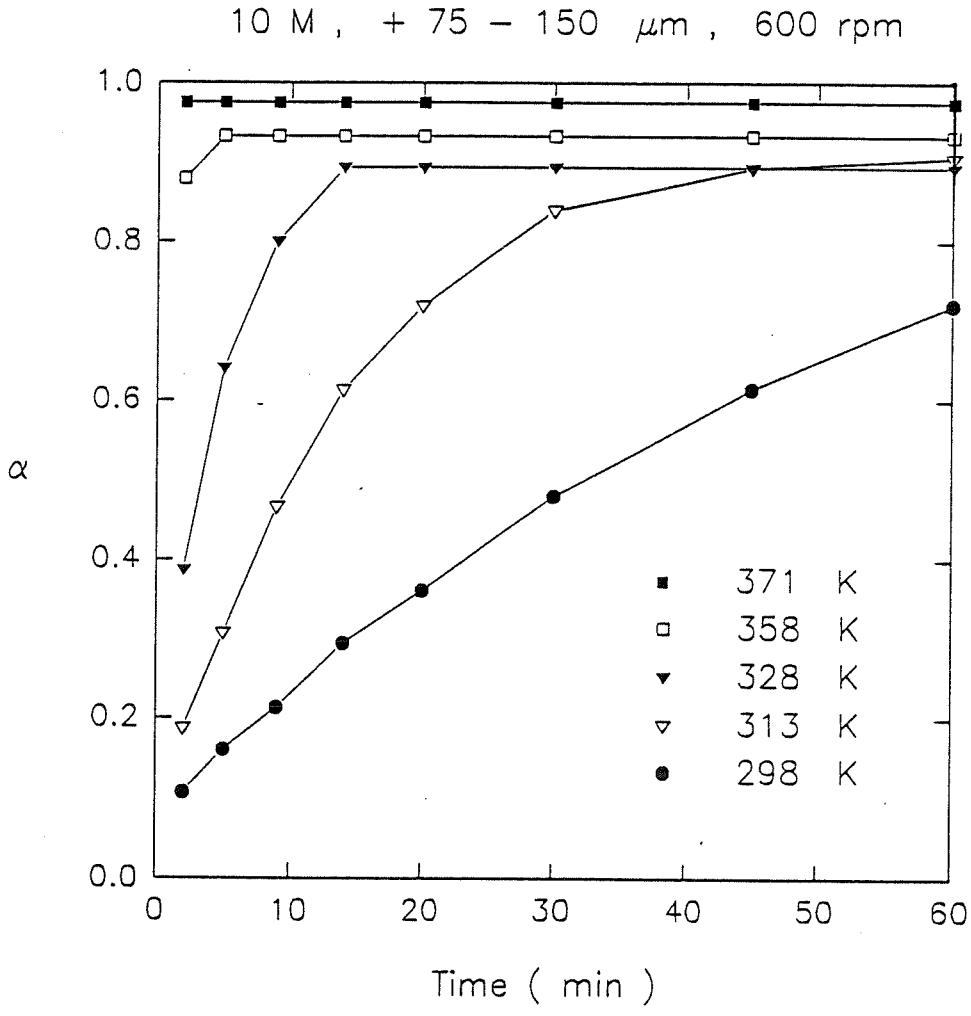

Figure 4.12 Effect of temperature on the leaching rate of roasted zinc concentrates

Figure 4.13 shows the effect of temperature on dissolution of the sintered mixture. Experiments using three temperature ranges were carried out in order to compare the leaching trend with that of the roasted zinc concentrates. As seen in this figure, increasing temperature increased the leaching rate.

4.2.5 Dissolution of Iron

Table 4.1 shows the dissolution of iron in NaOH solution as a function of the particle size of the roasted zinc concentrates. Although increasing particle size decreased the iron content in the concentrates, the iron dissolution is constant regardless of particle size. Figure 4.14 also shows the dissolution of iron as a function of NaOH concentration in the roasted zinc concentrates. As seen in this figure, the dissolution of iron increased as NaOH concentration increased. In 4 M NaOH solution, the dissolution increased with time. However, the maximum value was obtained after 5 minutes. The dissolutions of 6 and 8 M NaOH solutions reached maximum values within 2 minutes. As seen in Figure 4.14, the iron dissolution is the same between 6 and 8 M, but it suddenly increases between 8 and 10 M. This is due to the precision range of the atomic absorption spectrophotometer.

As seen in Table 4.1 and Figure 4.14, there is a limited dissolution of iron in the leached solution during alkaline leaching of the roasted zinc concentrates. The precipitation process which removes the ferric ion from the leached solution can be

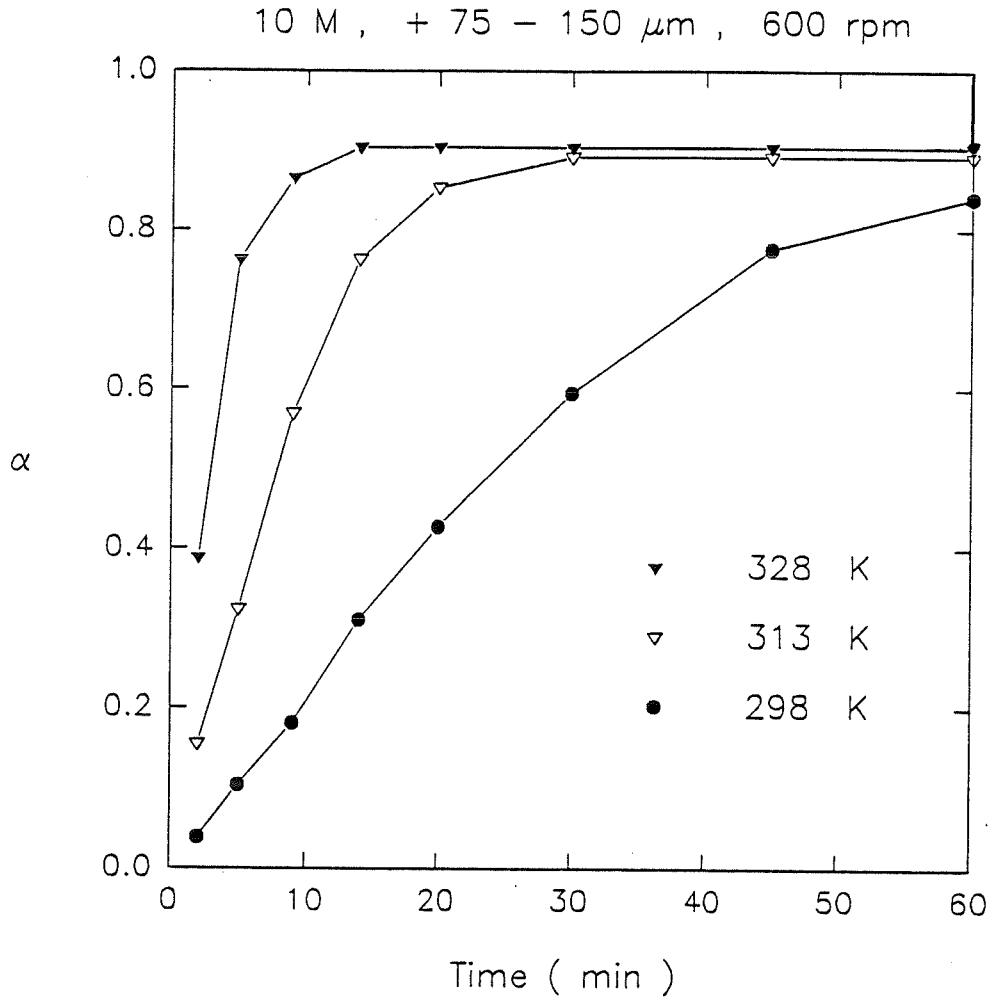

Figure 4.13 Effect of temperature on the leaching rate of sintered mixture

Table 4.1 The dissolution of iron in NaOH concentration as a function of particle size (10 M/l, 298 K, 600 rpm)

d_0 (μm)	Fe (%)	Fe(III) (g/l)
+ 20 - 38	13.60	0.01
+ 38 - 45	13.30	0.01
+ 45 - 63	12.35	0.01
+ 63 - 75	10.80	0.01
+ 75 - 150	10.80	0.01

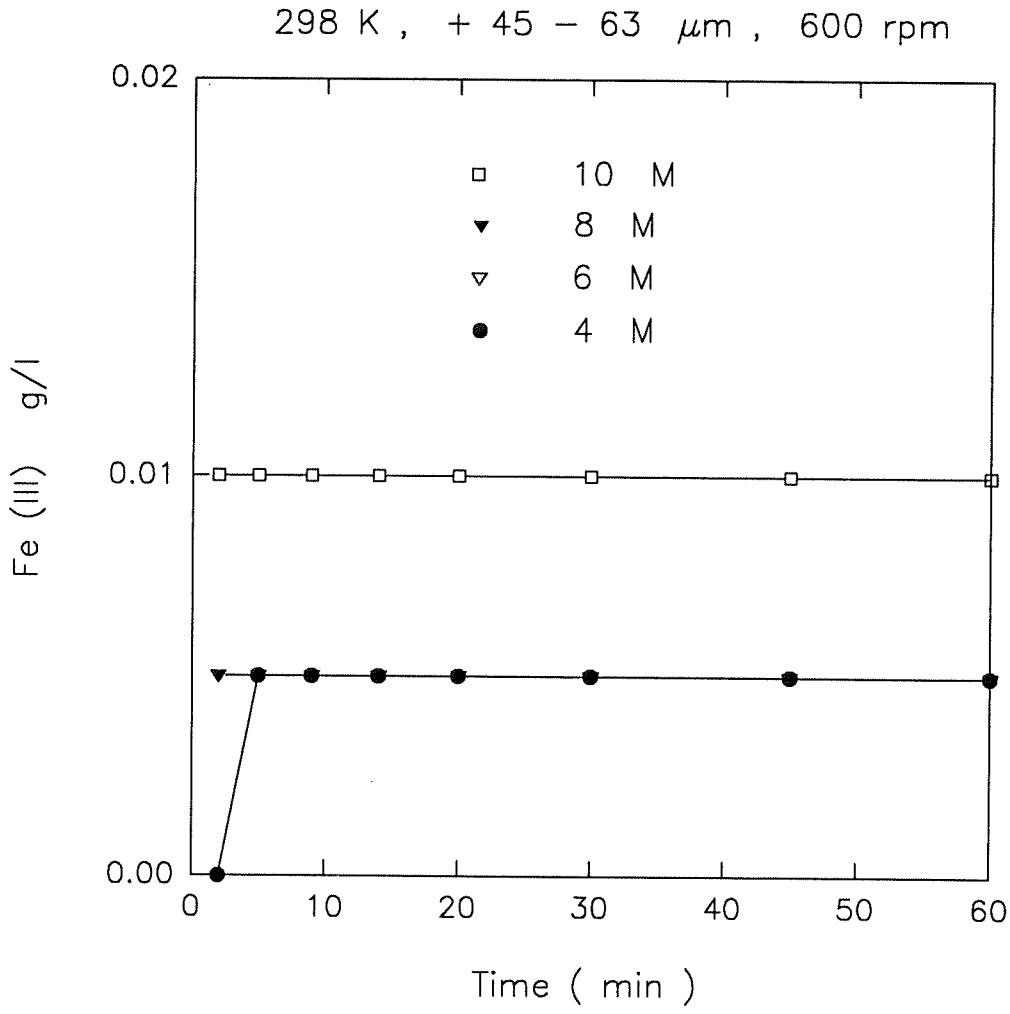

Figure 4.14 Dissolution of iron as a function of the NaOH concentration in roasted zinc concentrates

avoided. On the other hand, the precipitation process is required in the sulfate leaching process, because all of the iron is dissolved (15,16).

4.2.6 Morphology

Partially-leached particles of the roasted zinc concentrates were obtained after leaching. These particles were dried by evaporating water and sodium hydroxide, in order to investigate the morphology with the scanning electron microscope (SEM). Ethyl alcohol was used to evaporate water and sodium hydroxide, since sodium hydroxide is very soluble in ethyl alcohol, but zinc oxide and zinc ferrite are not (85). Ethyl alcohol forms the azeotrope with water and sodium hydroxide, and is very volatile. The dried particles were mounted, and polished sections made. By this means, cross-sections of the particles were made for morphological examination.

Figure 4.15 shows the typical result of partially-leached roasted zinc concentrates. This corresponds to $\alpha = 0.7$ and +75-150 μm in Figure 4.9. Figure 4.15-a shows the morphology of the particle. Figures 4.15-b and 4.15-c give the X-ray mapping of the distribution of iron oxide and zinc oxide throughout the particle, respectively. As seen in these figures, iron oxide exists outside of the particle, whereas zinc oxide remains inside. Moreover, the particle size remains unchanged even though leaching has been done.

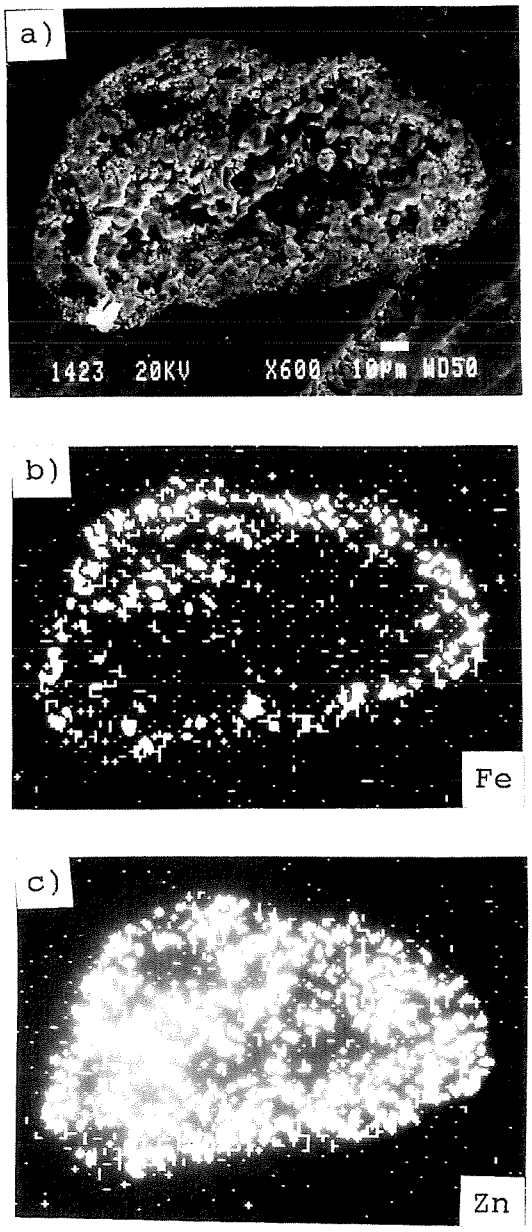

Figure 4.15 Morphology and X-ray mapping of partially-leached particle roasted zinc concentrates

4.3 PROCESS VARIABLES

Three kinds of materials were used: reagent grade pure zinc oxide and iron-containing zinc oxides, which are roasted zinc concentrates and sintered mixture.

4.3.1 Measurement of Kinematic Viscosity

A Cannon-Fenske capillary type viscometer of ASTM size number 100 was used to measure the kinematic viscosity of the NaOH solution as a function of temperature, using American National Standard ANSI/TAPPI method (86). Figure 4.16 shows the kinematic viscosity of each concentration of NaOH solution and of pure water as a function of temperature. The kinematic viscosity of pure water was obtained from the literature (85) as a point of comparison with that of each concentration of NaOH solution. As illustrated in this figure, when temperature increased and/or NaOH concentration decreased, the kinematic viscosity decreased. Also, as NaOH concentration increased from 6 to 8 to 10 M, kinematic viscosities increased, respectively, about 4, 6 and 10 times with respect to pure water.

4.3.2 Suspension of Particles

Figure 4.17 shows the effect of agitation speed on the dissolution of pure zinc oxide without baffles. The extractions of 8, 16, 76, 92 and 97 % were obtained within 5 minutes at 0, 200, 400, 600 and 1200 rpm, respectively. The results show that the

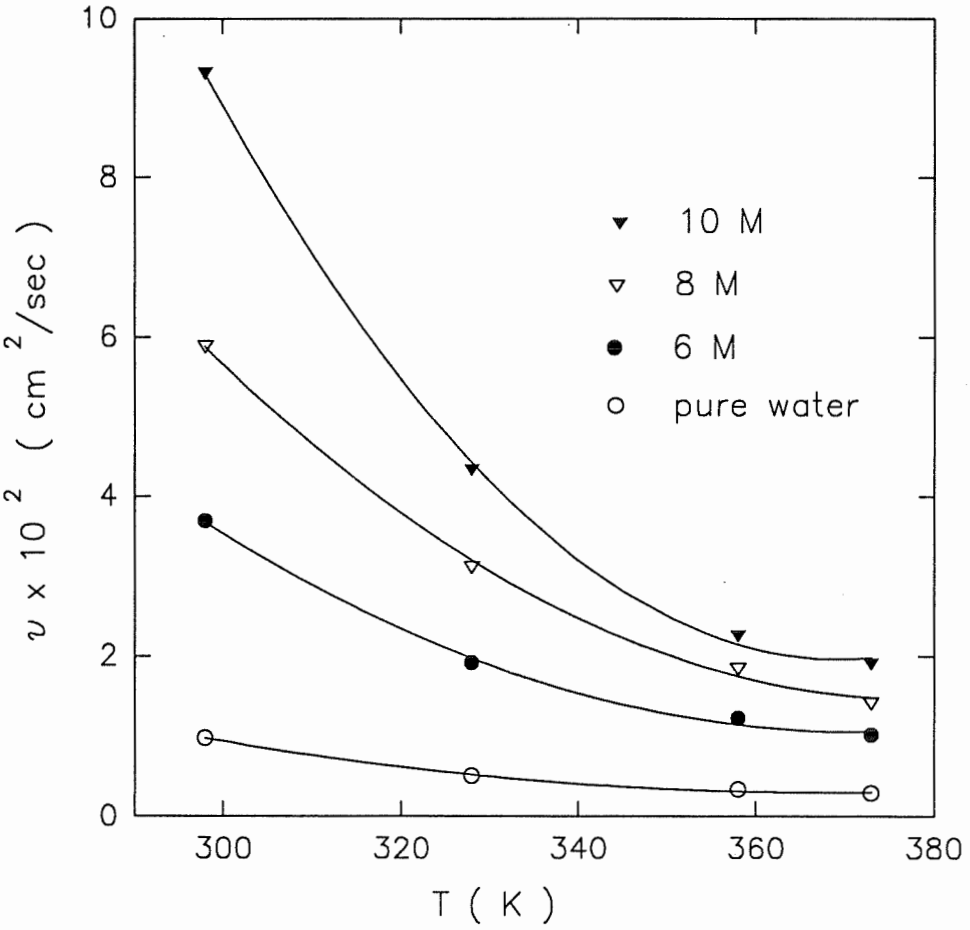

Figure 4.16 Kinematic viscosity of NaOH solution as a function of temperature

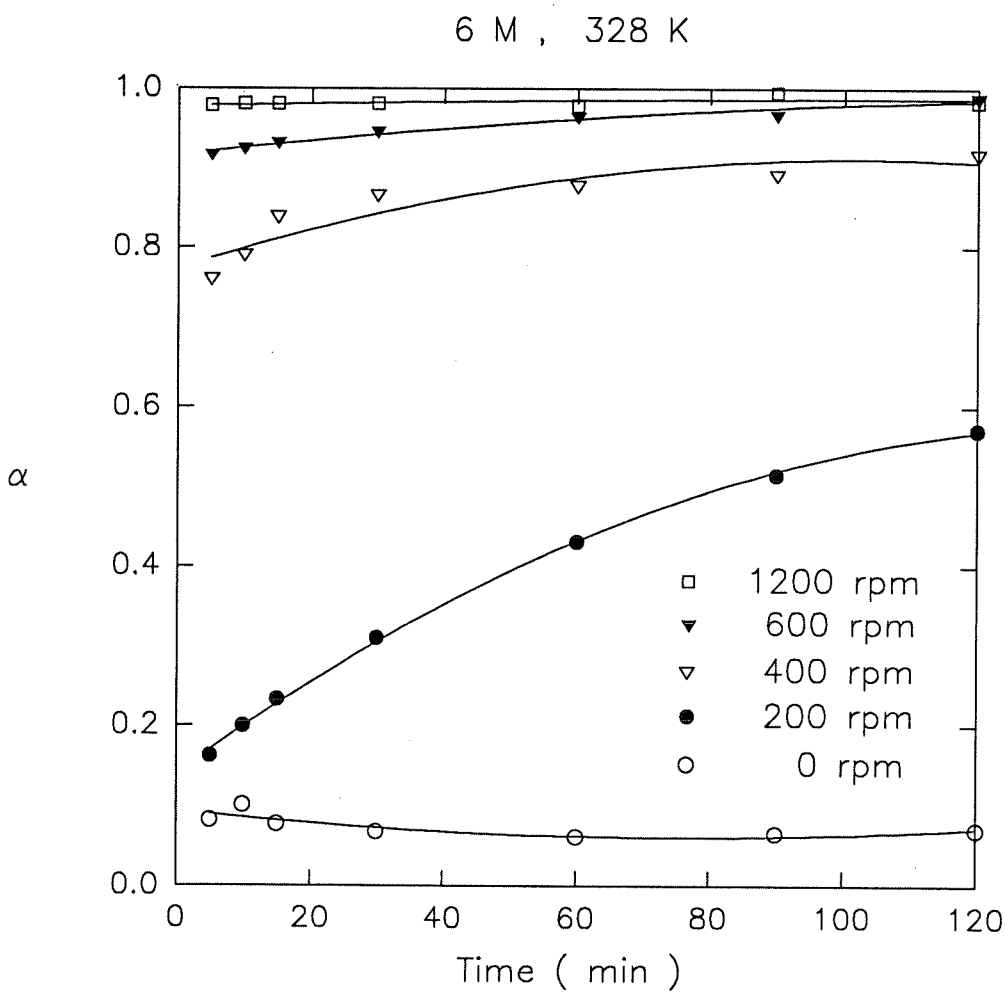

Figure 4.17 Effect of agitation speed on the dissolution of pure zinc oxide (+75-150 μm)

dissolution of pure zinc oxide did not progress at 0 rpm, i.e., passivation, whereas the dissolution of pure zinc oxide increased with time at 200 rpm. On the other hand, experiments at 400, 600 and 1200 rpm show that the dissolution of pure zinc oxide greatly increased at the beginning of the process.

As the agitation speed increased, the degree of particle suspension increased. As indicated in section 2.3.1, the degree of particle suspension can be judged visually. A mirror was placed beneath the reactor bottom to get the image of the reactor bottom. Figure 4.18 shows the suspension of particles as a function of the agitation speed without baffles. In Figure 4.18-a, an accumulation of particles is seen on the bottom of the reactor at 300 rpm. Only a small portion of the particles are suspended. However, in Figure 4.18-b, there is no accumulation, since they are completely suspended. This result was obtained using 600 rpm.

4.3.3 Precipitate

As stated in section 4.2.6, the partially-leached particles were dried by evaporating water and sodium hydroxide with ethyl alcohol, and scanning electron microscope (SEM) was used to investigate the morphology of precipitates.

Figure 4.19 shows the precipitate of a partially-leached pure ZnO particle reacted at 200 rpm, 328 K, 10 M. Its cross-section was prepared by breaking the particle, and

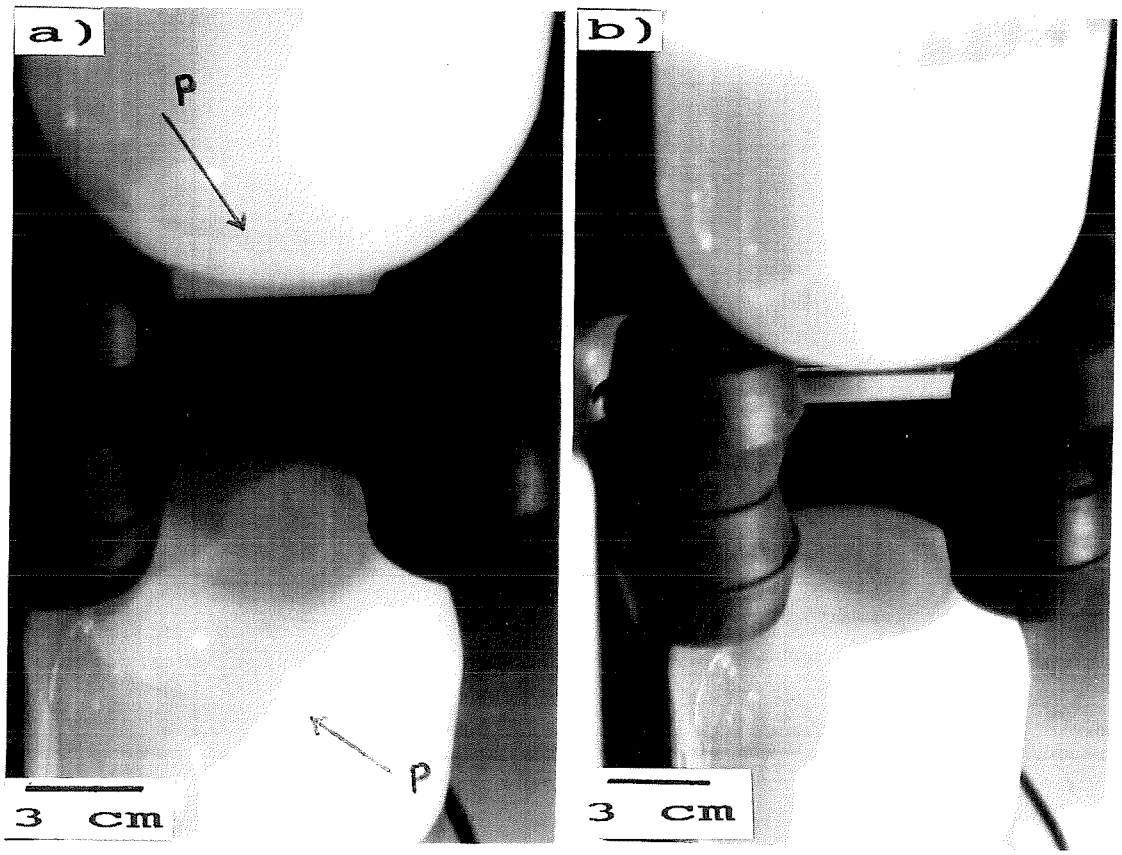

Figure 4.18 Suspension of particles (10 M, 298 K) a) 300 rpm

b) 600 rpm p indicates the accumulation of particles

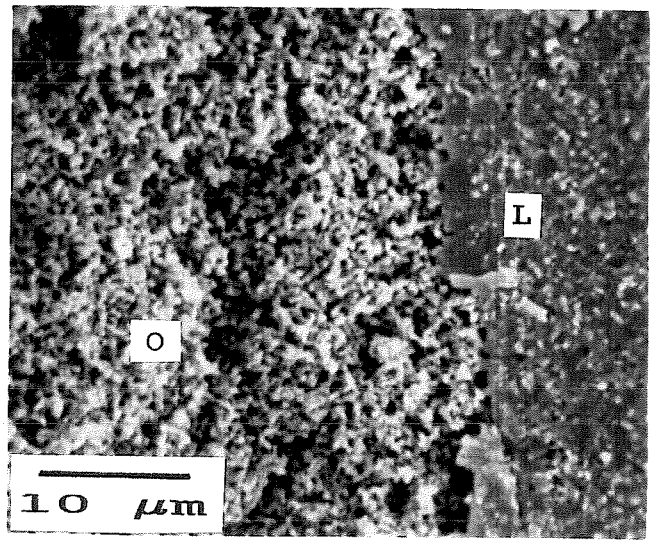

Figure 4.19 Formation of precipitate of partially-leached particle (200 rpm, 328 K, 10 M) L indicates precipitate and O original particle

no further treatment was carried out. As can be seen in this figure, the precipitate is more compact than the original particle, i.e., unreacted part, it therefore becomes more difficult for the $Zn(OH)_4^{2-}$ ion to diffuse into the bulk of the electrolyte. However, no precipitate appeared at 600 rpm.

Figure 4.20 shows the dissolution of pure zinc oxide at an agitation speed of 200 rpm. The extractions of 41, 57 % were obtained in 120 minutes at 298 and 328 K, respectively. As seen in this figure, the dissolution curves are parabolic, which indicates the formation of precipitate between zinc oxide and the solution through which reactants and products must diffuse. The 8 and 10 M solutions have the same leaching trends as the 6 M solution at 200 rpm.

4.3.4 Effect of Baffles

The effect of baffles on the dissolution of pure zinc oxide is shown in Figure 4.21. On the reactor wall, four vertical baffles were set equidistant from each other. The leaching rate was higher with baffles than without them at 200 and 400 rpm. The complete suspensions were obtained at 400 rpm and 600 rpm with baffles and without baffles, respectively. Thus, the leaching rate at 400 rpm with baffles was almost the same as that of 600 rpm without them. Also, the leaching rate in the presence of baffles increased as agitation speed increased from 200 to 400 rpm, since the particles were suspended. However, the leaching rates with baffles showed no significant differences

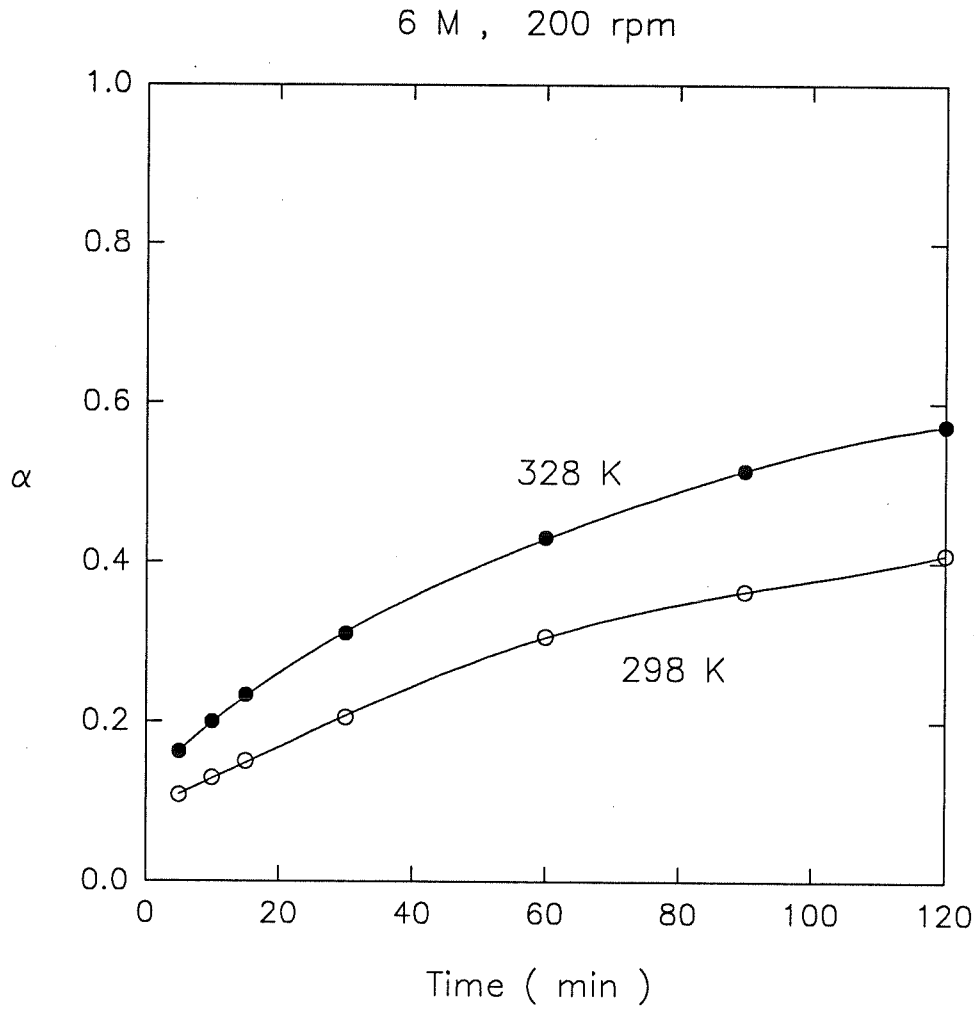

Figure 4.20 Dissolution of pure zinc oxide at 200 rpm (+75-150 μm)

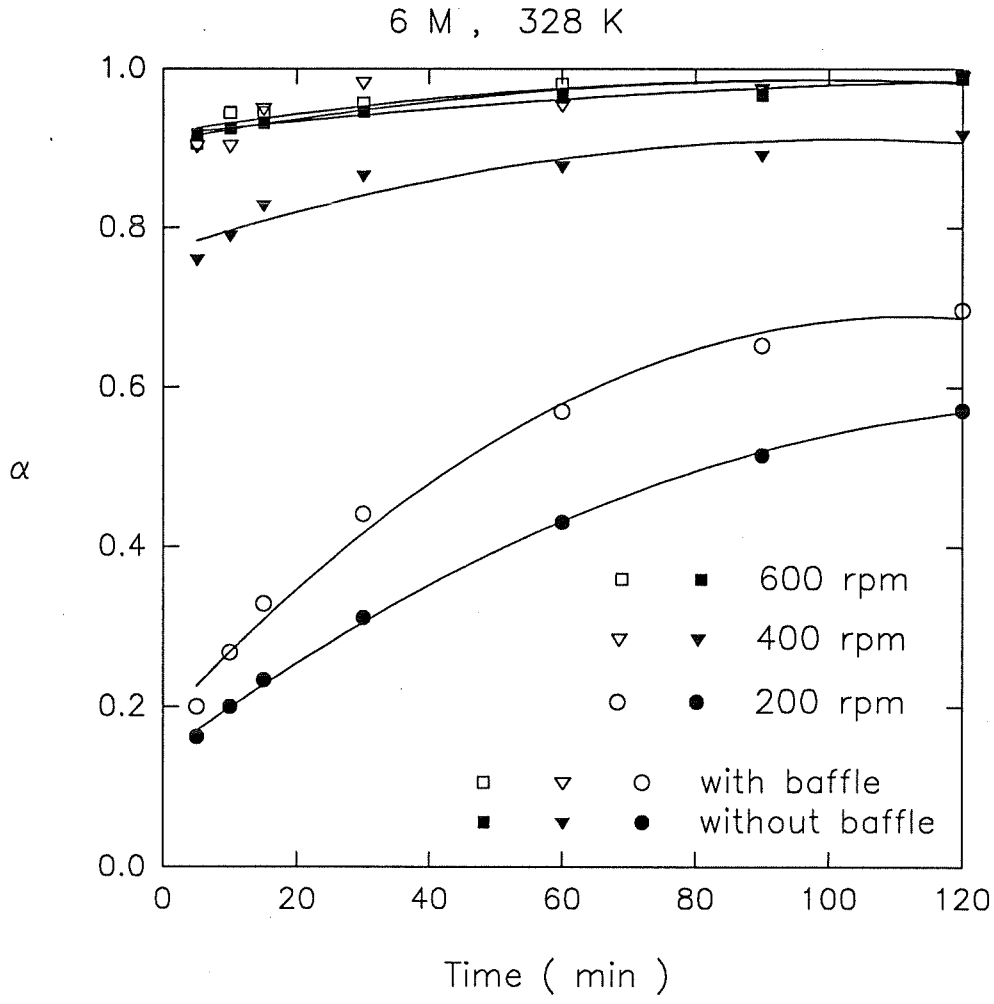

Figure 4.21 Effect of baffles on the dissolution of pure zinc oxide (+75-150 μm)

as the agitation speed increased from 400 rpm to 600 rpm.

The effect of the number of baffles on the dissolution of the roasted zinc concentrates is shown in Figure 4.22. In these experiments, four or eight vertical baffles were set at the same distance on the reactor wall respectively. As can be seen in this figure, the leaching rate was higher using eight baffles.

4.3.5 Effect of Degree of Particle Concentration

Figure 4.23 illustrates the effect of degree of particle concentration of the roasted zinc concentrates on the leaching rate. There exists an optimum degree of particle concentration which yields the highest leaching rate. Particle weights of 157.0, 100.0 and 66.0 g were used as high, medium and low degree of particle concentration in 10 M NaOH solution. These weights converted into 10.5, 6.9 and 4.7 wt%, respectively.

However, as explained in section 3.5, since each NaOH concentration has its own maximum solubility, the particle weights of high, medium and low degree of particle suspension varied depending with each NaOH concentration. Therefore, the particle weights of high degree of particle concentration at 10, 8 and 6 M NaOH solution were determined from their maximum solubility and the weight ratios were then determined for medium and low degree of particle concentration, respectively. The weight ratios of each degree of particle concentration were calculated as 1.0, 0.64 and 0.42.

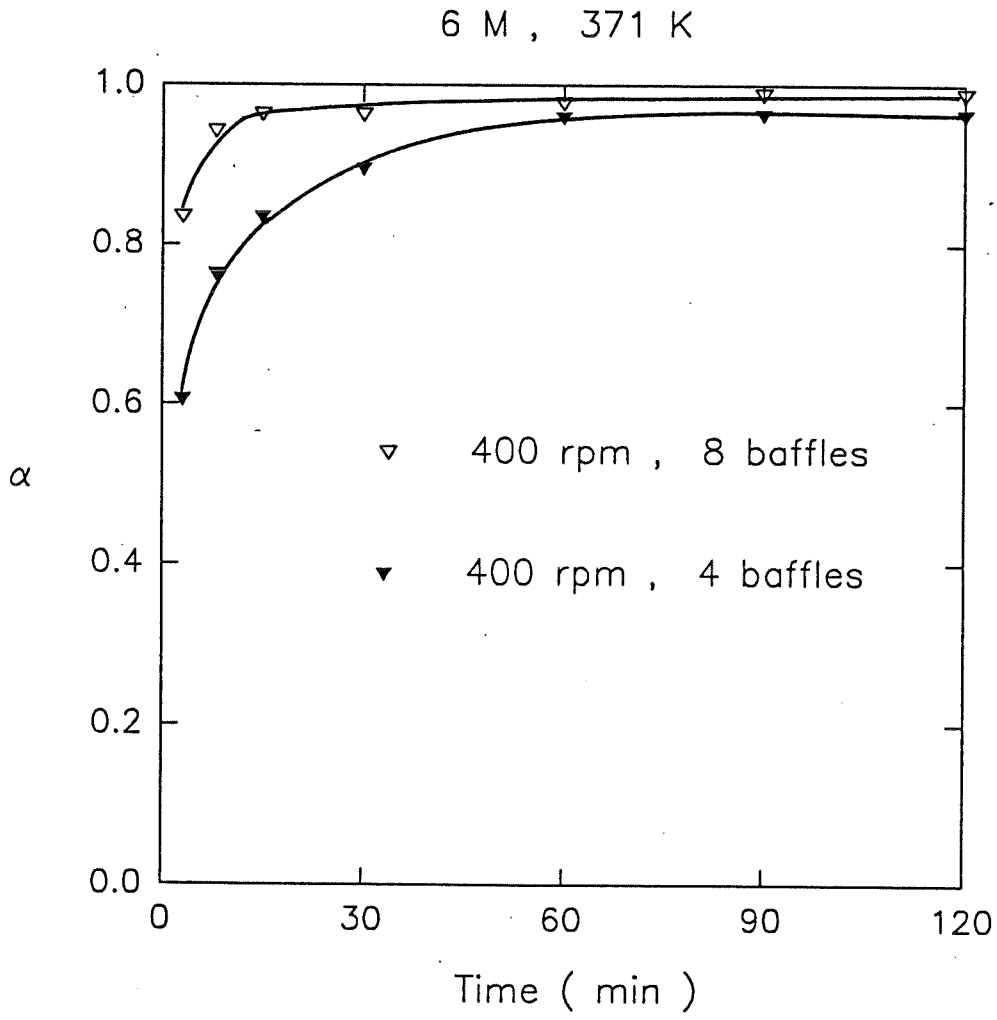

Figure 4.22 Effect of the number of baffles on the dissolution of roasted zinc concentrates

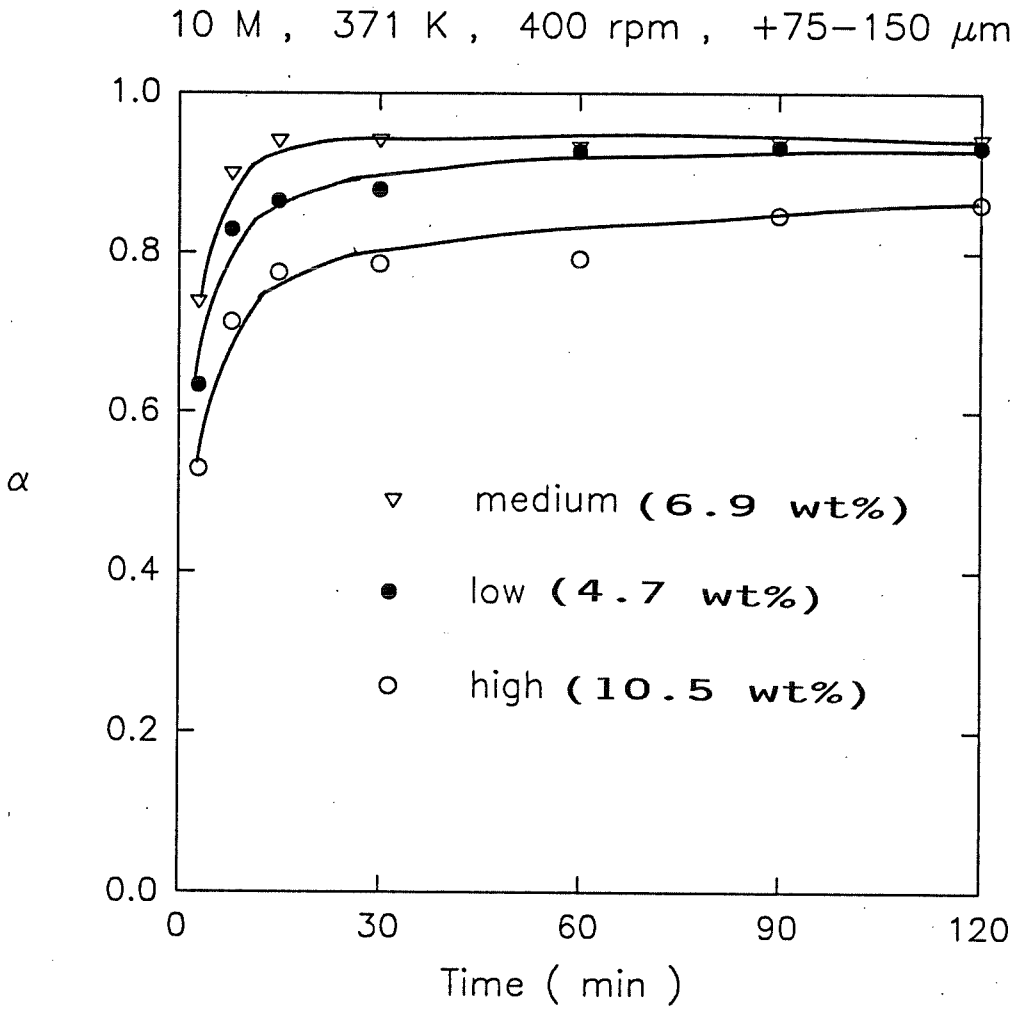

Figure 4.23 Effect of the degree of particle concentration on the dissolution of roasted zinc concentrates

4.3.6 Agitation Speed for Complete Suspension

Figure 4.24 shows agitation speed for complete suspension as a function of impeller-to-reactor diameter ratio and clearance ratio. Agitation speed for complete suspension decreased as the impeller-to-reactor diameter ratio increased from 0.23 to 0.69 and/or as the clearance ratio decreased from 0.3 to 0.05. The criterion for complete suspension is that no particles remain on the bottom of the reactor more than 1 second. This criterion were determined by the visual observation using a mirror placed beneath the reactor.

4.3.7 Effect of Clearance Ratio

Figure 4.25 shows the effect of clearance ratio on the leaching rate. Since the flow pattern is sensitive to the clearance ratio, as stated in section 2.3.3.1, there exists an optimum clearance ratio, which yields the highest leaching rate. In the case of $h/D_T = 0.1$, all particles move to the bottom of the reactor before they reach the reactor wall; they then turn up, making a larger surface area available for the leaching reaction. In the case of 0.3, the leaching rate is lowest, because of the difficulty in obtaining complete suspension.

4.3.8 Effect of Impeller-to-Tank Diameter Ratio

Figure 4.26 illustrates the effect of the impeller-to-tank diameter ratio on the dissolution of particles. As seen in this figure, there is an optimum ratio, which yields

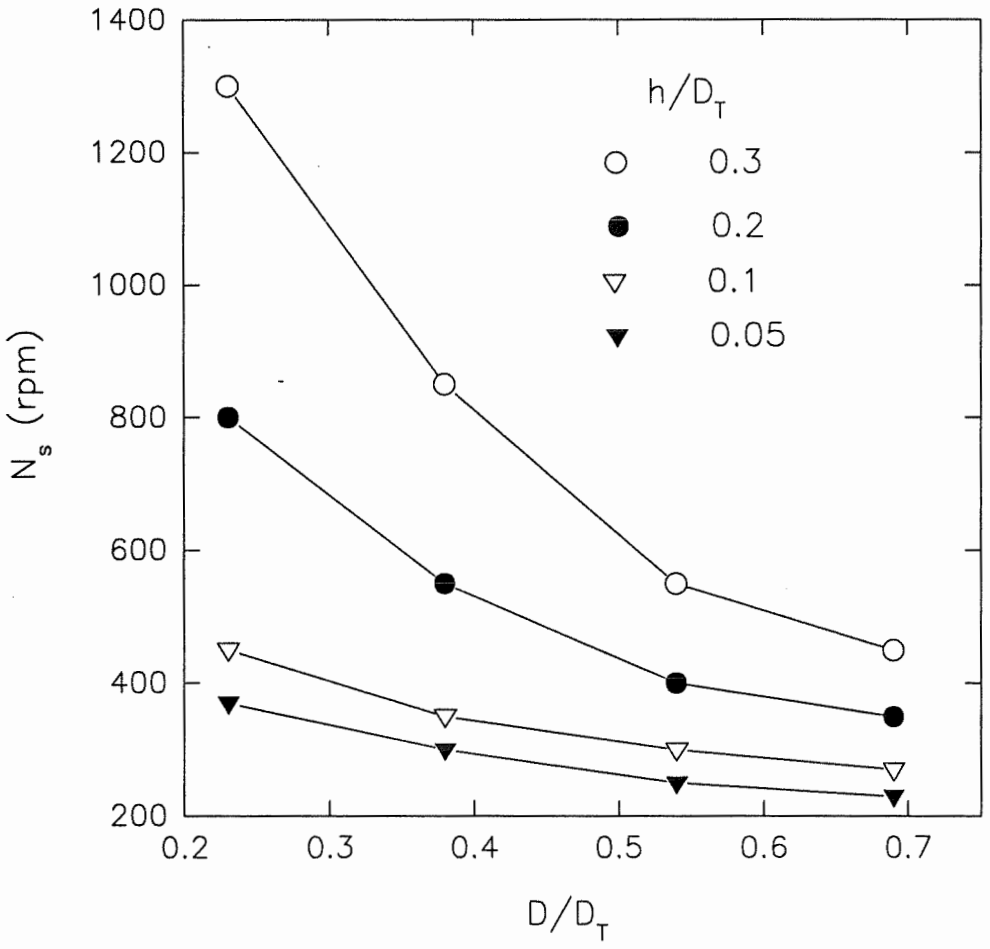

Figure 4.24 Effect of impeller-to-reactor diameter ratio and clearance ratio on the minimum agitation speed for complete suspension

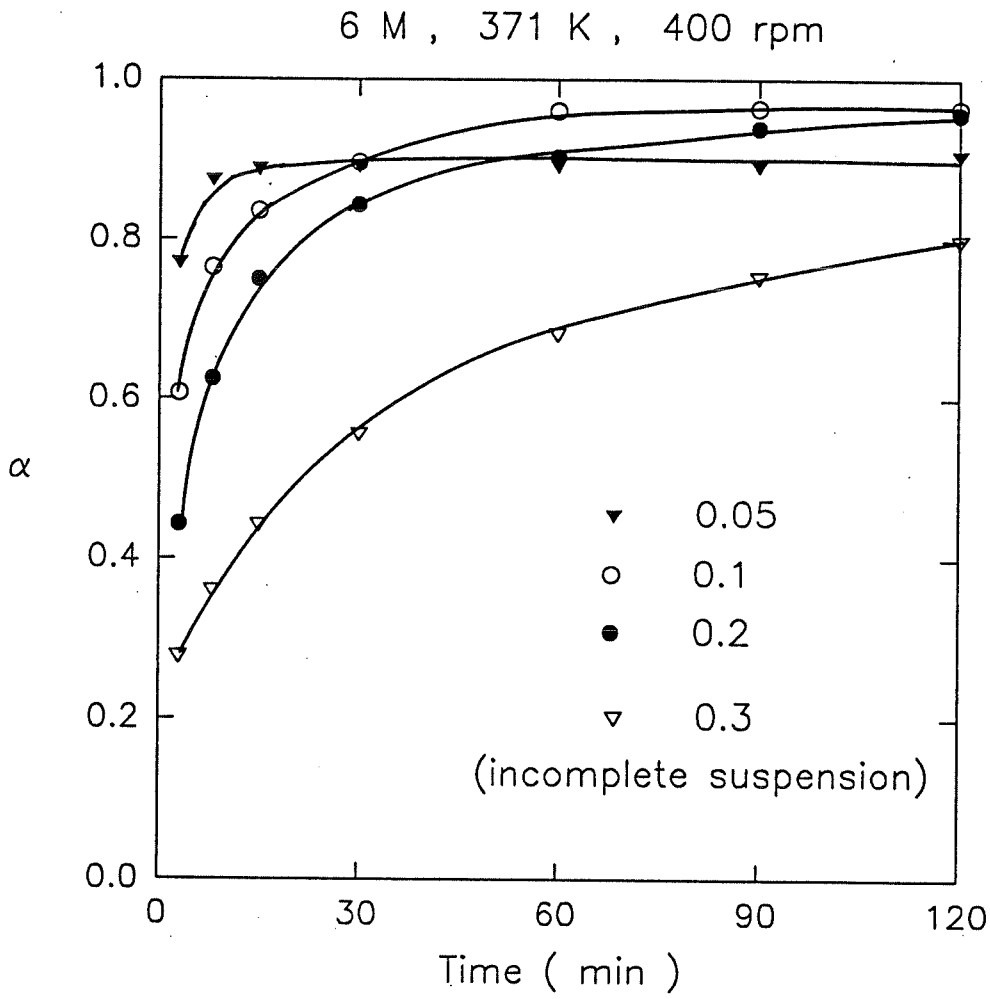

Figure 4.25 Effect of clearance ratio (h/D_T) on the dissolution of roasted zinc concentrates at $D/D_T = 0.38$.

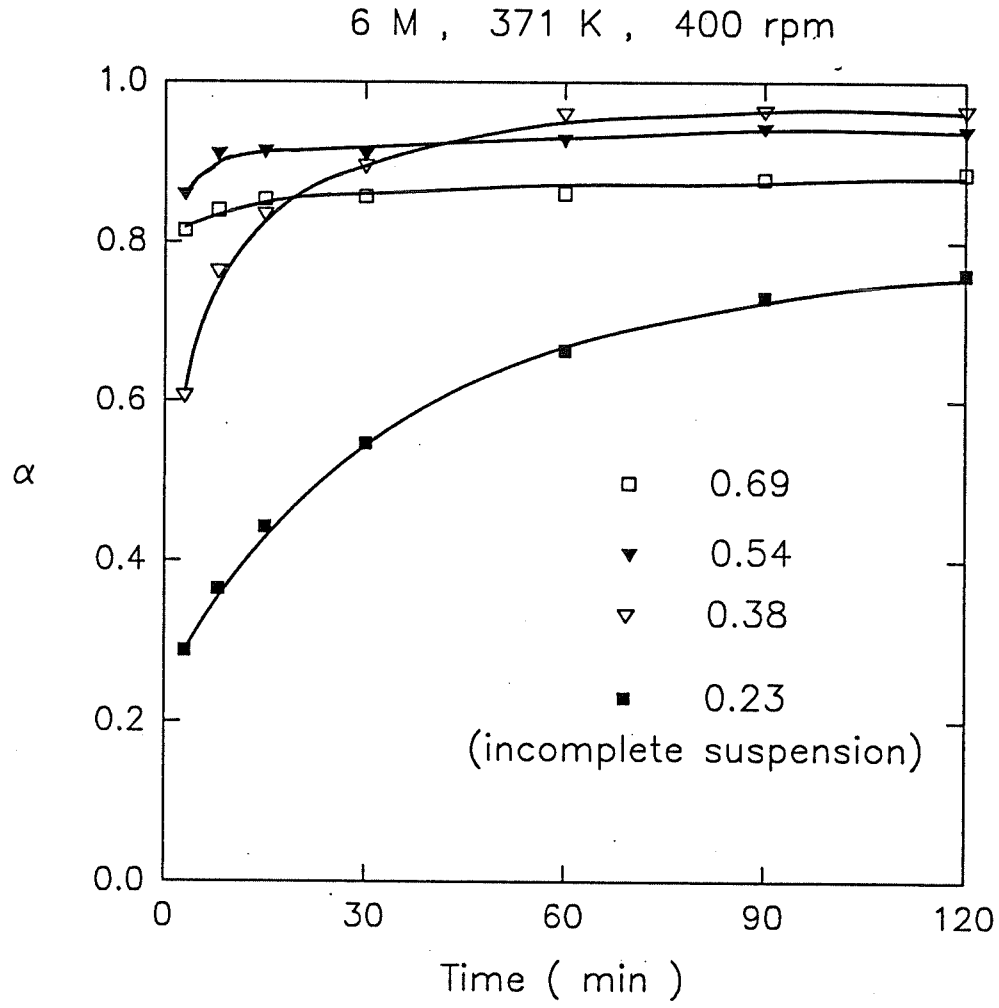

Figure 4.26 Effect of impeller-to-reactor diameter ratio (D/D_T) on the dissolution of roasted zinc concentrates at $h/D_T = 0.1$

the highest leaching rate. The leaching rate is, however, lowest for the value of 0.23, because it is difficult to obtain complete suspension.

CHAPTER 5

DISCUSSION

This chapter is divided into the same three parts as Chapter 4. Part one is the study of the kinetics of alkaline leaching of pure zinc oxide, and part two studies the kinetics of alkaline leaching of roasted zinc concentrates. Low particle concentrations were used in both studies. Part three studies the variables of leaching process using high concentration of particles.

5.1 LEACHING KINETICS OF PURE ZINC OXIDE

5.1.1 Data Treatment

In the dissolution of pure zinc oxide, as explained in section 2.2.1 and Figures 4.1 - 4.5, the particle size decreases, as the particles dissolve until they finally disappear. Thus, when spherical particles dissolve with no solid product layer build-up and with a fresh surface always exposed to the aqueous solution, a leaching rate relating the fraction reacted, α, and the leaching time, t, can be represented by the shrinking core model studied in detail in section 2.2.1.

$$1 - (1 - \alpha)^{1/3} = k\ t \qquad (5.1)$$

$$where: \quad k = \frac{k_r M \sigma C}{R \rho} \qquad (5.2)$$

Values of k can be obtained by plotting the linear relationship of the leaching time, t, vs $1 - (1 - \alpha)^{1/3}$. In most cases, the experimental data fit the shrinking core model extremely well, with linear correlation coefficients typically in excess of 0.99.

The specific rate constant, k_m, is given by

$$k_m = \frac{k R \rho}{M \sigma} \qquad (5.3)$$

For the spherical particles, the initial specific surface area is given by

$$S_o = \frac{3}{\rho R} \qquad (5.4)$$

Thus, the initial radius is related to the initial specific surface area by

$$R = \frac{3}{\rho S_o} \qquad (5.5)$$

Substitution of Equation (5.5) into Equation (5.3) gives:

$$k_m = \frac{3\,k}{M\,\sigma\,S_o} \qquad (5.6)$$

However, as shown in section 2.2.2, the rate-determining step can not be determined from kinetics alone if there is no build-up of solid product layer, since the shrinking core model with decreasing particle size has the same formula for the surface reaction control and the boundary layer diffusion control. Therefore, the effect of temperature and agitation speed on the observed kinetics must be evaluated in order to distinguish between the two.

5.1.2 Effect of Agitation Speed

Figure 5.1 analyzes the experimental results of Figure 4.1 with the shrinking core model. As illustrated in this figure, there exists an optimum agitation speed which yields the highest leaching rate. Over complete suspension, the leaching rate increased as the agitation speed increased from 400 to 600 rpm. However, it decreased as the agitation speed increased from 600 to 900 rpm.

The rate law for the dissolution process, which is controlled by diffusion through the boundary layer, is

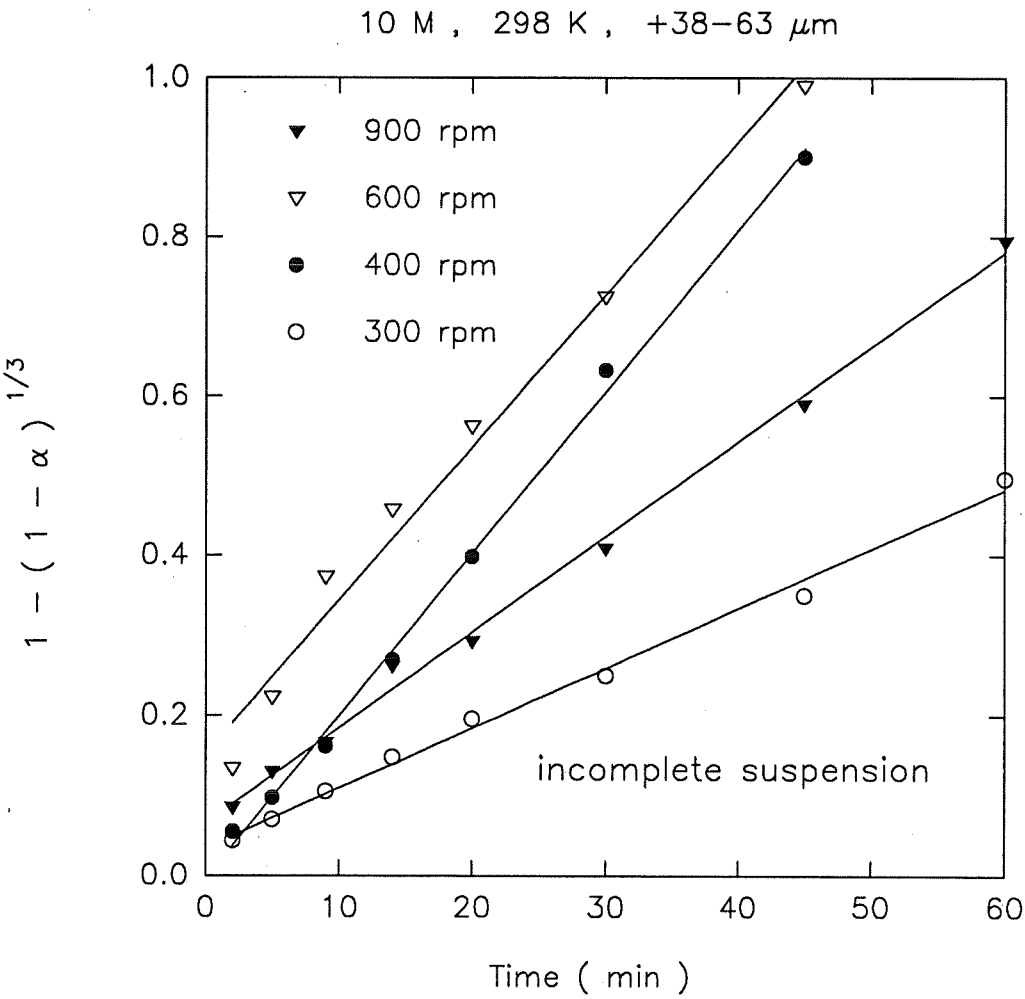

Figure 5.1 Effect of agitation speed on the leaching rate of pure zinc oxide analyzed by shrinking particle model

$$Leaching\ Rate \propto \frac{1}{\delta} \qquad (5.7)$$

Since the thickness of the boundary layer, δ, decreases with increasing agitation speed, the rate of dissolution consequently increased. However, further increases in the agitation speed increased the depth of the vortex, entraining air into the liquid (35,54). As a consequence, air pockets were formed and distributed between the liquid and the particles, interfering with the leaching reaction. Therefore the effective interfacial area between solution and particle is reduced.

5.1.3 Effect of Particle Size

Figure 5.2 is an analysis of the experimental results of Figure 4.3 using the shrinking core model. The slope is steeper as the particle size decreases.

The relationship between the leaching rate and the surface area of particles was analyzed. The rate constant, k, and the specific surface area, S_0, of each particle size were obtained from Figure 4.3 and Table 3.1, respectively, and are plotted in Figure 5.3, which shows a linear relationship between them. The results indicate that there is a proportionality between the leaching rate and the specific surface area.

In the classification of particles, it is very difficult to remove very fine particles

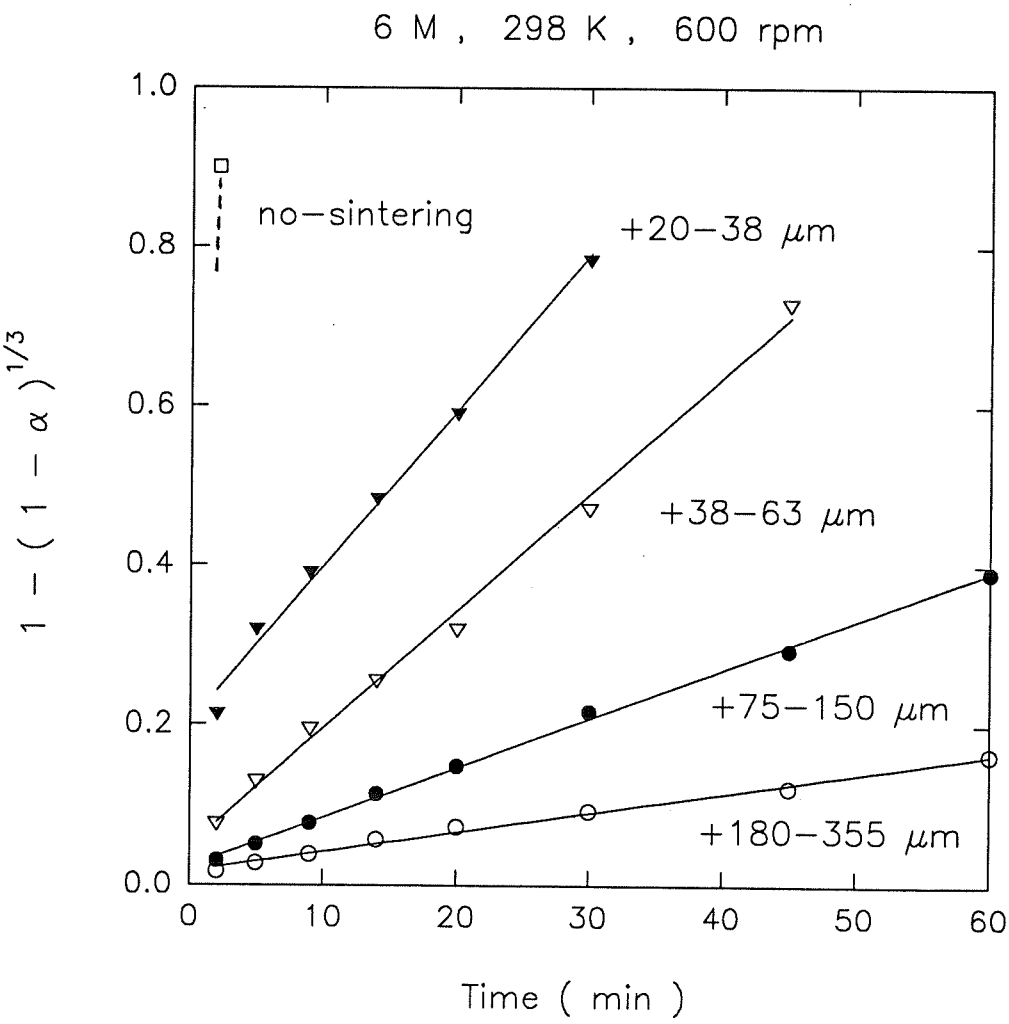

Figure 5.2 Effect of particle size on the leaching rate of pure zinc oxide analyzed by shrinking particle model

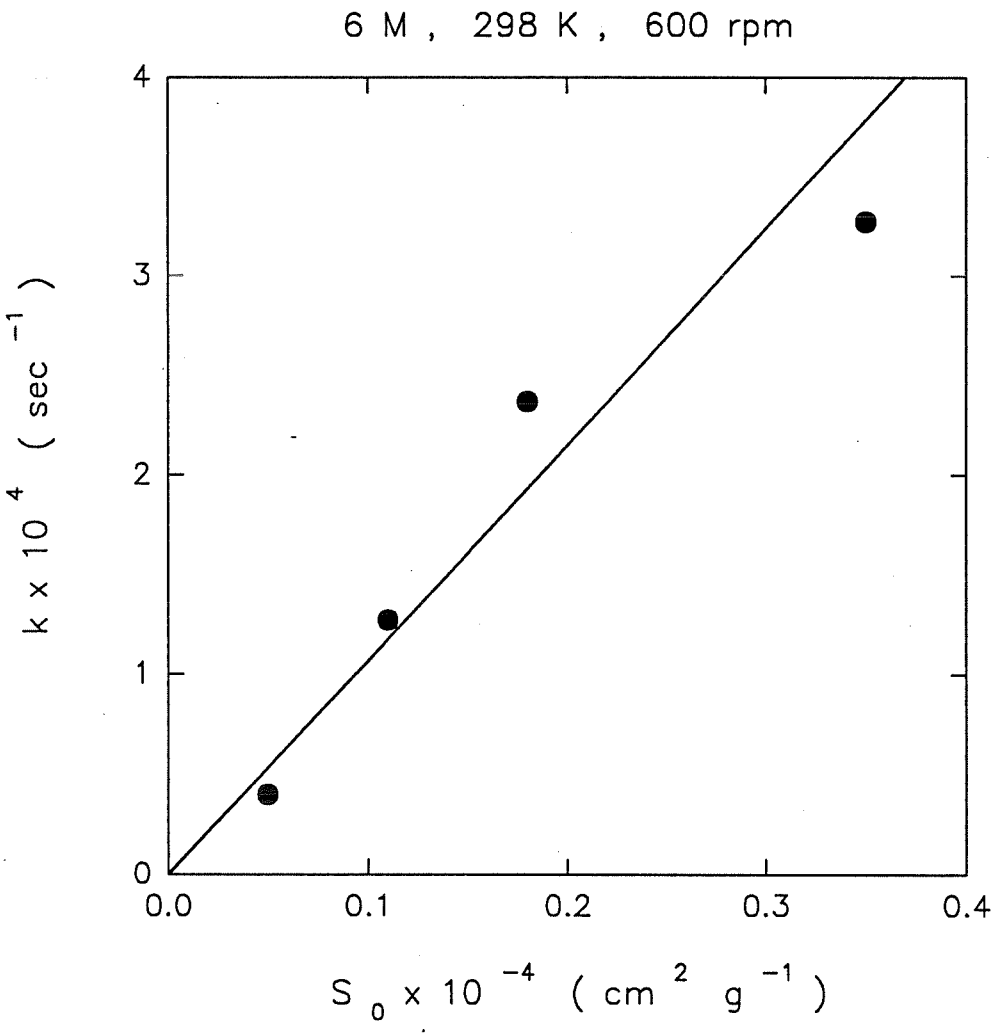

Figure 5.3 Relationship between rate constant and specific surface area

from each size fraction of Table 3.1, especially in the case of smaller-size fractions. These very fine particles result initially in an enhanced reaction rate, due to their rapid dissolution. The leaching rate therefore deviates from the origin, depending on the size of the particles, as seen in Figure 5.2.

5.1.4 Effect of NaOH Concentration

Figure 5.4 is an analysis of the experimental results of Figure 4.4 using the shrinking core model. The slope is steeper as the concentration increases; however, the proportionality decreases.

The relationship between the leaching rate and the NaOH concentration was analyzed. In Figure 5.5, the rate constants are plotted with respect to the concentration of the NaOH solution in order to calculate the dependence of leaching rate on the concentration. The plot of log k against log (NaOH) shows a marked change of slope with increasing NaOH concentration. Linear regression on the line gives the power dependencies of the leaching rate on NaOH concentration. These values decrease from 0.9 to 0.5 as the NaOH concentration goes from 4 to 10 M.

5.1.5 Effect of Temperature

In Figure 5.6, the experimental results of Figure 4.5 are analyzed using the shrinking core model. As can be seen in this figure, the slope becomes steeper as

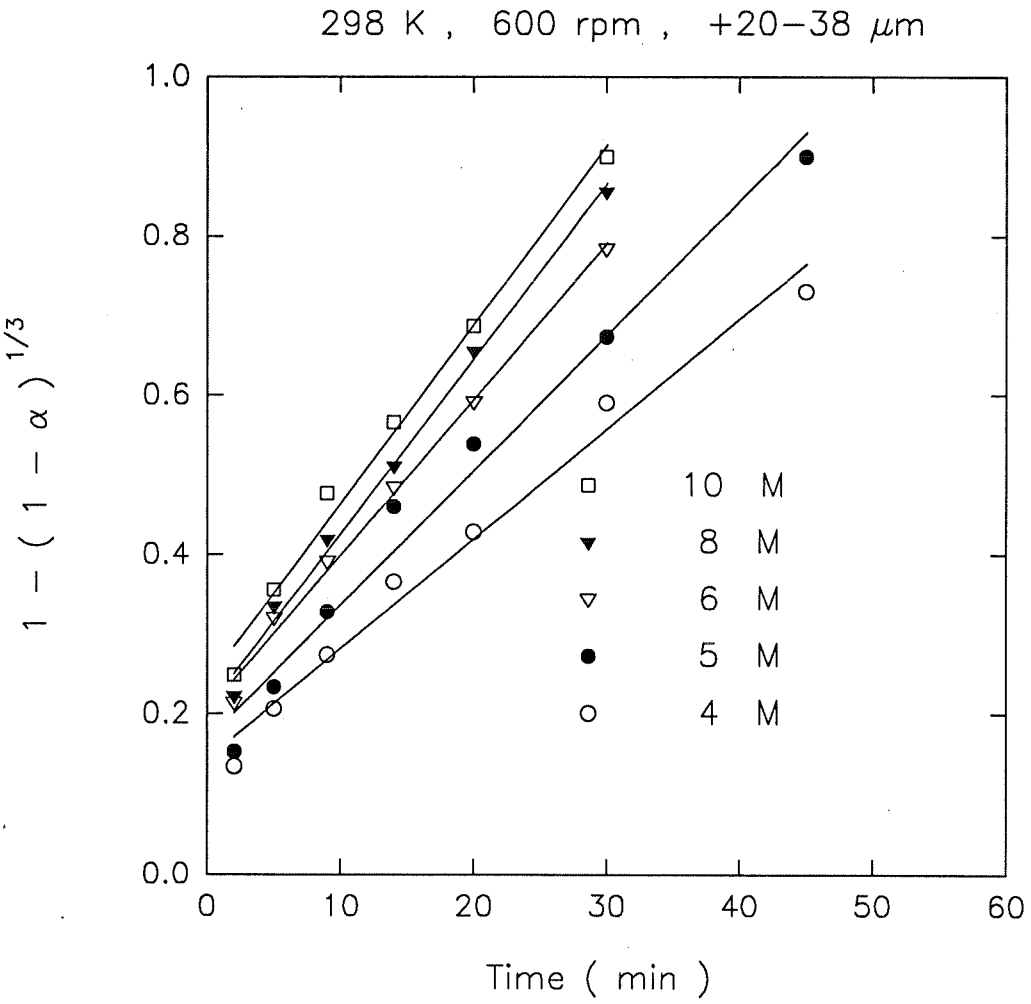

Figure 5.4 Effect of NaOH concentration on the leaching rate of pure zinc oxide analyzed by shrinking particle model

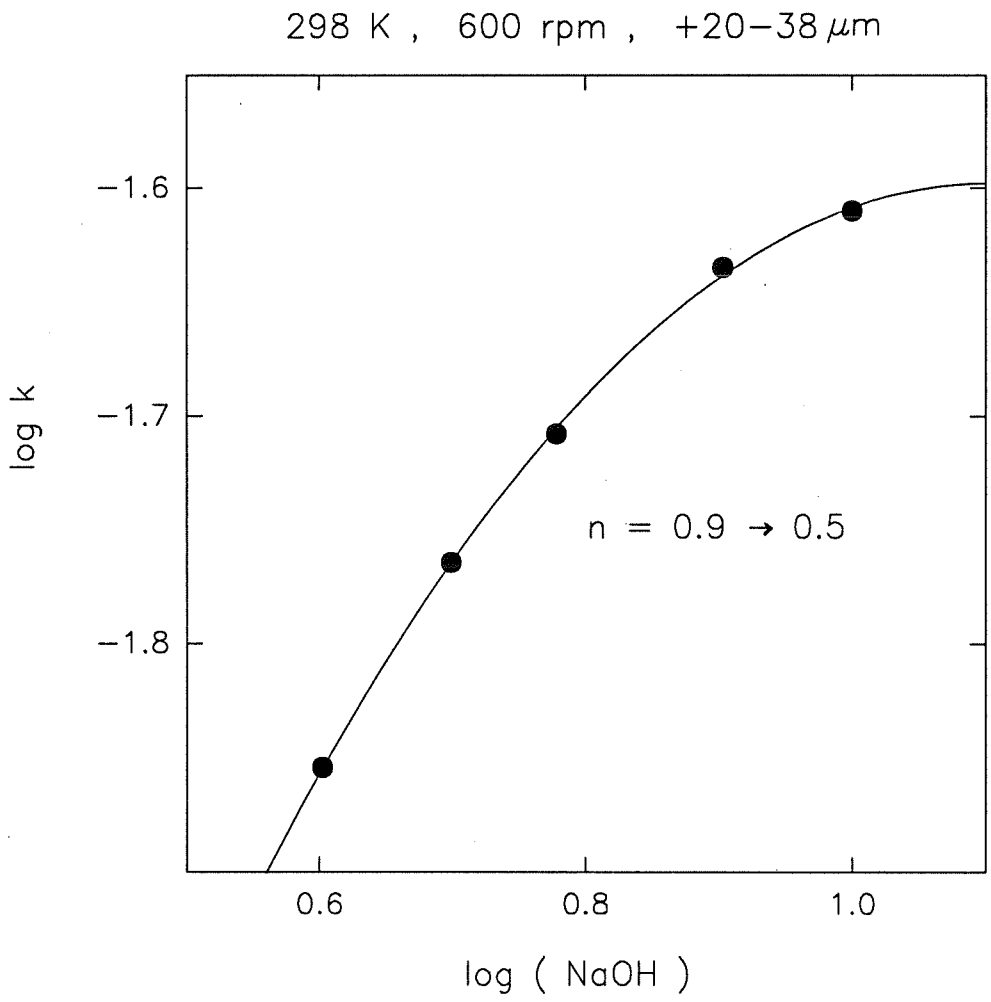

Figure 5.5 Change of power dependency on NaOH concentration

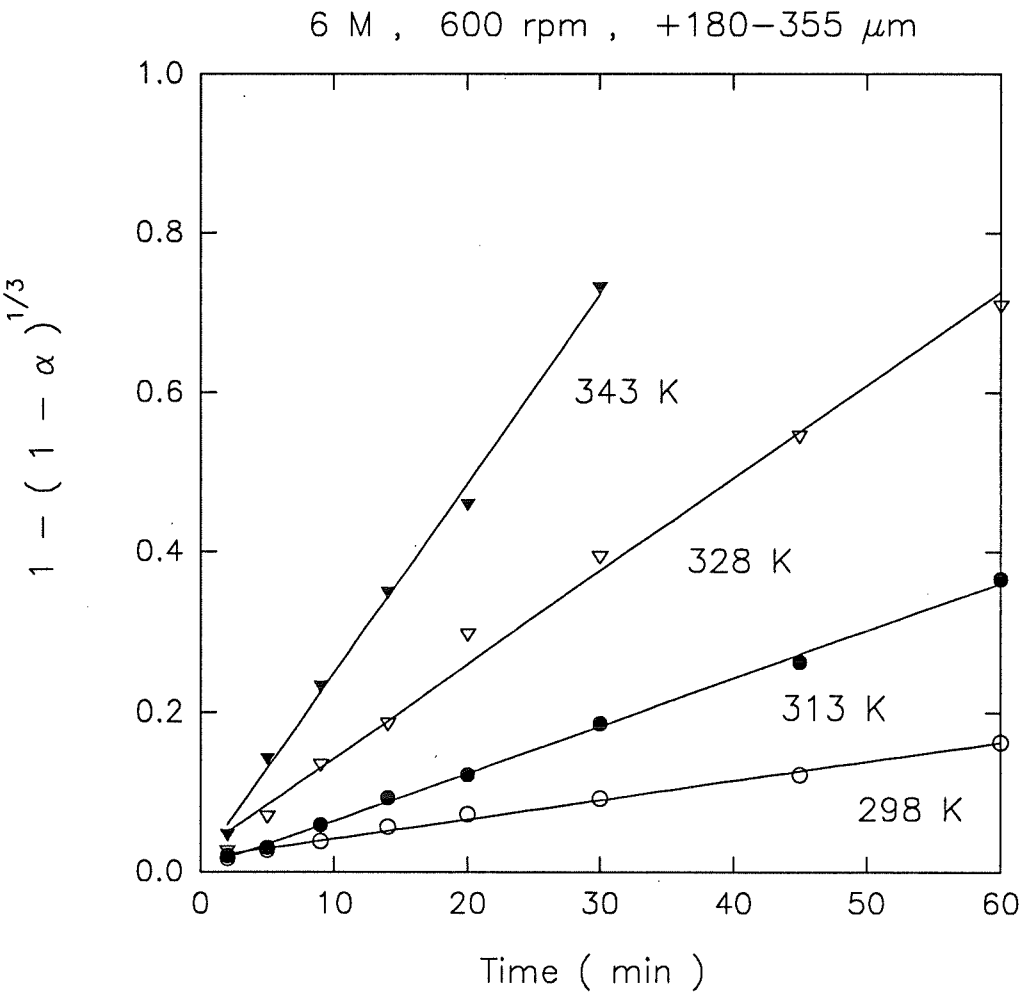

Figure 5.6 Effect of temperature on the leaching rate of pure zinc oxide analyzed by shrinking particle model

temperature increases.

The activation energy, 10 kcal/mol, was obtained using Figure 5.6, which is illustrated in Figure 5.7. The error range is $\pm$ 1 kcal/mol. According to Habashi (35), the activation energy of the diffusion-controlled process is characterized as being 1 to 3 kcal/mol, while it is usually greater than 10 kcal/mol for the surface-reaction-controlled process.

5.1.6 Mixed Control

The leaching process of zinc oxide in NaOH solution is governed by mixed control of surface reaction and boundary layer diffusion. This conclusion is based on the following experimental observations: 1) an activation energy of 10 kcal/mol was calculated, which indicates the surface reaction control; 2) the leaching rate was affected by agitation speed for complete suspension, which indicates the diffusion control.

Because the leaching rate is partially controlled by boundary layer diffusion, the contribution of diffusion on the leaching rate can be estimated separately by calculating the mass transfer coefficient. Mass transfer to suspended particles can be correlated by the following semi-empirical relationship as discussed in section 2.3.6:

$$k_t = \frac{D_d}{d}\left[2 + 0.6\left(\frac{d\,v_t}{\nu}\right)^{\frac{1}{2}}\left(\frac{\nu}{D_d}\right)^{\frac{1}{3}}\right] \qquad (5.8)$$

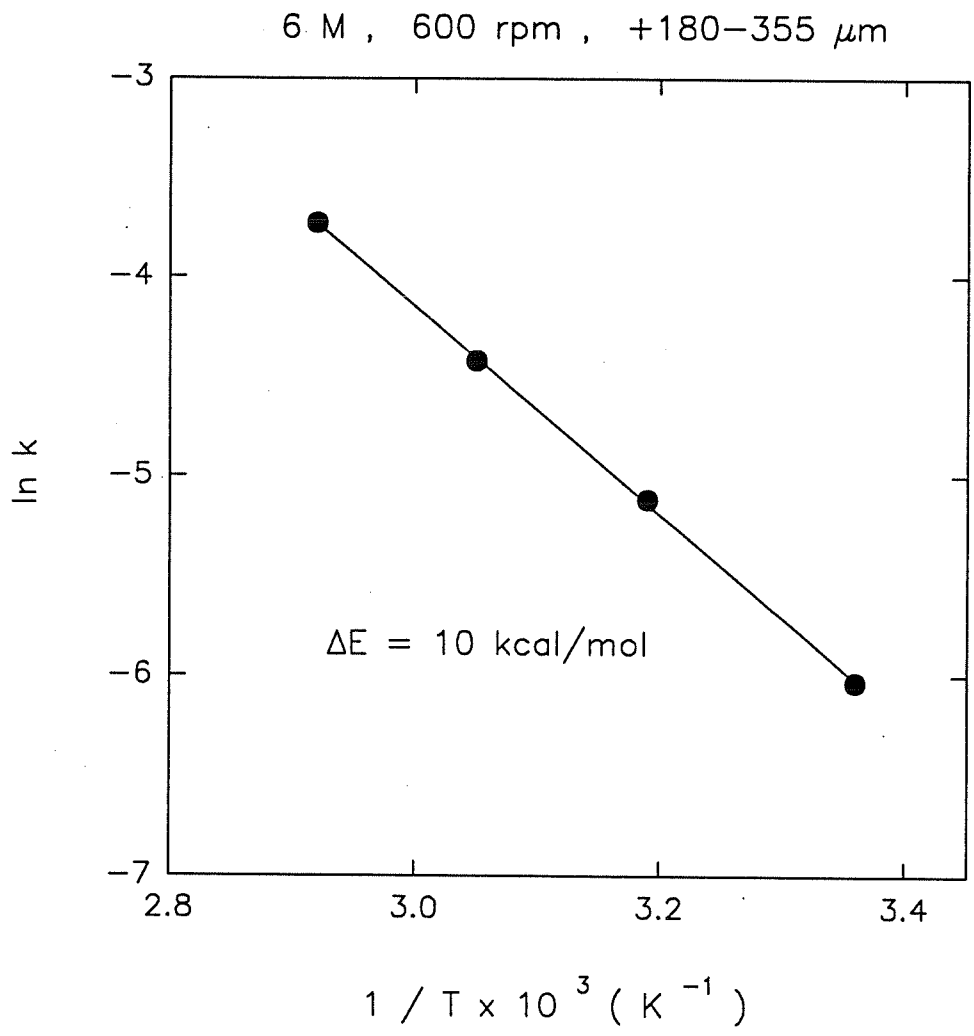

Figure 5.7 Activation energy from Arrhenius plot on the dissolution of pure zinc oxide

k_t may change with particle size, but it was calculated based on the initial particle size.

The free-settling terminal velocity, v_t, can be used for the slip velocity, v_s, of the particles. The free-settling terminal velocity is as follows (40,59):

$$v_t = \left[\frac{4\ g^2\ (\rho-\rho_f)^2\ d^3}{225\ \rho_f^2\ \nu}\right]^{0.33} \qquad (5.9)$$

The kinematic viscosity, ν, was obtained as a function of temperature, as shown in Figure 4.16.

If the leaching process is controlled by boundary layer diffusion, the ions involved are the OH^- and the zincate, $Zn(OH)4^{2-}$, since the global dissolution reaction of zinc oxide in NaOH solution can be expressed as follows:

$$ZnO + 2\ OH^- + H_2O = Zn(OH)_4^{2-} \qquad (5.10)$$

However, the diffusion coefficient of zincate is smaller than that of OH^- (87-89). This fact strongly suggests that the diffusion limitation is due to the zincate ion rather than to the OH^- ion. Therefore, in the case of diffusion control, the leaching rate is controlled by diffusion of the zincate ion. As explained in section 2.3.6, k_s can be obtained by multiplying 2 into k_t. Specific mass transfer coefficient can be calculated from the mass transfer coefficient by the following equation:

$$k_d = C_1 k_s \qquad (5.11)$$

Table 5.1 shows the results for the specific rate constant and the specific mass transfer coefficient. The diffusion boundary layer thicknesses of ZnO particles were calculated from the mass transfer coefficient. Boundary layer diffusion contributes to the leaching rate, because all values of these two specific constants have the same order of magnitude. As seen in this table, the relative importance of surface reaction control and diffusion control depends on their individual rates, which in turn depends on variables such as particle size, temperature and/or NaOH concentration. Increasing particle size, temperature and/or NaOH concentration make diffusion control more important. The change of the slope of power dependency on NaOH concentration is attributed to the importance of diffusion control as NaOH concentration increased.

In order to analyze the reaction steps producing zincate in the surface reaction control, the rate constant was plotted against the activity of NaOH, as shown in Figure 5.8. The NaOH activity was calculated as a product of the activity coefficient (90) and the corresponding molal concentration. The conversion of molar concentration to molal concentration was carried out by means of the published tables (85).

The rate constant, k, vs activity curve shown in Figure 5.8 is similar to the behavior for the leaching of cuprite in perchloric acid and beryllia in all acids (91).

Table 5.1 Calculation of specific rate constant and specific mass transfer coefficient (600 rpm)

T	C	d_0	k x 10^4	k_m x 10^9	k_s x 10^3	δ x 10^4	k_d x 10^9
K	M		sec^{-1}		cm sec^{-1}	cm	
		μm		mol cm^{-2} sec^{-1}			mol cm^{-2} sec^{-1}
298	6	20-38	3.37	3.64	9.60	3.5	3.24
298	6	38-63	2.37	4.85	7.77	4.4	3.08
298	6	75-150	1.27	4.26	6.24	5.5	2.02
298	6	180-355	0.40	2.95	5.52	6.2	1.65
298	6	180-355	0.40	2.95	5.52	6.2	1.65
313	6	180-355	1.00	7.37	9.19	6.0	3.49
328	6	180-355	2.00	14.70	13.13	5.7	4.98
298	6	20-38	3.37	3.64	9.60	3.5	3.24
298	8	20-38	3.87	4.08	6.84	3.7	2.46
298	10	20-38	4.09	4.31	4.41	3.8	1.67

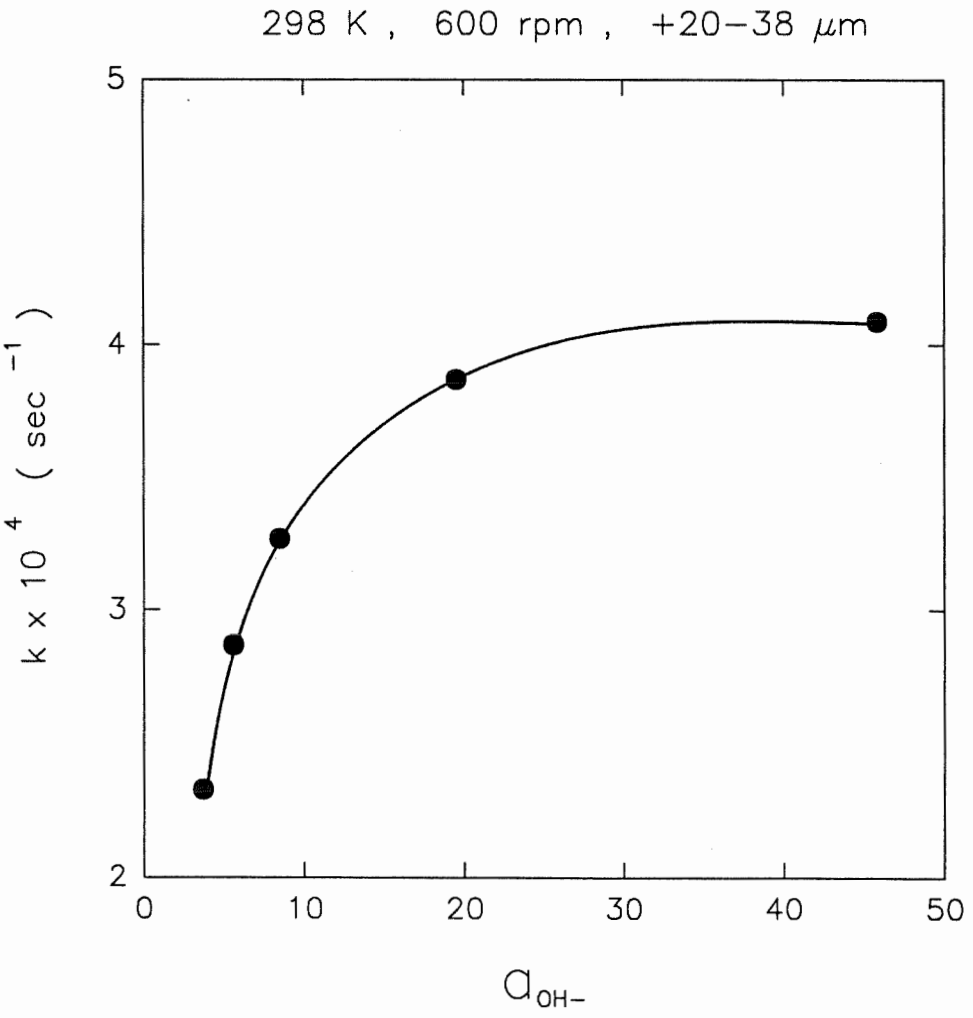

Figure 5.8 Relationship between rate constant and NaOH activity

Warren et al. (91) proposed the acid dissolution mechanism of these oxides according to the following equation:

$$Rate = \frac{k_1^* K_1^* a_{H^+}}{1 + K_1^* a_{H^+}} \qquad (5.12)$$

where k_1^* and K_1^* represent the equilibrium constant and the rate constant for the formation and desorption of the protonated complex, respectively.

The same equation can be altered to describe the dissolution of zinc oxide in NaOH solution according to Figure 5.8, as follows:

$$Rate = \frac{k_1 K_1 a_{OH^-}}{1 + K_1 a_{OH^-}} \qquad (5.13)$$

In this case, k_1 and K_1 represent the equilibrium constant and rate constant for the formation and desorption of the hydroxylated complex, respectively.

Therefore, the simple and approximate dissolution steps could be represented as follows:

$$[ZnO]^{\square} + H_2O \rightleftharpoons [Zn(OH)_2]^{\square} \qquad (5.14)$$

$$[Zn(OH)_2]^{\square} + OH^- \rightleftharpoons [Zn(OH)_3^-]^{\square} \qquad (5.15)$$

$$[Zn(OH)_{3-}]^{\square} \rightleftharpoons [\ ]^{\square} + Zn(OH)_3^- \qquad (5.16)$$

$$Zn(OH)_3^- + OH^- \rightleftharpoons Zn(OH)_4^{2-} \qquad (5.17)$$

where: $[\ ]^{\square}$ indicates the surface of the ZnO particle.

According to this scheme, the desorption reaction, i.e. Equation (5.16), is considered to be important.

5.1.7 Prediction of Leaching Time

Under mixed control of the dissolution of spherical pure zinc oxide, the leaching time required to attain a certain conversion is obtained as follows:

$$t_r = \frac{\rho}{(k_o M \sigma)} R C^{-n} \exp\left(\frac{\Delta E}{R T}\right) [1 - (1 - \alpha)^{\frac{1}{3}}] \qquad (5.19)$$

Substitution of Equation (5.5) into Equation (5.18) gives:

$$t_r = \left(\frac{3}{k_o M}\right) S_o^{-1} C^{-n} \exp\left(\frac{\Delta E}{R T}\right) [1 - (1 - \alpha)^{\frac{1}{3}}] \qquad (5.19)$$

k_o was obtained by extrapolating the Arrhenius plot, and ΔE was obtained from the effect of temperature. n was determined to be 0.6 from the effect of concentration of NaOH solution.

Now, t_r is given by

$$t_r = 2.1 \times 10^{-4} S_o^{-1} C^{-0.6} \exp\left(\frac{5170}{T}\right) \left[1 - (1-\alpha)^{\frac{1}{3}}\right] \quad (5.20)$$

The leaching time predicted by the mixed kinetic equation and that obtained from experimental data are compared under various conditions. Figure 5.9 shows the comparison of the calculated and the experimental leaching time between conversion and time as a function of particle size. The leaching time decreased as the particle size decreased. Figure 5.10 shows the comparison as a function of temperature. The leaching time decreased as the temperature increased.

It is very difficult to remove very fine particles in small size fractions of the particles. These very fine particles result in an enhanced leaching rate. Moreover, small particles have more irregular spherical form than large particles. Therefore, the calculated leaching times of larger particles were fitted well rather than those of small particles.

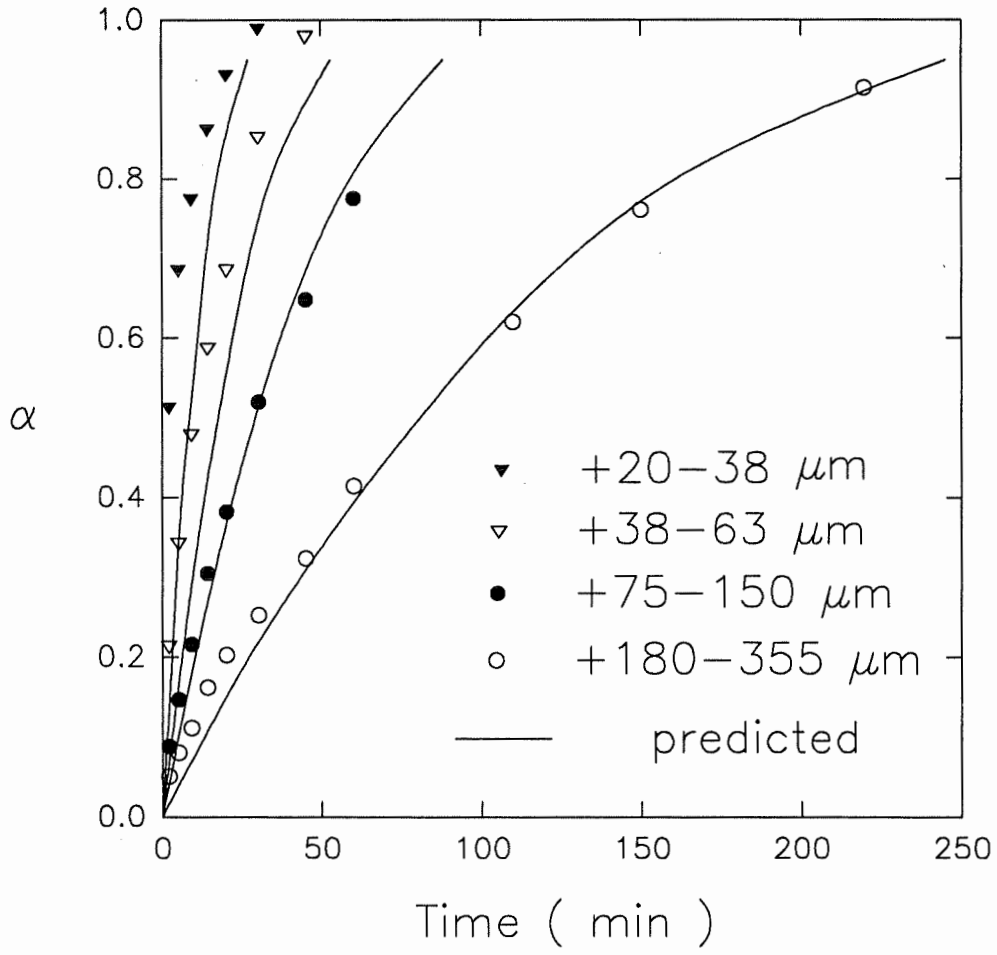

Figure 5.9 Comparison of the calculated and the experimental leaching time as a function of particle size

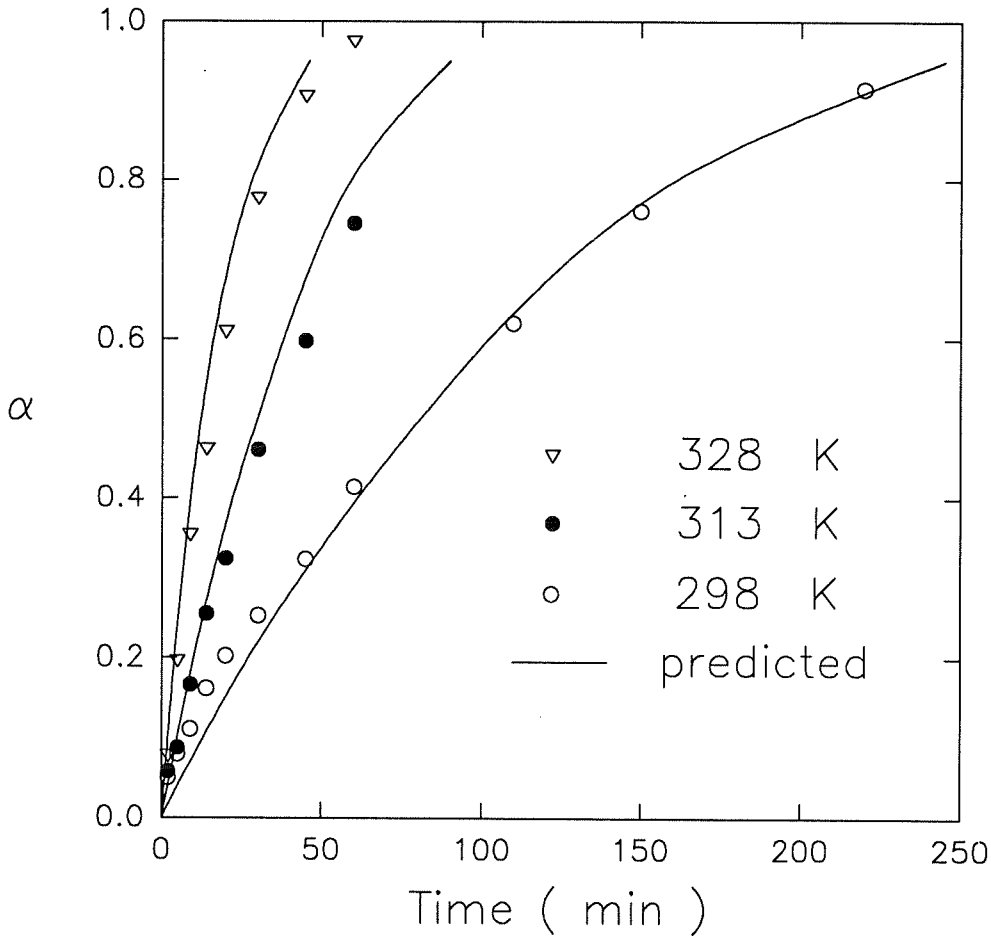

Figure 5.10 Comparison the calculated and the experimental leaching time as a function of temperature

5.2 LEACHING KINETICS OF ROASTED ZINC CONCENTRATES

5.2.1 Data Treatment

In the reaction of iron-containing zinc oxide, as seen in Figures 4.6, 4.7, 4.10 and 4.11, for complete suspension, the leaching rate is independent of the agitation speed and NaOH concentration. These results indicate the formation of a solid product layer. Moreover, as seen in Figure 4.15, the particle size does not diminish after the leaching proceeds. This result also indicates the formation of a solid product layer.

Thus, for the spherical particles, when a particle reacts with solid product layer build-up and with an active surface always exposed to the aqueous solution, the leaching rate related to the fraction reacted, α, and the leaching time, t, can be represented with the shrinking core model without diminishing the particle size discussed in detail in section 2.2.3.

As seen in Figures 4.6 and 4.7, diffusion through the fluid boundary layer is no longer the rate-determining step, because the leaching rate is independent of the agitation speed. Hence, the following shrinking core models are available, depending on control of diffusion through the solid product layer, surface reaction control or mixed control.

For surface reaction control,

$$1 - (1 - \alpha)^{\frac{1}{3}} = K_C\, t \qquad (5.21)$$

$$where: \quad K_C = \frac{M\, \sigma\, k_c\, C}{\rho\, R} \qquad (5.22)$$

For control by diffusion through a solid product layer,

$$1 - \frac{2}{3}\,\alpha - (1 - \alpha)^{\frac{2}{3}} = K_D\, t \qquad (5.23)$$

$$where: \quad K_D = \frac{2\, \sigma\, M\, D_e\, C}{\rho\, R^2} \qquad (5.24)$$

As seen in Equations (5.21) - (5.24), in the surface reaction control, the leaching time, t, is proportional to the initial mean radius of the particle, R, whereas in the case of control by diffusion through a solid product layer, it is proportional to R^2.

Equations (5.21) and (5.23) were developed on the assumption that a single resistance controls the leaching rate throughout the leaching process. However, the relative importance of the diffusion and the surface reaction may vary as the reaction progresses. Hence, as discussed in section 2.2.4, to account for the simultaneous action for the control by diffusion through the solid product layer and by the surface reaction is straightforward, since they act in series and are all linear in the concentration of the

solution.

$$[1-\frac{2}{3}\alpha-(1-\alpha)^{\frac{2}{3}}]+A[1-(1-\alpha)^{\frac{1}{3}}]=K_M\ t \qquad (5.25)$$

$$where:\quad K_M = \frac{M\ \sigma\ k\ D_e\ C}{\rho\ R^2} \qquad (5.26)$$

$$A = \frac{2\ D_e}{R\ k_c} \qquad (5.27)$$

The experimental data should yield a straight line when the left side of Equations (5.21), (5.23) and (5.25) is plotted against time t. α represents the fraction reacted at time t. K_C, K_D and K_M are apparent rate constants.

5.2.2 Rate-Determining Step

In the case of the formation of a solid product layer in the shrinking core model, the rate-determining step is the surface reaction during the early stage of the leaching process, whereas in later stage it is the diffusion through the solid product layer. The solid product layer is built up after the surface reaction and diffusion through it becomes important. Thus, it changes from the surface reaction to diffusion through the solid product layer as time proceeds.

The experimental results of Figure 4.9 were analyzed using the above theory.

Verification of the order and of possible changes in the rate-determining step during the leaching process may be obtained by determining how the dissolution of the roasted zinc concentrates is influenced by particle size.

Rewriting Equations (5.21) and (5.22) gives:

$$\log t = \log A_1 + \log R \tag{5.28}$$

$$where: \quad A_1 = \frac{[1 - (1 - \alpha)^{\frac{1}{3}}]\ \rho}{\sigma\ k_c\ C\ M} \tag{5.29}$$

If the leaching rate is controlled by the surface reaction, as seen in Equation (5.28), a plot of log t vs log R will give a slope of one.

Similarly, rewriting Equations (5.23) and (5.24) gives:

$$\log t = \log A_2 + 2 \log R \tag{5.30}$$

$$where: \quad A_2 = \frac{\rho\ [1 - \frac{2}{3}\ \alpha - (1 - \alpha)^{\frac{2}{3}}]}{2\ \sigma\ D_e\ C\ M} \tag{5.31}$$

If the leaching rate is controlled by diffusion through the product layer, as seen in Equation (5.30), a plot of log t vs log R will give a slope of two.

In order to verify the order and changes in the rate-determining step, the time needed to achieve the same fractional conversion for each particle size was obtained from Figure 4.9 against log R. The results are shown in Table 5.2. Based on this table, log t was plotted against log R, which is shown in Figure 5.11. Each line represents a constant value of α for each particle size. As seen in this figure, the slope is changed from two to one; the rate-determining step is changed from diffusion through the solid product layer to the surface reaction. Thus, during the early stage of the leaching process, the leaching rate is controlled by diffusion through the solid product layer, whereas in the later stage, it is controlled by the surface reaction.

5.2.3 Extension of Shrinking Core Model

As seen in Figure 5.11, our analysis of the experimental results could be fitted well mathematically with the shrinking core model. However, practically, two questions arise using this established shrinking core model with the results of this study.

First, at the beginning of the leaching process, the solid product layer does not exist; nevertheless, as presented in Figure 5.11, the equation for diffusion through the solid product layer fitted the results.

Table 5.2 Time needed to achieve the same fractional conversion for each particle size

log R	-2.8239	-2.6990	-2.6021	-2.4559	-2.2596
α			log t		
0.4			0.5052	0.8808	1.3463
0.5	0.3617	0.6435	0.7482	1.0828	1.5065
0.6	0.6990	0.8325	1.0128	1.2743	1.6325
0.7	0.9590	1.0607	1.2695	1.5211	1.7497
0.8	1.2529	1.4942	1.6031	1.7332	

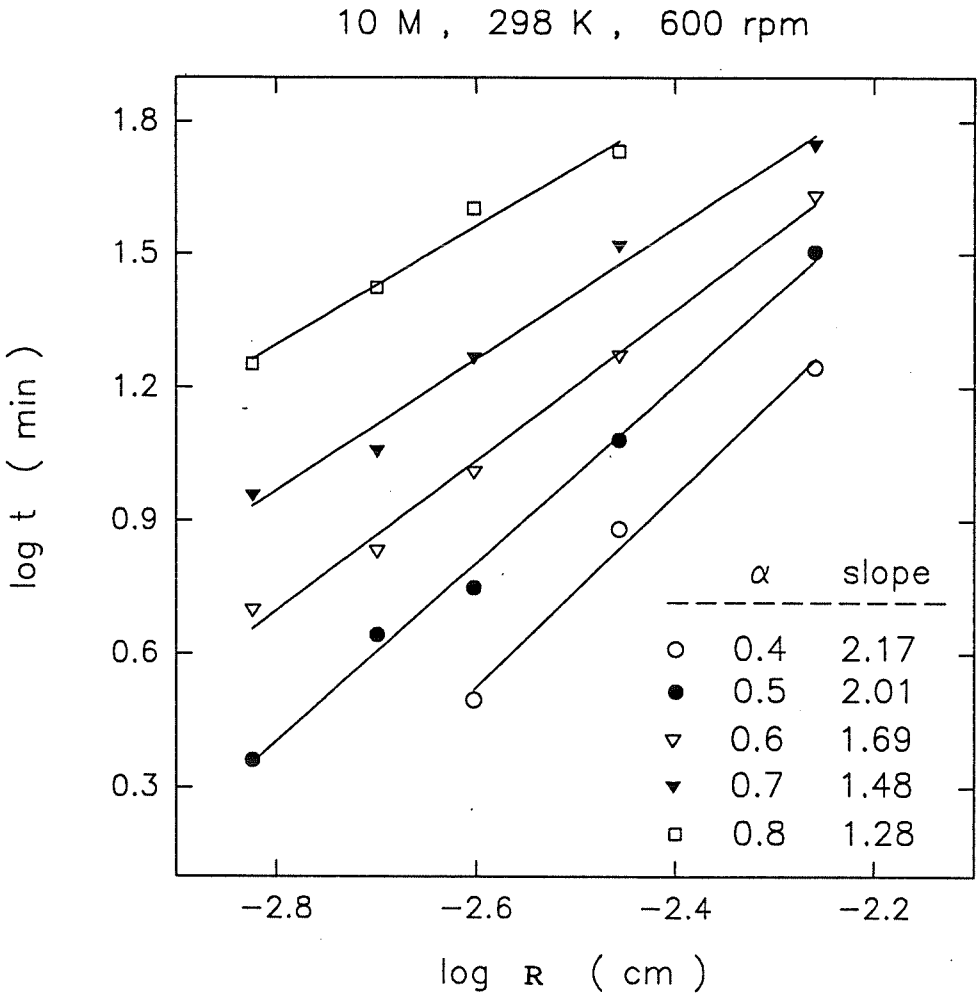

Figure 5.11 Times to reach a given fractional conversion based on the original particle size of roasted zinc concentrates

Second, as presented in Figure 5.11, in the later stage, i.e., even after build-up of the solid product layer, the rate-determining step changed to the surface reaction. Thus, even if the solid product layer is formed at certain time, diffusion through the solid product layer can not control the leaching rate. What controls the leaching rate during the early stage of the leaching rate ?

The solid layer of zinc ferrite provides resistance to diffusion of the fluid during the early stage of the leaching process. As seen in Figure 4.15, the particle size remained unchanged, and iron oxide still existed outside of the particle, enclosing the zinc oxide. Moreover, as seen in Figure 4.14 and Table 4, the dissolution of iron oxide is negligible. Thus, before leaching proceeded, a solid layer of zinc ferrite existed outside of the particle enclosing the zinc oxide.

It is suggested [22,23] that zinc ferrite forms outside of the particle during the roasting of zinc sulfide concentrates in three stages. The first stage involves the selective diffusion of iron to the particle surface, resulting in the formation of an iron oxide shell enclosing a largely unreacted zinc sulfide kernel. In the second stage, this kernel is oxidized to form zinc oxide. In the third stage, the iron oxide reacts with the zinc oxide to form zinc ferrite.

However, replacing the reactant solid layer of zinc ferrite as a diffusion barrier

with the solid product layer of the shrinking core model gives rise to two questions.

First, the fluid should diffuse to zinc oxide through the solid layer of zinc ferrite as in the shrinking core model, since the solid product layer is inert. If this happens, the rate-determining step can not be changed as the leaching process proceeds.

Second, in the shrinking core model, a sharp interface exists between two phases, with the result that the fluid cannot diffuse into the particle. Only solid diffusion could occur, but its rate is too slow to apply to our results.

Thus, the liquid should diffuse through the solid layer of zinc ferrite to arrive zinc oxide and during the diffusion, zinc oxide contained in the solid layer of zinc ferrite must be dissolved. In order to solve the above problems, the porosity of the particles should be considered.

In a porous solid, the mathematical expression for diffusion through a solid reactant layer is the same as for a solid product layer, since the fluid concentration has a gradient within the layer and drops to a very small value at the interface. Thus, when diffusion through the solid layer is rate-determining, there is no way to determine which of the two layers presents the resistance to the diffusion [39,92]. Therefore, diffusion through any solid layer can be the rate-determining step in the shrinking core model,

since the diffusion through a solid reactant layer can be extended to contain diffusion through the solid product layer.

The leaching process of the porous solid with the fluid involves the parallel occurrence of the surface reaction and diffusion through the solid layer. Thus, the effect of particle size on the leaching rate is vague, since the fluid concentration is constant everywhere; the reaction occurs uniformly throughout the particle if the surface reaction presents the major resistance to the overall progress of the process. However, if diffusion through the solid layer presents the major resistance, the process occurs in a narrow boundary of the interface, where the fluid concentration becomes zero. This situation corresponds to the shrinking core model. Under this situation, the measurement of an effective diffusivity makes it possible to predict the reaction rate. Moreover, in surface reaction control where the particle contains a narrow pore, the particle size affects the leaching rate.

Therefore, the shrinking core model can be applied to particles with any kind of porosity, in keeping with the topochemical reaction, since the sharp interface can be extended to include a porosity, which keeps the effect of particle size on the leaching rate.

5.2.4 Analysis with Extended Shrinking Core Model

The experimental results were analyzed using the extended shrinking core model, according to the rate-determining step as discussed in the above sections. All of the results were in good correlation with diffusion through the solid layer and the surface reaction. Figures 5.12.a and 5.12.b show the analysis of the results of Figure 4.9 with the extended shrinking core model. The two functions, $1 - 2/3\ \alpha - (1 - \alpha)^{2/3}$ in Equation (5.23), i.e., diffusion through the solid layer and $1- (1 - \alpha)^{1/3}$ in Equation (5.21), i.e., the surface reaction, are plotted against leaching time, t in Figure 5.12.a and 5.12.b, respectively.

As seen in Figure 5.12.a, during the early stage of the leaching process, the leaching rate is linear with respect to diffusion through the solid layer, while as seen in Figure 5.12.b, in the later stage, it is linear with respect to the surface reaction. Thus, as seen in Figure 5.12.c, it would appear that the rate-determining step is an additivity of diffusion through the solid layer and the surface reaction. The slopes of the lines are steeper as the particle size decreases. However, neither graph gives a linear relationship throughout the dissolution process.

Figure 5.13 also illustrates the analysis of the experimental results of Figure 4.12 with the extended shrinking core model. As seen in this figure, the rate-determining step is an additivity of diffusion through the solid layer and the surface reaction, which give

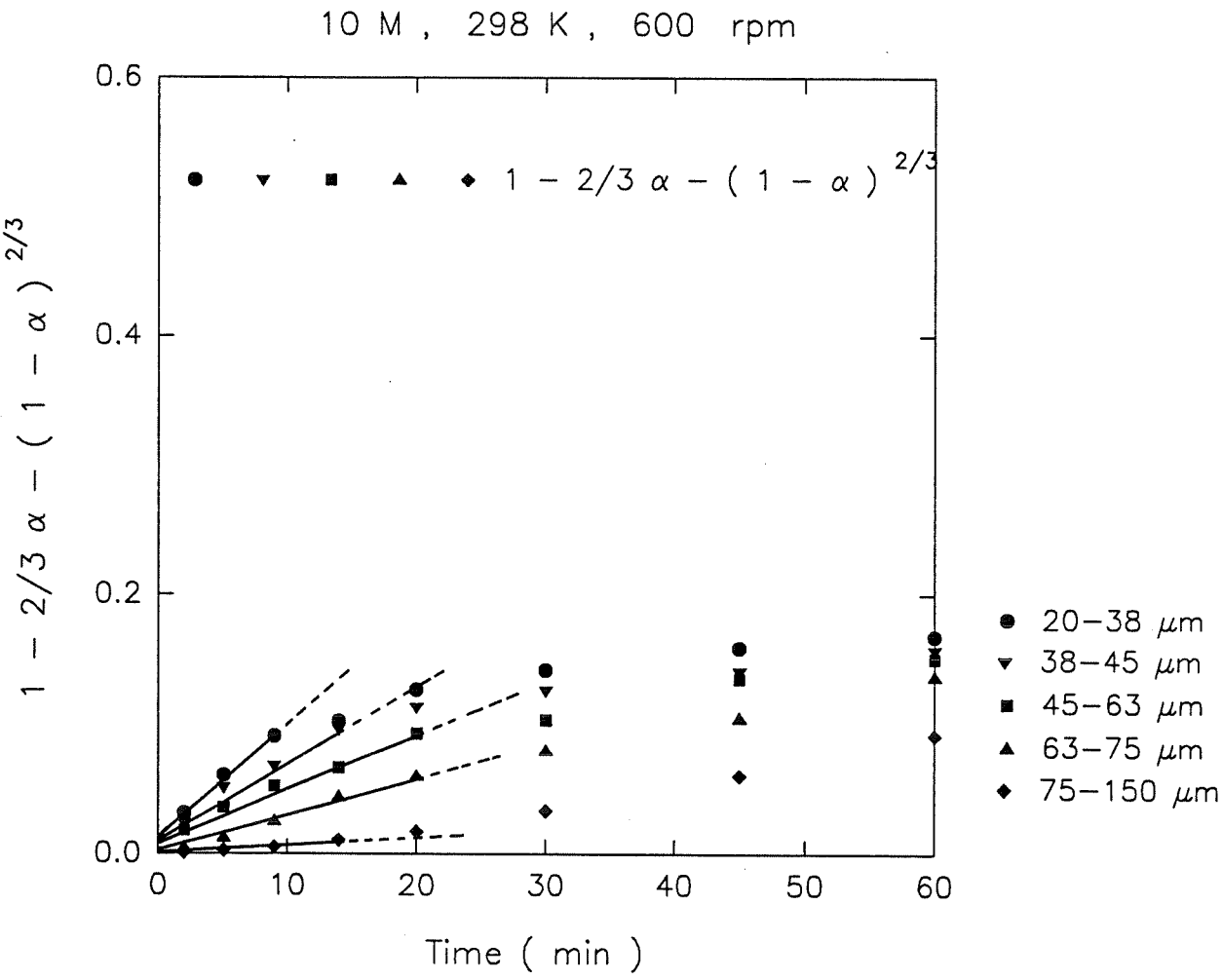

Figure 5.12.a Analysis of experimental results using Equation (5.23) of the shrinking core model as a function of particle size (data from Figure 4.9)

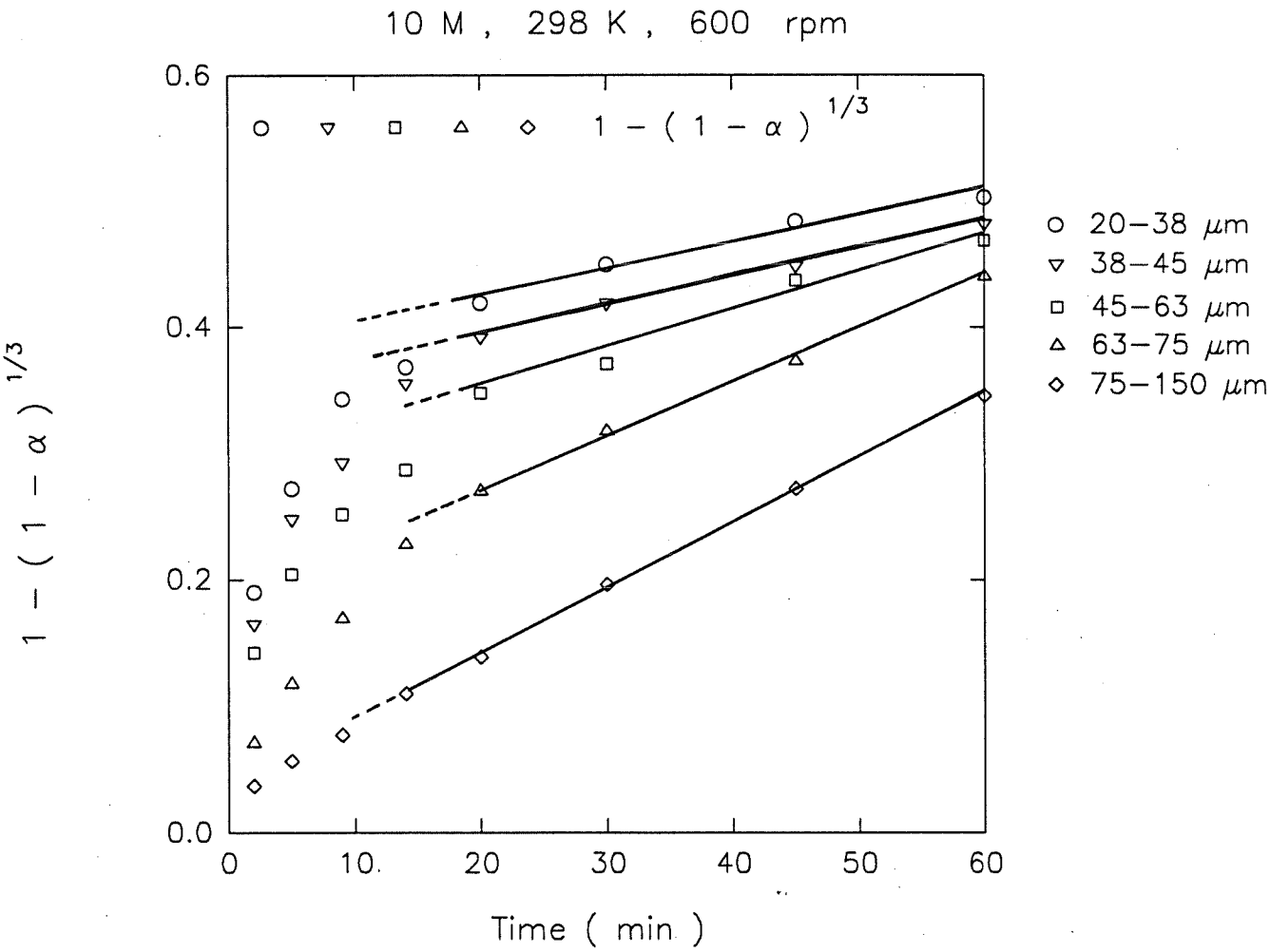

Figure 5.12.b Analysis of experimental results using Equation (5.21) of the shrinking core model as a function of particle size (data from Figure 4.9)

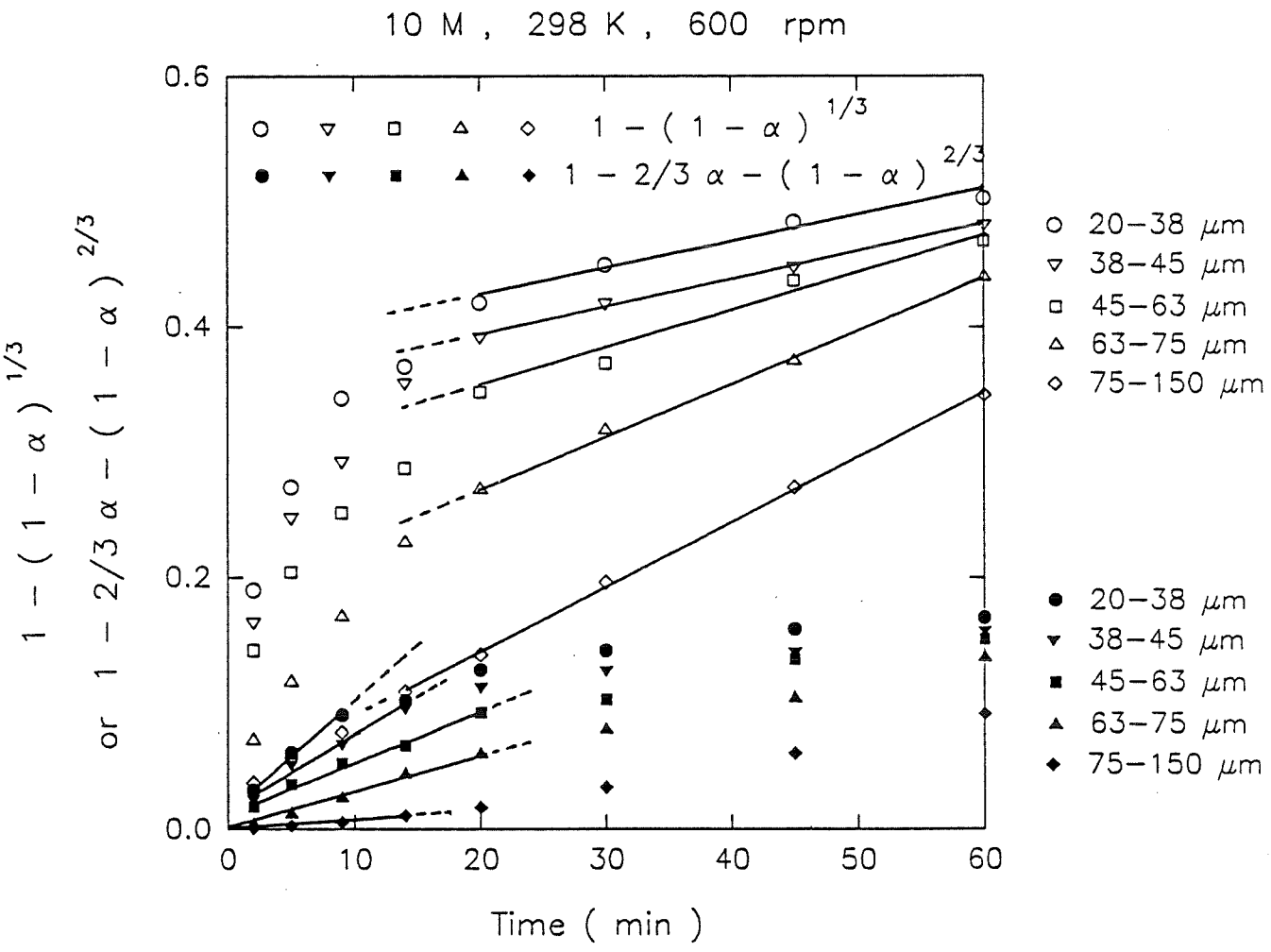

Figure 5.12.c Analysis of experimental results by the shrinking core model as a function of particle size (data from Figure 4.9)

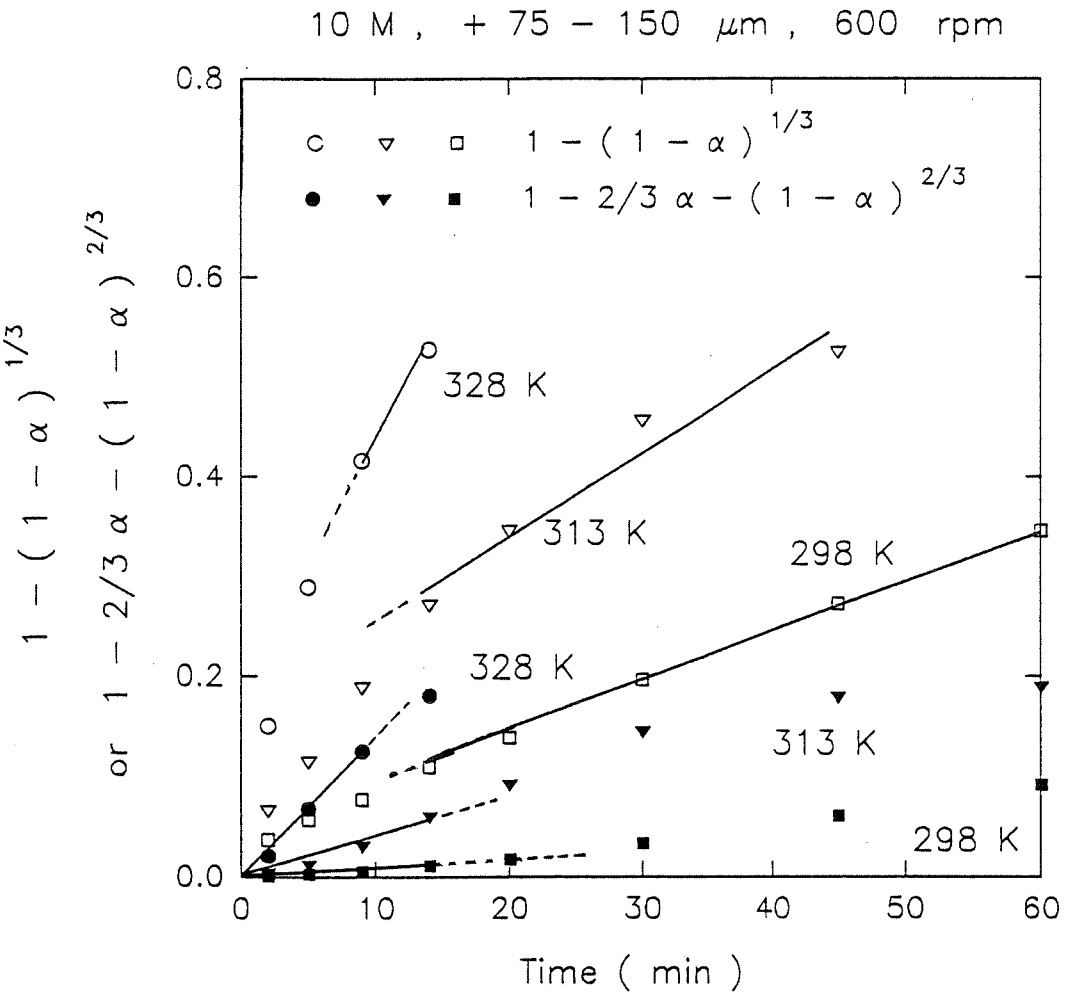

Figure 5.13 Analysis of experimental results by the shrinking core model as a function of temperature (data from Figure 4.12)

the same results as Figure 5.12. The slopes of the lines are steeper as the temperature increases.

5.2.5 Dissolution of Zinc Ferrite

As seen in Figure 4.15, zinc ferrite exists outside, enclosing the zinc oxide, so that it must be leached first. However, since the iron oxide of zinc ferrite does not dissolve, only zinc oxide forming zinc ferrite dissolves selectively. Thus, the fluid diffuses through the porous surface of the solid layer of zinc ferrite and reacts with the zinc oxide within the solid layer of zinc ferrite.

Since the leaching rate is faster near the surface than in the interior of the particle, due to the concentration gradient within the solid layer, zinc oxide near the surface of the solid layer of zinc ferrite is selectively dissolved to remain more porous iron oxide. The iron oxide thickens progressively from the selective dissolution of zinc ferrite.

After dissolving zinc oxide from the solid layer to form the more porous iron oxide, the fluid diffuses freely without resistance to the zinc oxide which is inside of the particle, so that the rate-determining step changes from diffusion through the solid layer to the surface reaction in the later stage of the leaching process.

Therefore, the global dissolution reaction of the roasted zinc concentrates in

alkaline solution can be expressed as follows:

$$ZnFe_2O_4 + 2\ OH^- + H_2O = Zn(OH)_4^{2-} + Fe_2O_3 \qquad (5.32)$$

$$ZnO + 2\ OH^- + H_2O = Zn(OH)_4^{2-} \qquad (5.33)$$

5.2.6 Determination of Effective Diffusion Coefficient, D_e, and Chemical Rate Constant, k_c

Since the leaching rate is controlled by diffusion through the solid layer during the early stage of the leaching process, the effective diffusion coefficient, D_e, can be determined from the slope of the linear portion of the graph when the data are plotted according to Equation (5.23),i.e., diffusion through the solid layer, as in Figure 5.12. The slope is K_D; D_e can then be obtained from known values of the other quantities. Similarly, since the leaching rate is controlled by the surface reaction in the later stage, the chemical rate constant, k_c, can be determined from the slope of the linear portion of the curve when the data are plotted according to Equation (5.21), i.e., the surface reaction, as in Figure 5.12. The slope is K_C; k_c can then be calculated from the known values of the other quantities.

Effective diffusion coefficients and chemical rate constants were calculated with Equations (5.24) and (5.22), respectively. The results are listed in Table 5.3. As seen in the table, increasing the particle size increases D_e and k_c. This is because decreasing

Table 5.3 Dependence of rate constant and effective diffusion coefficient on particle size (298 K, 600 rpm, 10 M)

d_0 (μm)	Zn (%)	Fe (%)	$ZnO:ZnFe_2O_4$ (mole ratio)	$D_e \times 10^7$ (cm^2/min)	$k \times 10^4$ (cm/min)
sintered mixture of zinc oxide and hematite					
+75-150	64.35	15.30	6 : 1	1.722	11.23
roasted zinc concentrates					
+20-38	57.60	13.60	6 : 1	1.047	1.080
+38-45	58.10	13.30	6 : 1	1.278	1.530
+45-63	58.80	12.35	7 : 1	1.699	2.748
+63-75	58.30	10.80	8 : 1	2.133	5.041
+75-150	62.30	10.80	9 : 1	2.200	9.780

the particle size increases the formation of zinc ferrite.

Figure 5.14 shows the results of X-ray diffraction analysis of the particles. Figures 5.14-a, 5.14-b and 5.14-c show X-ray diffraction of pure zinc oxide, pure zinc ferrite and pure hematite as standard samples, respectively. X-ray diffraction analysis identified zinc oxide, zinc ferrite and hematite as seen in Figures 5.14-a to 5.14-c. Figures 5.14-d and 5.14-e show X-ray diffraction of the roasted zinc concentrates and of the sintered mixture with a particle size of +75-150 μm, respectively. As seen in these figures, X-ray diffraction analysis shows that a hematite does not exist in the particles prior to the leaching reaction, which proves that during dead roasting, almost all of the iron converts to zinc ferrite [16,20,22]. In order to calculate the mole ratios between zinc ferrite and zinc oxide in the particles, the following assumptions have been made : 1) the rest of S is associated with Zn to sphalerite (ZnS), 2) the composition of zinc ferrite is $ZnFe_2O_4$. Under these assumptions, the mole ratios were approximately calculated. The results are listed in Table 5.3.

With the values of D_e and k_c, all of the results were plotted with Equation (5.25) in order to obtain the mixed control. The constant, A, in Equation (5.27) was calculated from the effective diffusion coefficient and the chemical rate constant. Table 5.4 shows the values of A. These values increased as the particle size decreased and the temperature increased.

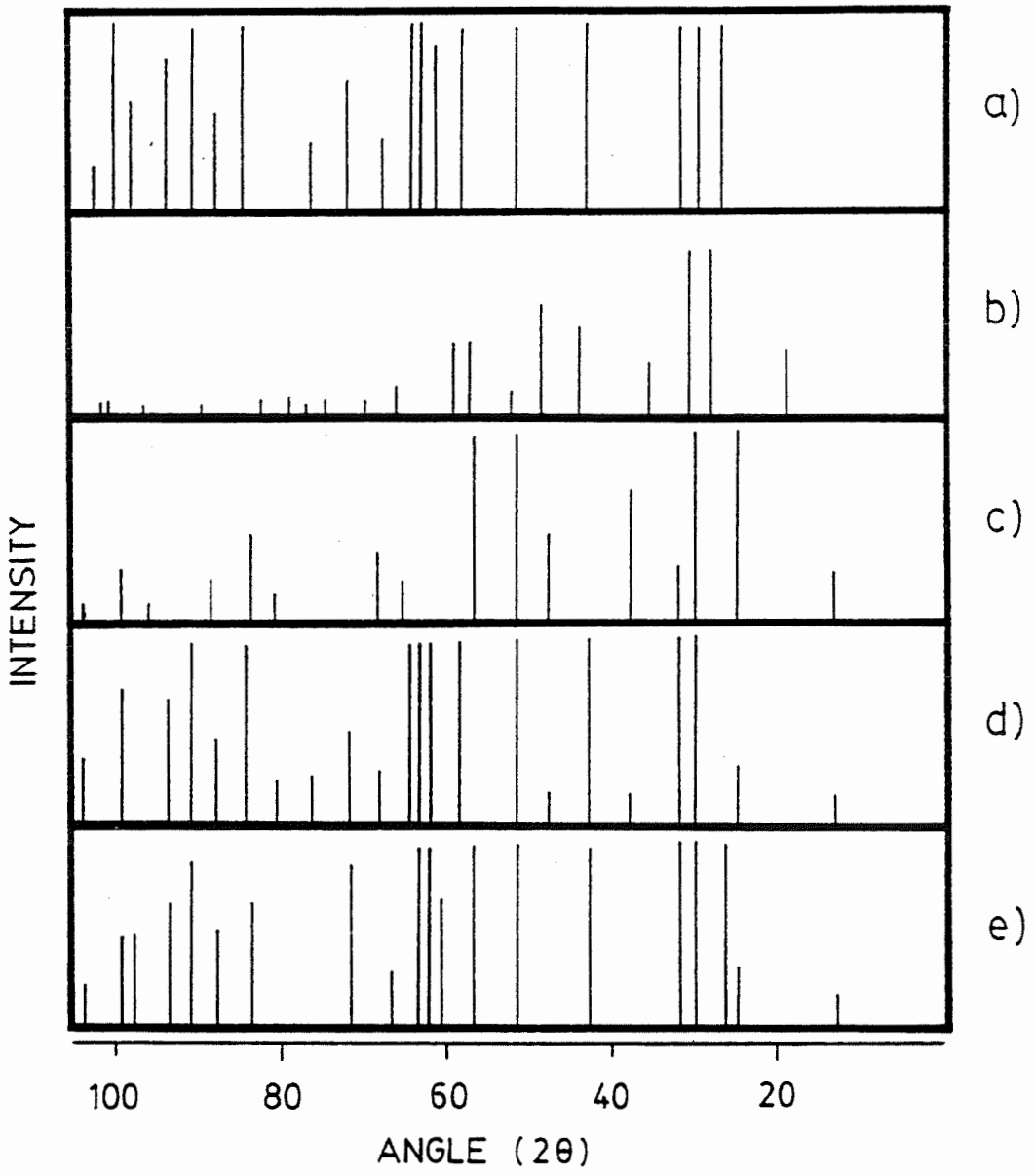

Figure 5.14 X-ray diffraction analysis of the particles (a: ZnO, b: Fe_2O_3, c: $ZnFe_2O_4$, d: sintered mixture of +75-150 μm, e: roasted zinc concentrates of +75-150 μm)

Table 5.4 Calculation of values of A.

d_0 (μm)	T (K)	A
+20-38		1.293
+38-45		0.835
+45-63	298	0.495
+63-75		0.242
+75-150		0.082
	298	0.082
+75-150	313	0.185
	328	0.214

Figure 5.15 analyzes the results with Equation (5.25). A linear relationship was not obtained throughout the dissolution process. Therefore, the leaching reaction can not be simultaneous control by diffusion through the solid layer and the surface reaction.

From Figure 5.13, the effective diffusion coefficient and the chemical rate constant can be obtained through the procedure given as above. The rate-determining step is also the additivity of diffusion through the solid layer and the surface reaction, which gives the same results as Figure 5.12. The sintered mixture also had the same leaching trend as the roasted zinc concentrates, as seen in Figure 4.13. Two constants were therefore obtained by the same process, as in the case for the roasted zinc concentrates. The results are listed in Table 5.5, and, as expected, the values of the constant increase as the temperature increases.

5.2.7 Calculation of Activation Energy

The activation energy for the leaching process can be obtained from the Arrhenius plot with Figure 5.13. It is reasonable to consider that there are two types of activation energy, since the rate-determining step consists of two stages. Figure 5.16 shows the calculation of the activation energy. The activation energy for control of diffusion through the solid layer is 16 kcal/mol, while that for surface reaction control is 11 kcal/mol.

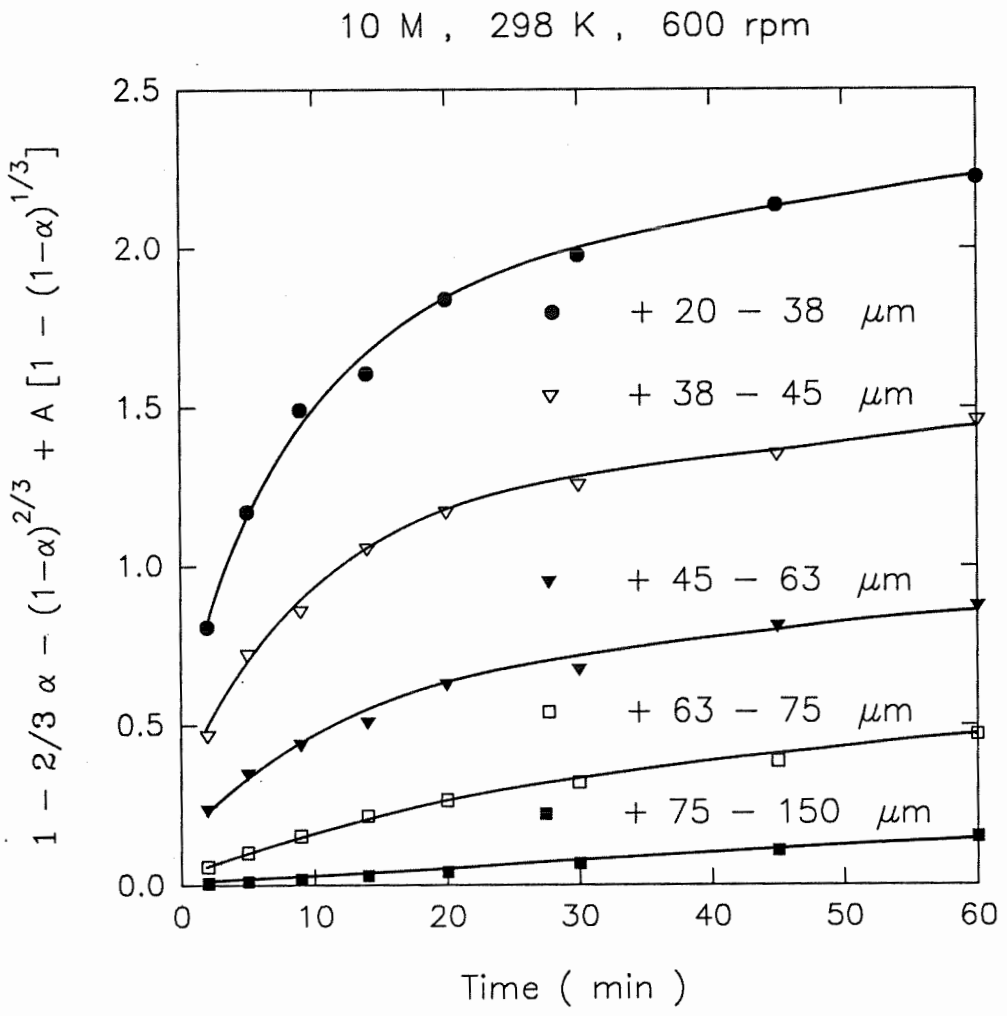

Figure 5.15 Analysis of experimental results using Equation (5.25)

Table 5.5 Dependence of rate constant and effective diffusion coefficient on temperature (10 M, 600 rpm, +75-150 μm)

T (K)	Zn (%)	Fe (%)	$ZnO:ZnFe_2O_4$ (mole ratio)	$D_e \times 10^6$ (cm^2/min)	$k \times 10^3$ (cm/min)
sintered mixture of zinc oxide and hematite					
298	64.35	15.30	6 : 1	0.172	1.123
313				1.150	1.867
328				4.880	2.608
roasted zinc concentrates					
298	62.30	10.80	9 : 1	0.220	0.978
313				0.796	1.562
328				2.498	4.245

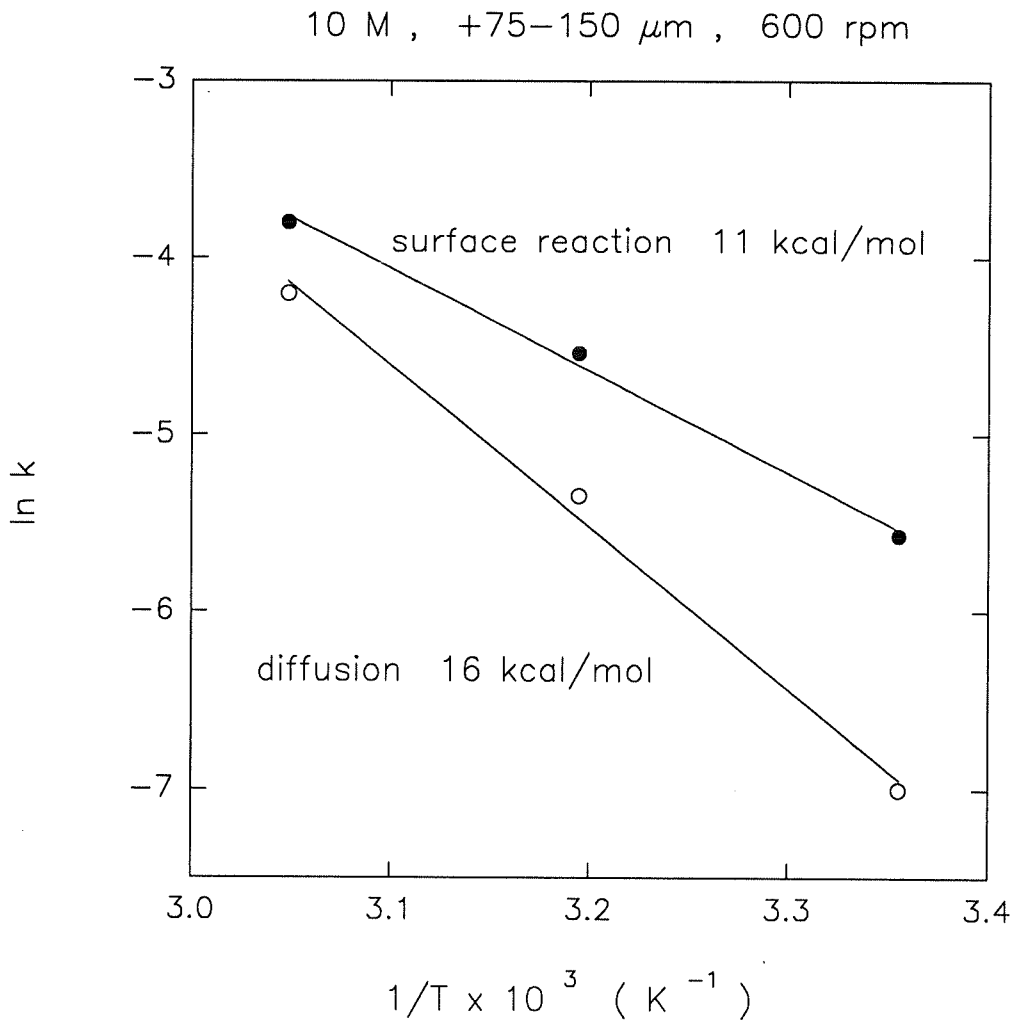

Figure 5.16 Activation energy from Arrhenius plot determined from the leaching rate of roasted zinc concentrates

Zinc ferrite is a double oxide consisting of a unit cell containing 32 oxygen ions that form a FCC lattice, with the metal cations distributed interstitially in two sublattices [67-69]. That is to say, zinc ferrite has strong bonds between zinc oxide and iron oxide. It has a spinel structure, and is therefore difficult to dissolve. Thus, the activation energy for zinc ferrite will be higher than that for zinc oxide.

5.2.8 Effect of Zinc Ferrite

Figure 5.17 shows the effect of zinc ferrite on the leaching rate, where three different kinds of particles were used. These particles are the sintered pure zinc oxide, the sintered mixture of pure zinc oxide and hematite and the roasted zinc concentrates. The sintered pure zinc oxide does not contain zinc ferrite, whereas the sintered mixture and the roasted zinc concentrates do.

As seen in this figure, the sintered pure zinc oxide of +20-38 μm, which has a specific surface area of 0.35 m^2/g, has a higher leaching rate than the sintered mixture of +75-150 μm with 0.38 m^2/g, even though two materials have almost the same surface area.

Also, the sintered pure zinc oxide of +75-150 μm, which has a specific surface area of 0.11 m^2/g, has the same leaching rate as the roasted zinc concentrates of +75-150 μm with 0.66 m^2/g, even though the surface area of the roasted zinc concentrates is 6

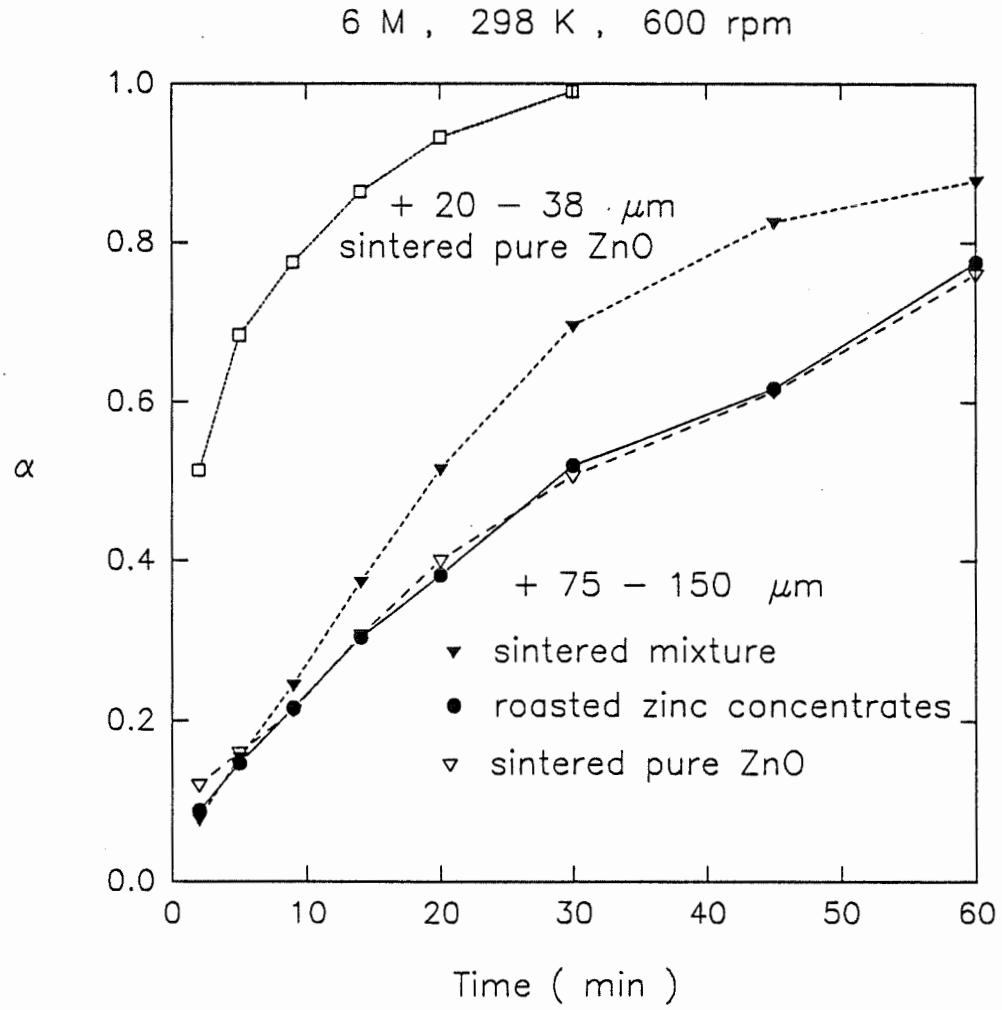

Figure 5.17 Effect of zinc ferrite on leaching rate

times higher than that of the sintered pure zinc oxide.

Therefore, the leaching rate of the roasted zinc concentrates and the sintered mixture are lower than those of the sintered pure zinc oxide, because zinc ferrite exists outside, enclosing the zinc oxide.

As illustrated in Figures 4.8 and 4.12, the absolute extraction percentage becomes higher and higher as particle size increases. For example, in +75-150 μm, the percentage is about 98 %, while in +20-38 μm, the percentage is about 93 %. As can be seen in Table 3.1, +20-38 μm particles have a larger surface area than +75-150 μm particles: 2.90 m^2/g and 0.66 m^2/g, respectively. On the other hand, as seen in Table 3.2, +20-38 μm particles have a lower Zn percentage and a higher Fe percentage than 75-150 μm particles: 57.60 % Zn, 13.60 % Fe and 62.30 % Zn and 10.80 % Fe, respectively. A particle size of +20-38 μm therefore has a higher leaching rate because of its larger surface area, as seen in Figure 4.9. However, +75-150 μm particles have a higher absolute extraction percentage, because of their higher Zn percentage and lower Fe percentage, i.e., lower zinc ferrite formation.

5.2.9 Effect of Impurities

As seen in Figure 5.17 and Table 3.1, the leaching rate of the sintered mixture, which has a specific surface area of 0.38 m^2/g, is faster than that of the roasted zinc

concentrates with 0.66 m^2/g. The rate constants of the former are greater than those of the latter, even though the two materials have the same leaching mechanism. Since, in the case of the roasted zinc concentrates, there exist some impurities such as copper, lead and cadmium, as seen in Table 3.3, part of the specific surface area should be regarded as non-active, which partially explains the difference in the leaching rate.

5.3 PROCESS VARIABLES

Three kinds of materials were used: reagent grade pure zinc oxide and iron-containing zinc oxides, which are roasted zinc concentrates and the sintered mixture.

5.3.1 Degree of Particle Suspension

Figure 5.18 is a schematic diagram of the particle suspension obtained from Figures 4.17 and 4.18. Three kinds of particle suspensions can be identified. The first is no-suspension; that is, all of particles remain on the bottom of the reactor. The second is partial suspension; that is, some part of the particles are suspended and the rest of them remain on the bottom of the reactor. The third is complete suspension; that is, no particles remain for more than one second on the bottom of the reactor.

Each suspension has its own characteristics. In no-suspension, ZnO particles accumulate on the bottom, so that the interface between the particle and the solution is small. However, in complete suspension, all of the particles are suspended in the liquid, and the interface between them greatly increases. In partial suspension, only some of the particles are suspended, and the interface between them is then between the two other cases.

Also, in no-suspension, there is a passivation at 0 rpm and the formation of a

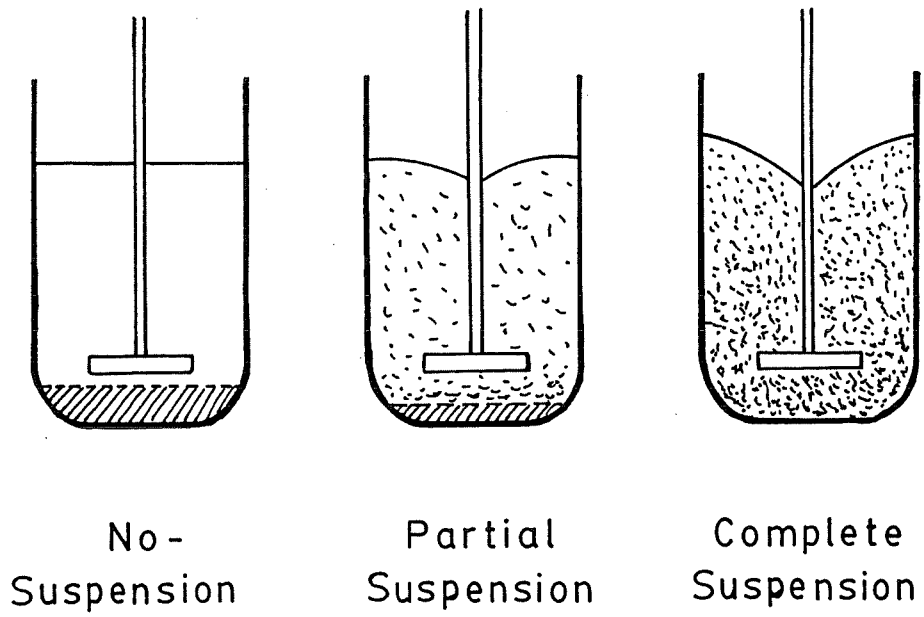

Figure 5.18 Schematic diagram of particle suspension as a function of agitation speed

precipitate at 200 rpm. However, there is no precipitate in complete suspension.

5.3.2 Formation of Precipitate

As seen in Figures 4.17, 4.19 and 4.20, the experiment using 0 rpm showed passivation, and that using 200 rpm formed a precipitate. Also, as discussed in section 5.1.6, the diffusion of $Zn(OH)_4^{2-}$ to the bulk of the electrolyte also constitutes the rate-determining step in the dissolution of pure zinc oxide in alkaline solution.

Based on the above facts, a three-stage scheme for the formation of precipitate can be proposed. First, the dissolution of zinc oxide produces zincate ions which accumulate near zinc oxide particle according to $ZnO + 2\ OH^- + H_2O \dashrightarrow Zn(OH)_4^{2-}$. Second, in the supersaturated zincate, zinc oxide film is precipitated from a layer of the electrolyte close to the particle surface, according to $Zn(OH)_4^{2-} \dashrightarrow ZnO + 2\ OH^- + H_2O$. Third, the zinc oxide film spreads out and gradually covers the particle surface, leading to passivation. This mode of film thickening is not unreasonable considering that $Zn(OH)_4^{2-}$ diffuses more slowly than OH^- (93). This proposal for the formation of precipitate agrees well with the dissolution-precipitation model (94-100).

Therefore, if there is no agitation, the precipitate accumulates to form a more compact precipitate which results in passivation.

However, the importance of an adequate hydrodynamic control in dissolution and passivation phenomena can be stressed. After passivation, zinc oxide can be reactivated by the addition of very small amounts of fresh hydroxide (101-103). The ease of dissolution of the precipitate in fresh electrolyte and the recovery of the electrode performance after the addition of fresh electrolyte suggests that even a small electrolyte circulation could help prevent passivation. Therefore, increasing the agitation speed from 0 rpm to 200 rpm prevents passivation and further increases in the agitation speed over complete suspension,i.e. 600 rpm, eliminate precipitation.

5.3.3 Complete Suspension

In an impeller-stirred vessel, the presence or absence of turbulence can be related to the impeller Reynolds Number, N_{Re} (53).

$$N_{Re} = \frac{D^2 N}{\nu} \qquad (5.34)$$

Table 5.6 shows N_{Re} which are calculated from Figure 4.16 and Equation (5.34). N_{Re} is less than 10 for laminar flow and greater than 10000 for turbulent flow (53). Therefore, the flow condition of the present work is intermediate or turbulent flow, because N_{Re} ranges from 900 to 49000. The N_{Re} for 400 and 1200 rpm can be obtained doubling N_{Re} values for 200 and 600 rpm, respectively.

Table 5.6 Calculation of impeller Reynolds number

C (M/l)	N (rpm)	T (K)	N_{Re}	α (5min)
6	200	298	2300	0.108
		328	4300	0.162
		358	6800	0.324
		371	8200	0.381
	600	298	6800	0.866
		328	13000	0.917
		358	20300	0.942
		371	24500	0.953
8	200	298	1400	0.125
		328	2700	0.210
		358	4500	0.248
		371	5300	0.377
	600	298	4200	0.887
		328	8000	0.962
		358	13400	0.976
		371	15800	0.982
10	200	298	900	0.087
		328	1900	0.124
		358	3700	0.222
		371	4300	0.325
	600	298	2700	0.837
		328	5700	0.912
		358	11000	0.933
		371	13000	0.953

As seen in Table 5.6, N_{Re} at 371 K, 200 rpm is greater than N_{Re} at 298 K, 600 rpm: 8200 and 6800, respectively. However, the leaching rate at 298 K, 600 rpm is higher than at 371 K, 200 rpm: 0.381 and 0.866, respectively. This is due to the fact that the agitation speed of 600 rpm produces the complete suspension, whereas that of 200 rpm produces no-suspension. Moreover, even though N_{Re} at 298 K, 600 rpm is less than for turbulent flow, a fast leaching rate is obtained. Therefore, the requirement for a fast leaching rate is to obtain complete suspension, not a turbulent flow.

5.3.4 Correlation for Complete Suspension

From Equation (2.35), can be written:

$$S = \frac{N_S \, D^{0.85}}{\nu^{0.1} \, d^{0.2} \, \left(\frac{g \, \Delta\rho}{\rho}\right)^{0.45} \, X^{0.13}} \qquad (5.35)$$

The clearance ratio (h/D_T) and impeller-to-reactor diameter ratio (D/D_T) were considered as a parameter, since the exponents of ν, d, $(g\ \Delta\rho)/\rho$, X and D were independent of impeller type, vessel size, h/D_T and D/D_T. Figure 5.19 shows the correlation between the dimensionless constant, s, and D/D_T as a function of h/D_T for the complete suspension:

$$When \ \frac{h}{D_T} = 0.3 \qquad S \propto \left(\frac{D}{D_T}\right)^{-0.34} \qquad (5.36)$$

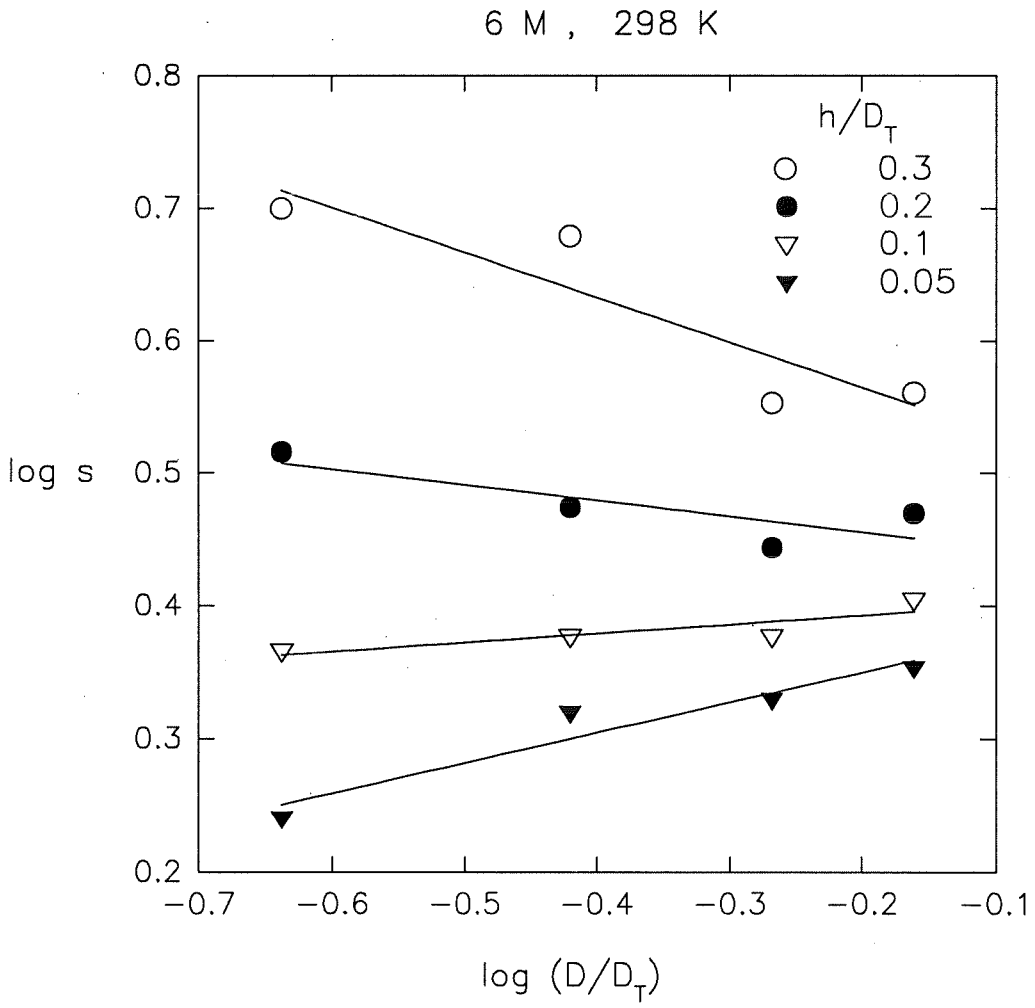

Figure 5.19 Correlation for complete suspension

$$When \ \frac{h}{D_T} = 0.2 \qquad s \propto \left(\frac{D}{D_T}\right)^{-0.12} \tag{5.37}$$

$$When \ \frac{h}{D_T} = 0.1 \qquad s \propto \left(\frac{D}{D_T}\right)^{0.07} \tag{5.38}$$

$$When \ \frac{h}{D_T} = 0.05 \qquad s \propto \left(\frac{D}{D_T}\right)^{0.23} \tag{5.39}$$

Equation (2.35) gives the following relationship between N_s and D:

$$N_s \propto D^{-0.85} \tag{5.40}$$

From Equations (5.35) to (5.40) we obtain:

$$When \ \frac{h}{D_T} = 0.3 \qquad N_s \propto D^{-1.19} \tag{5.41}$$

$$When \ \frac{h}{D_T} = 0.2 \qquad N_s \propto D^{-0.97} \tag{5.42}$$

$$When \ \frac{h}{D_T} = 0.1 \qquad N_s \propto D^{-0.78} \tag{5.43}$$

$$When \ \frac{h}{D_T} = 0.05 \qquad N_s \propto D^{-0.62} \qquad (5.44)$$

As seen in Equations (5.41) to (5.44), N_s decreases as D increases. However, dependence of the decrease of N_s on D increases as h/D_T increases. With higher h/D_T, it is beneficial to use larger agitator diameters.

5.3.5 Power Consumption

The correlation of agitation conditions in terms of power input per unit mass is of special interest to engineers, since power requirements can be related to both capital and operating costs. Power consumption per unit mass giving complete suspension is given by the following equation:

$$P_m = \frac{P}{\rho_l V} = \frac{N_p \rho_l N_s^3 D^5}{\rho V} \qquad (5.45)$$

Power number N_p for the pitched blade turbine is approximately 1.52 (52).

Table 5.7 shows the power consumption per unit mass as a function of agitation speed. Power consumption increases greatly with increasing agitation speed from 400 to 600 to 1200 rpm. However, as seen in Figure 4.17, in complete suspension, there is no significant difference in the leaching rate between 600 and 1200 rpm, without

baffles. Also, as seen in Figure 4.21, in complete suspension, there is no difference in the leaching rate with baffles between 400 and 600 rpm.

Table 5.7 Calculation of power consumption per unit mass as a function of agitation speed for complete suspension

N_s	(rpm)	400	600	1200
$P_m \times 10^4$	(kw/kg)	1.41	4.75	38.0

To reduce power consumption, it is therefore essential to use the minimum agitation speed required for complete suspension.

5.3.6 Avoidance of Vortex

As seen in Figure 4.1, with a low concentration of particles, the leaching rate increases as the agitation speed increases from 400 to 600 rpm, i.e., for complete suspension. This is because the particles are evenly distributed in the solution, and mass transfer increases; there is no interference here among the particles, even though a vortex is formed.

However, as seen in Figure 4.21, with high concentration of particles, the leaching rate does not increase as the agitation speed increases from 400 to 600 rpm. This is because the particles cannot be evenly distributed in the solution; there is then interference among the particles due to the formation of a vortex in which classification of the particles occurs.

Thus, as seen in Figure 4.17, as agitation speed further increases from 600 to 1200 rpm, the leaching rate increases little. This is because the vortex depth increases and interference among the particles increases at these agitation speeds, even though air entrainment in the pulp density is much less than in low concentrations, as in Figure 4.1.

Moreover, when 8 baffles are used instead of 4 (Figure 4.22), the vortex depth decreases, and the leaching rate increases, due to the diminished interference among particles.

Furthermore, as seen in Figure 4.26, three different impeller-to-reactor diameter ratios produced different vortex depths, resulting in different leaching rates. This is because the relative vortex depth may be considerably increased by using an agitator with a larger diameter. Thus, increasing the ratio increases the vortex depth and decreases the leaching rate.

To maximize the leaching rate, leaching reactors must therefore be designed to avoid the formation of a vortex over complete suspension.

5.4 SUGGESTION FOR FUTURE RESEARCH

Increasing the temperature increased the leaching rate of the pure zinc oxide and the iron-containing zinc oxide. Particulary, in the case of the roasted zinc concentrates, increasing the temperature increased the absolute extraction percentage, regardless of the particle size, as seen in Figures 4.8 and 4.12. Thus, in order to increase the leaching rate and the absolute extraction percentage, higher temperatures are necessary.

However, temperature can not be increased above the normal boiling point of the solution, because of the volatilization of the solution at atmospheric pressure. To operate the leaching process above the normal boiling temperature, a pressure higher than atmospheric pressure must be used, in other words, pressure leaching.

There are two kinds of pressure leaching (104,105): in the absence of oxygen (106) and in the presence of oxygen (107-109). For pressure leaching in the absence of oxygen, the ore is heated with the leaching agent at a temperature above the boiling point of the solution to achieve a high reaction rate. The leaching rate therefore depends on the total pressure. However, in the second case, the ore is heated with the injection of oxygen. The oxygen pressure has a greater effect on the leaching rate than the total pressure. The leaching rate therefore depends on the oxygen pressure, not on the total pressure.

In the pressure leaching of the roasted zinc concentrates, oxygen is not needed and the leaching rate depends on the total pressure. Based on the present work, further development work is suggested as a function of the total pressure in order to study the relationship and the optimization between the total pressure and the parameters of the present work.

The following experimental techniques should therefore be explored:

1) periodic sampling in keeping the total pressure

2) the method to verify complete suspension in an autoclave.

CHAPTER 6

CONCLUSIONS

The dissolution of pure zinc oxide and roasted zinc concentrates in alkaline solution has been studied under the various experimental parameters. These conclusions are divided into three parts: leaching kinetics of pure zinc oxide, leaching kinetics of roasted zinc concentrates and process variables.

1) Leaching Kinetics of Pure Zinc Oxide

- The dissolution of zinc oxide in NaOH solution occurs under the condition of mixed control of the surface reaction and diffusion through the boundary layer.

- The relative importance of the surface reaction control and the diffusion control depends on their individual rates, which depends on the variables.

- The equation for the leaching time required to attain a certain conversion was found to be in good agreement with experimental data.

- An activation energy of 10 kcal/mol was obtained from the shrinking core model and Arrhenius plot.

- The leaching rate increases with increasing agitation speed for complete suspension. However, increasing agitation speed above the agitation speed required for complete suspension decreases the leaching rate.

- The leaching rate increases with increasing NaOH concentration, but the power dependency of NaOH concentration on the leaching rate decreases with increasing NaOH concentration.

- The rate of dissolution increases with decreasing particle size, and a linear relationship exists between the leaching rate and the specific surface area.

2) Leaching Kinetics of Roasted Zinc Concentrates

- The shrinking core model can be applied to particles with any kind of porosity, in keeping with the topochemical reaction.

- In the shrinking core model, diffusion through any solid layer can be the rate-determining step.

- The dissolution of roasted zinc concentrates in NaOH solution is controlled by diffusion through the zinc ferrite layer during the early stage of the leaching process and the surface reaction on the zinc oxide in the later stage.

- Activation energies of 16 and 11 kcal/mol are obtained from the Arrhenius plot for diffusion through the zinc ferrite layer and the surface reaction on the zinc oxide, respectively.

- The zinc ferrite layer changes to the porous iron oxide as leaching proceeds; it thickens progressively due to the selective dissolution of zinc ferrite.

- The leaching rate is independent of agitation speed for complete suspension and/or with NaOH concentrations ranging from 4 to 10 M.

- The effective diffusion coefficient and the chemical rate constant increase as particle size and/or temperature increase.

- The absolute extraction percentage increases as the particle size and/or temperature increase.

3) Process Variables

- A leaching reactor should be designed to secure complete suspension of particles with a minimum of power consumption.

- The requirement for a fast leaching rate is to obtain complete suspension, not a turbulent flow.

- The agitation speed for complete suspension decreases as the agitator diameter increases, but the dependence of the decrease increases as the clearance ratio increases.

- The formation of precipitates takes place in three stages: dissolution, supersaturation and thickening.

- The employment of baffles over complete suspension increases the leaching rate.

- For a higher leaching rate, a vortex must be avoided over complete suspension.

REFERENCES

1) Burney, H.S. and Talbot, J.B., "Report of the Electrolytic Industries for the Year 1990", J. Electrochem. Soc., Vol. 138, No. 10, October 1991, p 3140-3172.

2) Temple, D.A., "Zinc-from Mine to Market, Some Views on the Industry", Int. Sym. Extractive Metallurgy of Zinc, Tokyo, MMIJ, 1985, p 3-18.

3) Darlington, W.B. and Woo, M.Y.C., "Report of the Electrolytic Industries for the Year 1981", J.Electrochem.Soc., Vol. 129, No. 8, August 1982, p 275c-294c.

4) Bartlett, R.W. and Malmquist, D.E., "Changing Energy Economics in Non-ferrous Hydrometallurgy", J. Met., Aug. 1984, p 36-40.

5) Sider, M. and Piron, D.L., "Comparaison de la Consommation, La Technique, Nov.-Dec. 1989, p 15-18.

6) St-Pierre, J. and Piron, D.L., "Electrowinning of Zinc from Alkaline Solution", J. Appl. Electrochem., 16, 1986. p 447-456.

7) Brown, A.P., Melsenhelder, J.H. and Yao, N.-P., "The Alkaline Electrolytic Process for Zinc Production: a Critical Evaluation", Ind. Eng. Chem. Prod. Res. Dev., Vol. 22, No. 10, 1983, p 263-272.

8) Kellogg, H.H., "Energy Use in Zinc Extraction", Lead-Zinc-Tin '80, AIME, New York, 1980, p 28-47.

9) St-Pierre, J. and Piron, D.L., "Electrowinning of Zinc From Alkaline Solutions at High Current Densities", J. Appl. Electrochem., 20, 1990, 163-165.

10) Piron, D.L., "Recent Improvement in Zinc Alkaline Hydro-metallurgy", Proceedings of the International Symposium on Electro-Metallurgical Plant Practice, 20th Annual Hydrometallurgical Meeting, 1990, p 129-140.

11) Pourbaix, M., "Atlas des équilibres électrochimiques à 25 °C", Gauthier-Villars, Paris, 1963.

12) Jackson, E., "Hydrometallurgical Extraction and Reclamation", Ellis Horwood Limited, 1986, Chapters 1-2.

13) Peters, E., "The Physical Chemistry of Hydrometallurgy", Int. Sym. on Hydrometallurgy, 1973, Chicago, Chapter 10.

14) Dirkse, T.P., "The Nature of Zinc-Containing Ion in Strongly Alkaline Solution", J. Electrochem. Soc., Vol. 101, 1954, p 328-331.

15) Morgan, S.W.K., "Zinc and Its Alloys", Industrial Metals Series, Macdonald and Evans, Chapters 3 & 6, 1977.

16) Gordon, A.R. and Pickering, R.W., "Improved Leaching Technologies in the Electrolytic Zinc Industry", Metall. Trans. B, Vol. 6B, March 1975, p 43-53.

17) Merrill, C.C. and Lang, R.S., "Experimental Caustic Leaching of Oxidized Zinc Ores and Minerals and the Recovery of Zinc from Leach Solutions", Rep. Invest. US Bureau of Mines, 6576, 1965.

18) Baroch, C.T., Hillard, R.V. and Lang, R.S., "The Caustic Electrolytic-Zinc Process", J.Electrochem.Soc., 1953, p 165-172.

19) Frenay, J.N. and Hissel, J., "Zinc and Lead Recovery from Iron- and Steel-Making Dusts; Pilot Study of a Caustic Soda Process", ATB Metallurgy XXIV, No. 3, 1984, p 233-237.

20) Eacott, J.G., Robinson, M.C., Busse, E., Burgener, J.E. and Burgener, P.E., "Techno-economic Feasibility of Zinc and Lead Recovery from Electric Arc Furnace Baghouse Dust", CIM Bulletin, Sept. 1984, p 75-81.

21) Frenay, J., Hissel, J. and Ferlay, S., "Recovery of Lead and Zinc from Electric Steelmaking Dusts", Recycle and Secondary Recovery of Metals, The Metallurgical Society of AIME, 1985, p 195-201.

22) Graydon, J.W. and Kirk, D.W., "A Microscopic Study of the Transformation of Sphalerite Particles during the Roasting of Zinc Concentrate", Metall. Trans. B, Vol. 19B, February 1988, p 141-146.

23) Graydon, J.W. and Kirk, D.W., "The Mechanism of Ferrite Formation from Iron Sulfides during Zinc Roasting", Metall. Trans. B, Vol. 19B, October 1988, p 777-785.

24) Lastra, R., Rowlands, N. and Finch, J.A., "Evidence of Variable Zn/Fe in Zinc-Ferrites Produced from Roasting of Zinc Sulphide Concentrate", Scanning Microscopy, Vol. 2, No. 3, 1988, p 1427-1436.

25) Anderson, W.W., Rajcevic, H.P. and Opie, W.R., "Pilot Plant Operation of the Caustic Leach-Electrowin Zinc Process", TMS paper selection, The Metallurgical Society of AIME, paper A81-52, 1981.

26) Meek, R.L., "An Alkaline Process for Electrolytic Zinc", Proceedings, Extractive Metallurgy Division of AIME, Symposium, 1969, p 306-319.

27) Rogers, G., Simkovich, G. and Osseo-Asere, K., "The Effect of Point Defects on the Dissolution of Zinc Oxide in Sodium Hydroxide Solutions", Hydrometallurgy, 10, 1983, p 313-328.

28) Frenay, J., "Traitement Hydrométallurgique de Matériaux Oxyde de Zinc", Ph.D. Thesis, Laval University, Quebec, June, 1989.

29) Habashi, F., "Dissolution of Minerals and Hydrometallurgical Processes", Naturwissenschaften, No. 70, 1983, p 403-411.

30) Uhl, V.W. and Gray, J.B., "Mixing - Theory and Practice", Vol. III, Academic Press, 1986, Chapter 12.

31) Raghawa, K.S.M.S., Rewatkar, V.B. and Joshi, J.B., "Critical Impeller Speed for Solid Suspension in Mechanically Agitated Conditions", AIChE Journal, Vol. 34, Aug., 1988, p 1332-1340.

32) Beale, C, Oldshue, J.Y. and Sternad, G., "Mixing and Leaching in 1400 m^3 tanks at Rossing", Hydrometallurgy, Research, Development and Plant Practice, March 6-10, 1983, p 859-873.

33) Oldshue, J.Y., "Solid-Liquid Mixing in Hydrometallurgy", Unit Process in Hydrometallurgy, 1964, p 21-42.

34) Yagi, S. and Kunii, D., "Fluidized-Solids Reactors with Continuous Solids Feed", Chem. Eng. Sci., 1961, p 364-391.

35) Habashi, F., "Principles of Extractive Metallurgy", Vol. 1, 1969, p 111-252.

36) Levenspiel, O., "Chemical Reaction Engineering", Wiley, New York, 1972, p 357-377.

37) Bartlett, R.W., "Conversion and Extraction Efficiencies for Ground Particles in Heterogeneous Process Reactors", Metall. Trans., Vol. 2, Nov. 1971, p 2999-3006.

38) Wadsworth, M.E. and Sohn, H.Y., "Rate of Process of Extractive Metallurgy", Plenum Press, 1976, Chapter 3.

39) Wen, C.Y., "Noncatalytic Heterogeneous Solid Fluid Reaction Models", Industrial and Engineering Chemistry, Vol. 60, No. 9, 1968, p 34-54.

40) Mohemius, A.J. and Katungu, G., "Kinetics of Acid Leaching of Zinc Oxide", I. Chem. E. Symposium Series No. 87, p 635-642.

41) Terry, B. and Monhemius, A.J., "Acid Dissolution of Willemite($(Zn, Mn)_2 SiO_4$) and Hemimorphite($Zn_4Si_2O_7 (OH)_2 H_2O$)", Metall. Trans. B., Vol. 14B, 1983, p 335-346.

42) Beckstead, L.W., Munoz, P.B., Sepulveda J.L., Herbst J.A., Miller J.D., Olson F.A. and Wadsworth, M.E., "Acid ferric sulfate leaching of attritor-ground chalcopyrite concentrate", Int. Symp. on Copper Extraction and Refining, J.C. Yannopoulos and J.C. Agawal, eds., 105th AIME Annual Meeting, Las Vegas, Nevada, Feb. 22-26, 1976, p 611-632.

43) Bobeck, G.E. and Su, H., "The Kinetics of Dissolution of Sphalerite in Ferric Chloride Solution", Metall. Trans. B, Vol. 16B, 1985, p 413-424.

44) Pholman, S.L. and Olson, F.A., "A Kinetic Study of Acid Leaching of Chrysocolla Using a Weight Loss Technique", Solution Mining Symposium, 1974, p 446-459.

45) Uhl, V.W. and Gray, J.B., "Mixing - Theory and Practice", Vol. II, Academic Press, 1967, Chapter 9.

46) Baldi, G., Conti, R. and Alaria, E., "Complete Suspension of Particles in Mechanically Agitated Vessels", Chem. Eng. Sci., Vol. 33, 1978, p 21-25.

47) Conti, R., Sicardi, S. and Specchia, V., "Effect of the Clearance on Particle Suspension in Agitated Vessels", Chem. Eng. J., 22, 1981, p 247-249.

48) Narayanan, S., Bhatia, V.K., Guha, D.K. and Rao, M.N., "Suspension of Solids by Mechanical Agitation", Chem. Eng. Sci., 24, 1969, p 223-230.

49) Nienow, A.W., "Suspension of Solid Particles in Turbine Agitated Baffled Vessels", Chem. Eng. Sci., Vol. 23, 1968, p 1453-1459.

50) Zwietering, Th.N., "Suspending of Solid Particles in Liquid by Agitators", Chem. Eng. Sci., Vol. 8, 1958, p 244-253.

51) Nienow, A.W., "Dissolution Mass Transfer in a Turbine Agitated Baffled Vessel", Can. J. Chem. Eng., Vol. 47, June, 1969, p 248-258.

52) Chapman, C.M., Nienow, A.W., Cooke, M. and Middleton, J.C., "Particle-Gas-Liquid Mixing in Stirred Vessels: Part I. Particle-Liquid Mixing", Chem. Eng. Res. Des., Vol. 61, 1983, p 71-81.

53) Perry, R.H. and Green, D.W., "Perry's Chemical Engineer's Handbook", 6th Edition, 1984, Section 19.

54) Rieger, F., Ditl, P. and Novak, V., "Vortex Depth in Mixed Unbaffled Vessels", Chem. Eng. Sci., Vol. 34, 1979, p 397-403.

55) Bird, R.B., Stewart, W.E. and Lightfoot, E.N., "Transport Phenomena", John Wiley & Sons, Inc., 1960, Part I & III.

56) Ayazi Shamlou, P. and Koutsakos, E., "Solids Suspension and Distribution in Liquids under Turbulent Agitation", Chem. Eng. Sci., Vol. 44, No. 3, 1989, p 529-542.

57) Brian, P.L.T., Hales, H.B. and Sherwood, T.K., "Transport of Heat and Mass Between Liquids and Spherical Particles in an Agitated Tank", AIChE J., Vol. 15, No.5, 1969, p 727-733.

58) Levins, D.M. and Glastonbury, J.R., "Application of Kolmogoroff's Theory to Particle-Liquid Mass Transfer in Agitated Vessels", Chem. Eng. Sci., Vol. 27, No. 3, 1972, p 537-543.

59) Harriott, P., "Mass Transfer to Particles: Part I. Suspended in Agitated Tanks", AIChE J. Vol. 8, No. 1, 1962, p 93-102.

60) Levins, D.M. and Glastonbury, J.R., "Particle-Liquid Hydrodynamics and Mass Transfer in Agitated Vessel", Trans. Instn. Chem. Engrs., Vol. 50, 1972, p 132-146.

61) Nienow, A.W., "Agitated Vessel Particle-Liquid Mass Transfer: A Comparison between Theories and Data", Chem. Eng. J., Vol. 9, 1975, p 153-160.

62) Mathewson, C.H., "Zinc-The Science and Technology of Metal, Its Alloys and Compounds", 1970, Hafner Publishing Company, Inc.

63) Sandra, T. and Bradt, R.C., "Grain Growth in Sintered ZnO and ZnO-Bi_2O_3 Ceramic", J. Am. Ceram. Soc., 73, 1, 1990, p 106-114.

64) Zivkovic, M., Mikijelj, V., Radic, S.M. and Rastic, M.M., "Surface Area Reduction During ZnO Sintering", Materials Science Research, Vol. 13, Sintering Process, Edited by Kuczynski, G.C., p 479-483.

65) Gupta, T.K. and Coble, R.L., "Sintering of ZnO", J. Am. Ceram. Soc., Vol. 51, No. 9, 1968, p 521-528.

66) Asokan, T., Iyengar, G.N.K. and Nagabhushana, G.R., "Studies on Microstructure and Density of Sintered ZnO-Based Non-Linear Resistors", Journal of Materials Science, Vol. 22, 1987, p 2229-2236.

67) Kolta, G.A., El-Tawil, S.Z., Ibrahim, A.A. and Felix, N.S., "Kinetics and Mechanism of Zinc Ferrite Formation", Thermochimica Acta, Vol. 36, 1980, p 359-366.

68) Duncan, J.F. and Stewart, D.J., "Kinetics and Mechanism of Formation of Zinc Ferrite", Trans. Faraday Soc., Vol. 63, 1967, p 1031-1041.

69) Parker, R., Rigen, C.J. and Tinsley, C.J., "Solid-State Reaction between Zinc Oxide and Ferric Oxide", Trans. Faraday Soc., Vol. 65, 1969, p 219-224.

70) Weir, D.R., "Some Recent Developments in Hydrometallurgy", Can. Metall. Q., Vol. 23, No. 4, 1984, p 353-363.

71) Yeager, E. and Salkind, A.J., "Techniques of Electrochemistry", Wiley-Interscience, Vol. 1, 1972, Chapter 4.

72) Clyde Orr, Jr and Dallavalle, J.M., "Fine Particle Measurement-Size, Surface and Pore Volume", The Macmillan Company, 1959, Chapter 7.

73) Jaycock, M.J., "The Krypton BET Method", Particle Size Analysis edited by M.J. Groves, Heyden & Son Ltd, 1978, p 308-320.

74) Matthews, G.P., "Experimental Physical Chemistry", Clarendon Press, Oxford, 1985, p 73-79.

75) Operating manual of The FlowSorb 2300, Micromeritics Instrument Corporation, 1985.

76) Svarovsky, L., "Solid-Liquid Separation", Chemical Engineering Series, Butter Worth & Co Ltd, 1977, Chapter 7.

77) Hsu, H.-W., "Separations by Centrifugal Phenomena", Techniques of Chemistry, Vol. XVI, John Wiley & Sons, 1981, Chapters 1,2 & 7.

78) Elwell, W.T. and Gidley, J.A., "Atomic Absorption Spectrophotometer", Pergamon Press, 1971, Chapters 2,6 & 7.

79) Rubeska, I. and Moldan, B., "Atomic Absorption Spectrophotometer", CRC Press, 1966, Chapter 1.

80) St-Pierre, J. and Piron, D.L., "A Model for the Potential Oscillation of the Zinc Electrode Polarized Cathodically in an Alkaline Medium", J. Electrochem. Soc., Vol. 134, 1987, p 1689-1695.

81) St-Pierre, J. and Piron, D.L., "Mechanism of Cathodic Potential Oscillations of the Zinc Electrode in Alkaline Solutions", J. Electrochem. Soc., Vol. 137, 1990, p 2491-2497

82) Piron, D.L., "Electrochimie de Base pour Ingénieurs", Edition de l'École Polytechnique de Montréal, 1979.

83) Metals Handbook, 9th Edition, Vol. 13, p 21-24.

84) Piron, D.L.,"The Electrochemistry of Corrosion", published by NACE, 1991, Houston, Texas.

85) Handbook of Chemistry and Physics, 68th Edition, CRC Press, 1987, B131, B144, D12.

86) American National Standard ANSI/TAPPI, "Viscosity of Pulp (Capillary Viscometer Method)", 1978.

87) Dirkse, T.P., "Passivation Studies on the Zinc Electrodes", Power Sources, 2, 1970, p 485-493.

88) Dirkse, T.P., Technical Report No. AFAPL-TR-72-87, Contract No. S33651-70-C-1022, Project 3145, Calvin College, Grand Rapides, MI, December 1972.

89) McBreen, J., Report No. N68-15716, Contract No. NAS5-10231, Yandrey Electric Corp., New York, June 1967.

90) Dobos, D., "Electrochemical Data", Elsevier Scientific Publishing Company, 1975.

91) Warren, I.H. and Devuyst, E., "Leaching of Metal Oxides", Inter. Symp. on Hydrometallurgy, 1973, p 229-264.

92) Szekely, J., Evans, J.W. and Sohn, H.Y., "Gas-Solid Reactions", Academic Press, 1976, Chapters 3 & 4.

93) Chang, Y.-C. and Prentice, G., "A Model for the Anodic Dissolution of the Zinc Electrode in the Prepassive Region", J. Electrochem. Soc., Vol. 136, No. 11, 1989, p 3398-3403.

94) Nagy, Z. and Bockris, J.O'M., "On the Electrochemistry of Porous Zinc Electrodes in Alkaline Solutions", J. Electrochem. Soc., Vol. 119, No. 9, 1972, p 1129-1136.

95) Dirkse, T.P. and Hampson, N.A., "The Anodic Behaviour of Zinc in Aqueous KOH Solution - I. Passivation Experiments at Very High Current Densities", Electrochim. Acta, vol. 16, 1971, p 2049-2056.

96) Powers, R.W. and Breiter, M.W., "The Anodic Dissolution and Passivation of Zinc in Concentrated Potassium Hydroxide Solutions", J. Electrochem. Soc., Vol. 116, No. 6, 1969, p 719-729.

97) Hampson, N.A., Shaw, P.E. and Taylor, R., "Anodic Behaviour of Zinc in Potassium Hydroxide Solution - II. Horizontal Anodes in Electrolytes Containing Zn(II)", Br. Corrs. J., Vol. 4, 1969, p 207-211

98) McBreen, J. and Cairns, E.J., "The Zinc Electrode", Advances in Electrochemistry and Electrochemical Engineering, Vol. 11, Edited by Gerischer, H. and Tobias, C.W., 1978 John Wiley & Sons.

99) Liu, M.-B., Cook, G.M. and Yao, N.P., "Transient Current Distributions in porous Zinc Electrodes in KOH Electrolyte", J. Electrochem. Soc., Vol. 129, 1982,

p 239-246.

100) Katan, T., Savory, J.R. and Yao, N.-P., "Observations of an Operating Zinc-Pore Electrode", J. Electrochem. Soc., Vol. 126, No. 11, 1979, p 1835-1841.

101) Szpak, S. and Gabriel, C.J., "The Zn-KOH System: The Solution-Precipitation Path for Anodic ZnO Formation", J. Electrochem. Soc., Vol. 126, No. 11, 1979, p 1914-1923.

102) Shan, X., Ren, D., Scholl, P. and Prentice, G., "Coulometric and Ellipsometric Measurements of Passive Film Thickness on Zinc Electrodes in KOH Solution", J. Electrochem. Soc., Vol. 136, No. 12, 1989, p 3594-3598.

103) McKubre, M.C.H. and Macdonal, D.D., "The Dissolution and Passivation of Zinc in Concentrated Aqueous Hydroxide", J. Electrochem. Soc., Vol. 128, No. 3, 1981, p 524-530.

104) Habashi, F., "Principles of Extractive Metallurgy", Vol. 2, 1975, p 111-252.

105) Derry, R., "Pressure Hydrometallurgy: a Review", Minerals Science and Engineering, Jan. 1972, p 1-24.

106) Adamson, A.N., "Alumina Production: Principles and Practice", The Chemical Engineer, June 1970, p 156-171.

107) Martin, M.T. and Jankola, W.A., "Cominco's Trail Zinc Pressure Leach Operation", CIM Bulletin, April 1985, p 77-81.

108) Parker, E.G., "Oxidation Pressure Leaching of Zinc Concentrates", CIM Bulletin, May 1981, p 145-150.

109) Forward, F.A. and Veltman, H., "Direct Leaching Zinc-Sulfide Concentrates by Sherritt Gordon", J. Metals, N.Y., Vol. 11, 1959, p 836-840.